DESIGN OF WATER TUNNEL TO MEASURE WALL PRESSURE SIGNATURES DUE TO TUNNEL BLOCKAGE AND WAKE EFFECTS

THESIS

Kurt A. Lautenbach
Captain, USAF

AFIT/GAE/AA/88D-20

DEPARTMENT OF THE AIR FORCE
AIR UNIVERSITY
AIR FORCE INSTITUTE OF TECHNOLOGY

Wright-Patterson Air Force Base, Ohio

DISCLAIMER NOTICE

THIS DOCUMENT IS BEST QUALITY PRACTICABLE. THE COPY FURNISHED TO DTIC CONTAINED A SIGNIFICANT NUMBER OF PAGES WHICH DO NOT REPRODUCE LEGIBLY.

AFIT/GAE/AA/88D-20

DESIGN OF WATER TUNNEL TO MEASURE WALL PRESSURE SIGNATURES DUE TO TUNNEL BLOCKAGE AND WAKE EFFECTS

THESIS

Kurt A. Lautenbach
Captain, USAF

AFIT/GAE/AA/88D-20

Approved for public release; distribution unlimited

AFIT/GAE/AA/88D-20

DESIGN OF WATER TUNNEL TO MEASURE WALL PRESSURE SIGNATURES DUE TO TUNNEL BLOCKAGE AND WAKE EFFECTS

THESIS

Presented to the Faculty of the School of Engineering

of the Air Force Institute of Technology

Air University

In Partial Fulfillment of the

Requirements for the Degree of

Master of Science in Aeronautical Engineering

Kurt A. Lautenbach

Captain, Unites States Air Force

December 1988

Approved for public release; distribution unlimited

Preface

In this study, a water tunnel with a ten inch square test section was designed and constructed for the purpose of taking wall pressure signature data. This data is useful in analyzing solid blockage and wake blockage of the tunnel and can be collected without a priori knowledge of model geometry even in cases with separated flow. Previous studies in wind tunnels have shown that this technique allows for accurate measurements on models which are large in relation to the tunnel test section size. This is the first time such a study has been attempted in a water tunnel. Eventually, I hope that development of this technique in water leads to an aerodynamic test facility where indirect force measurements can be made simultaneously with excellent flow visualization.

I now take this opportunity to thank Maj L. Hudson for his guidance during this project. I also thank Professor H. Larson , Lt Col P. King and Dr. A. Nejad for their many helpful suggestions in the design of the hardware involved. Finally, I especially thank my wife Joanne for filling in for me at home while I was neglecting my family in the interests of higher education.

Kurt A. Lautenbach

Table of Contents

List of Figures

List of Tables

List of Symbols

$\bar{A}$	vector
b	Model span, or width
b_s	Line source span
B	Tunnel width, or nozzle width
C_p	Pressure coefficient
E	Young's modulus [psi]
ϕ	Cylindrical coordinate angle from y-axis or Perturbation velocity potential
Φ	Velocity potential, or spherical coordinate angle
H	Tunnel height
Γ	Surface of Ω
Γ_1	Boundary surface of Ω where u is known
Γ_2	Boundary surface of Ω where q is known
L	Nozzle length
μ	Doublet strength
M	Generalized nozzle radius
$\hat{n}$	Unit normal vector
P	Pressure, or point
psi	Pounds per square inch
psig	Gage or differential pressure, pounds per square inch
q	$\partial u/\partial n$, normal derivative of u
$\bar{q}$	Known value of q on Γ_2
Q_s	Source or sink strength for solid blockage

Q_w	Source or sink strength for wake blockage
r	Cylindrical coordinate, radius from x-axis, or in nozzle, generalized cylindrical radius
$\bar{r}$	Generalized non-dimensional radius in nozzle
R	Spherical coordinate, radius from origin, or in nozzle, cylindrical coordinate radius from x-axis
R_s	Radius of sphere
σ	Stress [psi]
θ	Spherical coordinate, angle from x-axis, or in nozzle, smaller of angle from y-axis or z-axis
θ	Spherical coordinate angle
t	thickness
u	Local velocity, or velocity potential
$\bar{u}$	Known value of u on Γ_1
Δu	Perturbation velocity
U	Free stream velocity
U_∞	Free stream velocity
Ω	Domain for volume integral
w	integrating factor, weighting function
x	Rectangular coordinate, direction of free stream flow
$\bar{x}$	Non-dimensional x
y	Rectangular coordinate, width
z	Rectangular coordinate, height

AFIT/GAE/AA/88D-20

Abstract

This thesis describes the design and construction of a new test section for the AFWAL Aero Propulsion Lab six-inch water tunnel in building 18. The new test section has a ten-inch square cross section and is designed to measure wall pressure signatures caused by solid and wake blockage of the flow due to the separation bubble which forms around bluff bodies immersed in the flow. The wall pressure signature for a spherical model is predicted. Applications of the method and associated requirements for instrumentation are discussed.

DESIGN OF WATER TUNNEL TO MEASURE WALL PRESSURE SIGNATURES DUE TO TUNNEL BLOCKAGE AND WAKE EFFECTS

I. Introduction

Water Tunnels are often used to provide flow visualization data which is analogous to the air flows studied in low speed wind tunnel experiments. However, force and pressure data are generally not collected in water tunnel experiments due to the complexity of obtaining and mounting waterproof pressure transducers and force balances compatible with the small models and fluid speeds typically used. Typical flow velocities in flow visualization studies reduce the Reynold's number to a laminar flow region. Nonetheless, information concerning the vorticular nature of the flow is considered of extreme utility in comparison to full scale behavior. Indeed, excellent agreement has been observed between water tunnel experimental results and flight test results in many cases involving separated vortex flows and complex vortex interaction [7:6-7].

In this study, a water tunnel is used which has had a new test section designed to resemble a typical wind tunnel test section. A water tunnel is distinguished from a water channel in that the channel has a free surface between the water and air, and partially or fully submerged models are

tested usually for marine applications. In an experiment involving a free surface, gravity forces are important and the Froude number must be considered [7:5]. In a low speed wind tunnel and in this study, the model is fully immersed in the fluid and no free surface is involved. The predominant forces present are viscous and inertial, therefore Reynold's Number is the appropriate measure of model similarity for scaling purposes.

It has long been recognized that the flow about a body, particularly an aircraft, in a wind or water tunnel is not the same as the flow about the same body in an unconfined space. The difference between the two flows is not due to the fact that in actual flight an aircraft moves through essentially still fluid while in a test tunnel a moving fluid flows around a stationary body. Instead, the difference is because streamlines in a closed test section tunnel are not free to displace away from the body due to the presence of tunnel walls. The difference between the wall constrained case and the infinite field case is further complicated by the effect of the boundary layer on the tunnel walls, viscous wake, compressibility, and a few other factors as well [29:chap 6]. Except for compressibility, it is expected that these effects are not unique to wind tunnels and could be observed in a water tunnel.

It is common knowledge that all of the above mentioned tunnel flow effects cause inaccuracy in experimental

measurements, and that these inaccuracies may be avoided by using models which are small in comparison to the tunnel test sections. Unfortunately, small models are difficult to instrument and difficult to build accurately. Further, they must be tested at larger velocity for the Reynold's number to match the full scale case and large velocity increases the Mach number on the model with the result that complete flow similarity is often impossible to maintain between the two cases. From the point of view of obtaining accurate data, the ideal case is to test on a full scale model. This is prohibitively expensive in both construction and operation. Thus we are faced with the necessity of using rather larger models than the ideal for a given tunnel facility, and then calculating corrections to the measured pressure or force data.

Recent wind tunnel experimenters have developed methods to use wall pressure signature data to estimate tunnel blockage, estimate wall interference, analyze wake and vortex flows, and calculate compressibility effects [27]. This research will utilize flow pressure signatures on the water tunnel walls to analyze the flow properties. From this signature, the flow past the body can be computationally modeled. Due to the preliminary nature of this study, potential flow theory is used for the flow modeling, but more complicated theories are equally applicable. Even in cases where a large separation bubble

surrounds the model, the flow outside the separation bubble and away from the small boundary layer on the tunnel wall is essentially potential flow, thus it should be possible to calculate pressures along a separation bubble or even on the model itself starting only with wall pressure signature data. It is also possible to make predictions of the wall pressure signatures based on either model geometry or based on separation bubble geometry as observed in flow visualization experiments which are well established as water tunnel research techniques [7,32].

The long term objective of this research is to develop the use of wall pressure signature measurement in a wind tunnel while also developing a potential flow computer model of the flow in the tunnel. This will enable the calculation of pressures on the model with fairly simple experiments since the model will not necessarily be instrumented as models generally are for wind tunnel experiments with pressure ports on the model and complex force measuring mounting systems. Instead, the instrumentation will be associated with the tunnel test section only, and will remain the same for different models. However, the reduction of the water tunnel wall pressure signature data will be fairly complex.

The computation method which is most applicable to this research is known variously as paneling theory, boundary element method, boundary integral equation method, boundary

integral solution, and other similar names [4:46]. One of the features of this method which distinguishes it from finite elements methods is that only the boundary surface of the domain of interest is discretized, rather than discretization of the entire domain. According to Brebbia [4:1], the boundary element method involves smaller matrix equations and produces less numerical error than would a finite element formulation of the same problem.

Since the experimental portion of this investigation is to be accomplished in a water tunnel, it should be a straight forward task to obtain flow visualization studies to verify the computed results. Eventually, a method could be developed to make corrections to flow visualization studies to account for the presence of the water tunnel walls just as methods have already been developed to account for the difference in measured forces on models in a free stream and in a flow confined to a wind tunnel.

The six inch water tunnel located at Wright-Patterson Air Force Base, Ohio, Building 18 ,room 23 is the designated facility for the experimental portion of this thesis. Arrangements to use this facility have been made through the sponsor of this research, Dr. Abdollah S. Nejad of Air Force Wright Aeronautical Laboratories, Aero Propulsion Laboratory, Experimental Research Branch. Renovations to the test section of the water tunnel have been designed and constructed. Preliminary instrumentation available consists

of manometers to measure static pressure on the water tunnel test section walls and dynamic pressure upstream of the test section and at various cross sections of the test section. Flow visualization capabilities consist of both dye and air bubble injection systems.

II. LITERATURE REVIEW

The recent literature concerning tunnel corrections calculated from wall pressure measurements in closed solid-walled wind tunnels assuming incompressible flow was extensively reviewed. No like material was found concerning water tunnels. There is a large body of knowledge concerning wall pressure measurements in transonic flow facilities, ventilated wall (boundary layer control and streamline control) tunnels, and flexible adaptive wall wind tunnels which is similar in some ways to the present subject but not applicable to this research. In addition to the recent material concerning wall pressure measurements, this literature review also presents an overview which points out the major historical trends in this type of research and the approximate period in which the different types of wind tunnel correction methods were developed. Although the major theme of this research is to take indirect force measurements by means of wall pressure signatures and it depends on knowledge of the contribution of the test section walls on the flow characteristics, it seems that the only use for this type of analysis so far has been to calculate wind tunnel corrections. The order of discussion will roughly follow the chronological order of the source material.

Many of the papers reviewed for this study included references to work done around 1930, especially to work done by H. Glauert and by L. Prandtl. These early papers are mentioned because they were the earliest encountered references to the calculation of tunnel wall corrections.

According to Joppa [20:7], a solution is given in Tragflugeltheorie, Volume II, C, Gottingen Nachrichten, 1919, by L. Prandtl for a circular wind tunnel which uses a mathematical model including only one pair of vortices outside of the tunnel to balance the effect of the trailing vortex pair inside the tunnel on the walls. This solution does not correct for the lifting line bound vortex and therefore fails to predict longitudinal variations which are known to exist.

Joppa also states that "The Interference of Wind Channel Walls on the Aerodynamic characteristics of an Aerofoil," Air Research Committee (Great Britain) Reports and Memoranda number 867, 1923 by H. Glauert, gives a solution for a rectangular wind tunnel. Another paper by Glauert, "Wind Tunnel Interference on Wings, Bodies, and Airscrews." Air Research Committee (Great Britain) Reports and Memoranda number 1566, September, 1933 was also frequently encountered in the bibliography of the documents reviewed in this study.

Glauert used a doubly infinite series of images of vortex lines with the tunnel walls taken as planes of symmetry

between vortex lines in and out of the tunnel to calculate the effect of the tunnel walls on the flow.

Rae, in the latest revision of the well known book on wind tunnel testing originally written by Alan Pope, explains an imaging system like Glauert's in detail at the beginning of the chapter on wind tunnel wall corrections [29:chap 6]. Imaging is a very useful technique but is easily applied only to rectangular cross section test sections and requires detailed knowledge of the geometry of the test object and of the flow characteristics about the test object. Thus, while imaging can be applied to wing models at low angle of attack, separated flow around a bluff body or aircraft models at high lift conditions especially with partially stalled airfoils are not adequately handled with this technique [20]. This imaging system, but based on a matrix of discrete doublets to model flow around a sphere, was used as a design aid in the present study. According to Moses, [26] other well-known shortcomings of imaging methods, also called singularity methods, are that complicated models, especially powered models, are difficult to represent by simple singularities, and that wall boundary layers and wakes invalidate the potential flow assumptions used.

A wind tunnel correction method applicable to bluff bodies of various aspect ratios, including stalled lifting bodies or wings was presented in 1963 [25]. An important finding of this empirically based development was

that the effect of wall constraint on drag was larger on an axisymmetric body (three dimensional) than was the effect on drag of a body of infinite aspect ratio (two dimensional) by a factor of 5/2. This factor also seems applicable to partially or fully stalled lifting bodies since the stalled regions of such flows were found to have much the same properties as in the axisymmetric case. The chapter on wind tunnel wall corrections in Rae and Pope's book [29:chap 6] gives a fairly complete description of Maskell's method and indicates that the method is widely used today.

An important limitation of Maskell's method is that it is only an adjustment to the dynamic pressure due to solid blockage of a tunnel test section. Although this may be the most important correction to measured lift, drag, and velocity, the calculated correction does not vary in the longitudinal direction and therefore does not provide accurate corrections concerning moment measurements.

With the advent of high speed computers came more sophisticated methods of tunnel corrections. One of the methods, developed by Heysen [17,18,19], involves modeling the tunnel with a vortex lattice and extending a one dimensional array of point sources from the aircraft model location to model the downwash. The location of the line of point sources is adjusted iteratively. This method is applicable to low-speed high lift models and includes corrections to measurement of moments and stability data.

Another method using vortex lattice theory is that of Joppa [20] where an attempt was made to calculate the wake trajectory and the wake shift due to the presence of tunnel walls. The tunnel is again modeled as a vortex lattice, and the lifting surface trailing vortices are modeled in segments which are located iteratively by including the effects of downwash on the location of the vortex. This method is applicable to swept wings in any shape tunnel. Both of these methods are also reviewed by Rae and Pope [29:chap 6] under the subject of downwash corrections.

Tunnel correction methods which depend on wall pressure signatures have been developed by Hackett et al [10-16] and by Ashill et al [1-3]. These methods have only been used in wind tunnels thus far, but there do not seem to be any factors which make it impossible to apply the methods in a water flow, although there are some challenging design problems involving pressure measuring instrumentation. The design problems are addressed later in this thesis.

Hackett's first method [11,13,15] depends on the characteristic wall pressure signature of a blunt body asymptotically approaching a pressure coefficient value of zero upstream while the pressure coefficient asymptotically approaches a non zero value downstream which depends on the size of the wake. The wall pressure signature is decomposed into a symmetric part which is due to solid blockage and an anti-symmetric part which is due to wake blockage. This

decomposition is accomplished iteratively until the maximum value of the symmetric part occurs at the same approximate longitudinal station as the inflection point of the anti-symmetric part. Figure 1 shows this configuration.

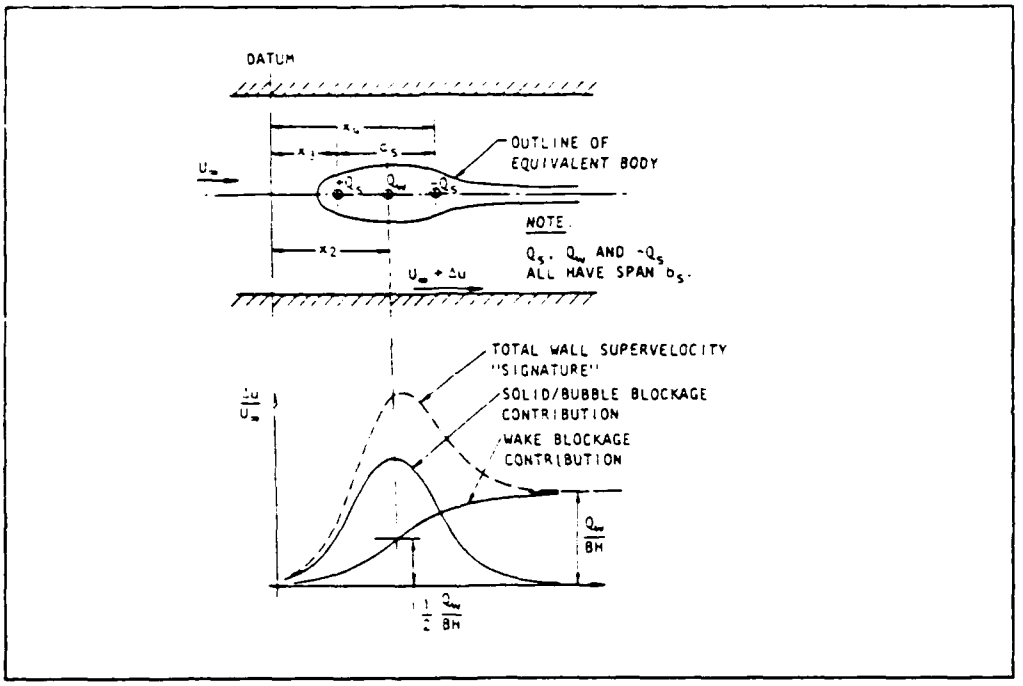

[16]

Figure 1. Wall Pressure Signature Decomposition

The information gained from the decomposed wall pressure signature is used to calculate the location and strength of a pair of line sources of equal but opposite strength (the downstream entity is actually a line sink) near the wind tunnel model location and a line source (balanced by a sink far downstream for the purpose of maintaining continuity) between the previously mentioned pair.

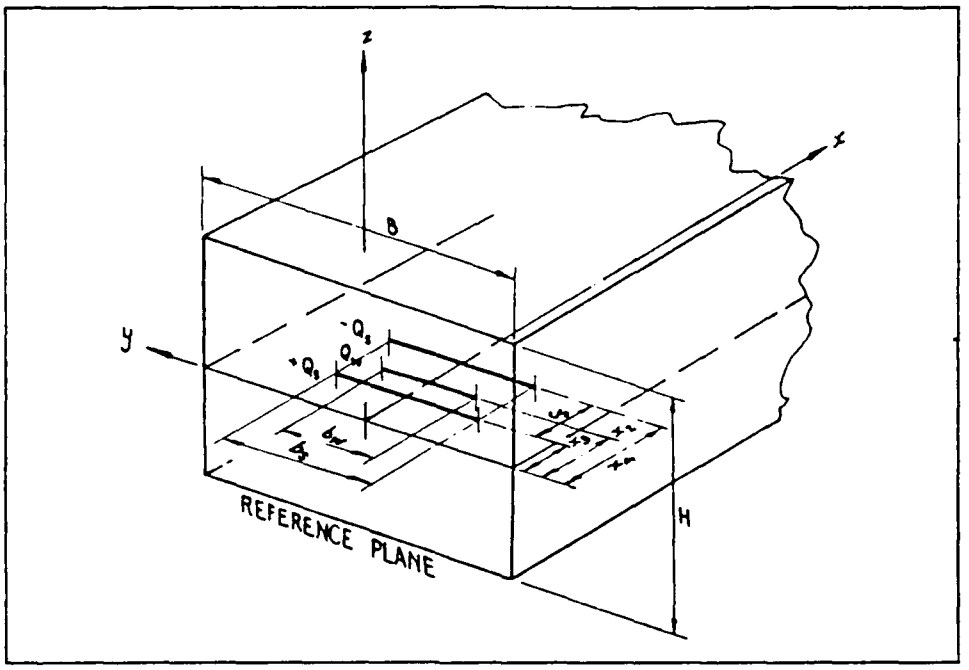

[13]

Figure 2. Location of Line Sources and Sinks

A two dimensional array of images is used to represent the tunnel walls in the case of a rectangular tunnel. The array of images is not doubly infinite but instead extends outwards from the tunnel in a plane perpendicular to the tunnel axis for only a few images then a source panel is used to represent the rest of the images as in Figure 3. This source panel contribution is much faster to compute and introduces only a small error.

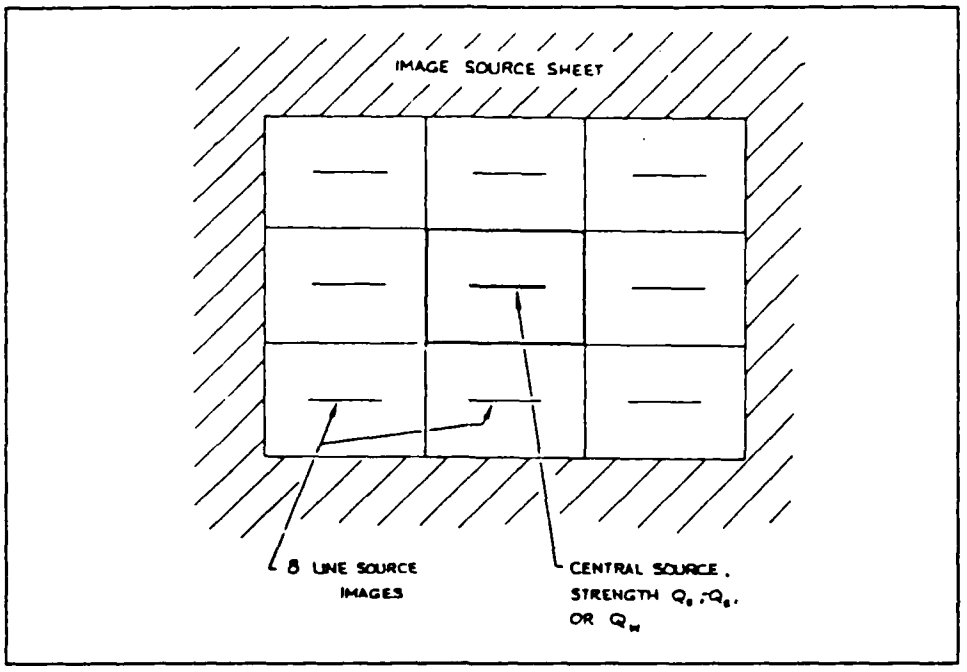

[13]

Figure 3. Image Array and Source Sheet

After the location and strength of these sources has been computed, the flow field in the wall constrained case and the unconstrained case can be calculated and the difference between these two flows can be used to correct measured velocities and pressures at any location in the wind tunnel.

The method has been used in tunnels with nonrectangular cross sections [15] but the imaging becomes more complicated in these cases. It has been established that this technique produces valid corrections for a variety of model geometries including flat plates normal to the flow, spheres, and automobile models mounted on the tunnel floor. Further, the

corrections seem to allow for useful data to be taken at larger tunnel cross section blockage ratios than other correction methods, up to 13.7% in the case of sphere models. Hackett obtained consistent results from tests performed in different sized wind tunnels and with a variety of model sizes in each tunnel. The method was also verified by Walker and Wiseman [36] for a flat plate mounted normal to the flow where it was found that various plate sizes could be corrected to produce essentially the same drag coefficient. Rae and Pope explain Hackett's method in some detail under the subject of wind tunnel blockage corrections [29:chap6]. Hackett implemented the method using look-up charts as it proved to be too slow to implement on-line in the tunnel with the available computers.

Further development, resulting in another method [12] applicable to winged vehicles, solved the slow computer limitation. In Hackett's second method, the tunnel walls are again modeled by imaging, but the solid and wake blockage are modeled by a single row of vortex panels centered in the wind tunnel. The geometry of the vortex panels is assumed and the strengths left as the unknowns. Since there are more data points (the wall pressure measurements) than unknowns (vortex strengths), the solution can be calculated without iteration by a least squares matrix technique. This produces a correction system that can be used on-line in the testing environment.

Ashill has used a boundary integral formulation to calculate the wall induced velocities and upwash at fighter aircraft, automobile, and flat plate models in a wind tunnel [1,3]. Results more accurate than those obtained by Maskell were reported and were accomplished using only about 80 wall pressure measurement locations on all walls in the wind tunnel. Zhou has also reported accurate corrections on an airfoil model using essentially the same formulation as Ashill [36]. Basically, the method involves calculating the perturbation potential function due to the tunnel walls and model.

$$\Phi = u - U_{\infty}x$$

Where Φ is velocity potential,

u is perturbation potential,

U_{∞} is free stream velocity, and

x is in the direction of free stream velocity.

The wall pressure data is used to gain accurate knowledge of the perturbation potential. Another perturbation potential may be calculated for the flow about the model in the same free stream flow but without the tunnel walls included. The difference between the two perturbation potentials is that due to the presence of the tunnel walls. The integral equations used in this method are amenable to Boundary Element Method (BEM) solution.

Again, although almost all of the literature reviewed referred to wind tunnel experiments, the recent emphasis on development of wall pressure signature techniques seems to point to a measurement technique which could be accomplished in a water tunnel with less complication than other wind tunnel force and pressure measurement methods. Also, most of the previous applicable research was aimed at calculating tunnel corrections to the desired free stream flow condition, but the desired eventual result from this research is to measure forces on a model in a flow without instrumenting the model, but instead by instrumenting the water tunnel.

III. Tunnel Flow Analysis

Potential flow theory is used as a first approximation to the flow expected in a ten inch square cross section water tunnel with a five inch diameter sphere model centered in the tunnel. Assuming incompressible, inviscid flow allows the use of the simple mathematical model of a doublet aligned along the same axis as a uniform flow. In two dimensional flow, this would produce a model of flow about a cylinder. In three dimensions, this superposition results in flow about a sphere which is most easily described in spherical coordinates as shown in Figure 4.

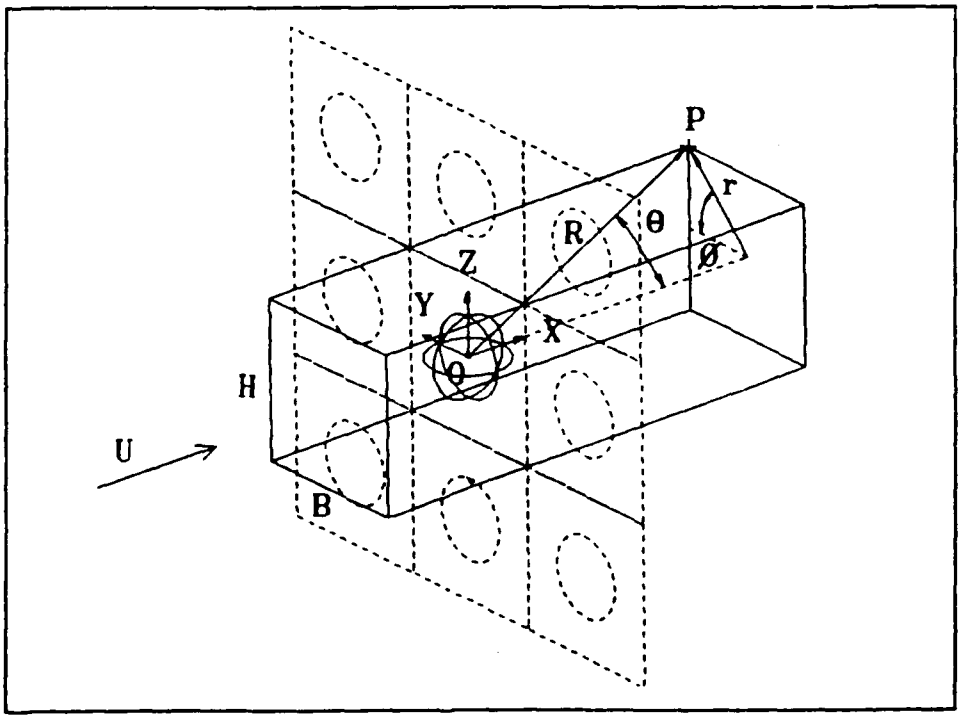

Figure 4. Coordinates for Sphere in Tunnel Imaging

Ignoring, for the moment, the tunnel walls and the array of doublet images in the YZ plane which are also shown in the figure above, the velocity potential in spherical coordinates is given by [21]

$$\Phi(R,\theta,\phi) = UR\cos\theta + \frac{\mu\cos\theta}{4\pi R^2}$$

where Φ = velocity potential

R = distance from global origin to point

θ,ϕ = angles defined in figure above

U = free stream velocity

μ = doublet strength

The velocity at any point outside of the sphere is [21]

$$u_R = \frac{\partial\Phi}{\partial R} = \left(U - \frac{\mu}{2\pi}\frac{1}{R^3}\right)\cos\theta$$

$$u_\theta = \frac{1}{R}\frac{\partial\Phi}{\partial\theta} = -\left(U + \frac{\mu}{4\pi}\frac{1}{R^3}\right)\sin\theta$$

$$u_\phi = \frac{1}{R\sin\theta}\frac{\partial\Phi}{\partial\phi} = 0$$

The radius of the sphere is [21]

$$R_s = \sqrt[3]{\frac{\mu}{2\pi U}}$$

Note that this configuration is axisymmetric which leads to $u_\phi = 0$, but with the doublet images included in the analysis then u_ϕ is not in general equal to zero.

The velocity components in the rectangular coordinate system are given by

$$\begin{bmatrix} u_x \\ u_y \\ u_z \end{bmatrix} = \begin{bmatrix} \cos\theta & -\sin\theta & 0 \\ \cos\phi\cdot\sin\theta & \cos\phi\cdot\cos\theta & -\sin\phi \\ \sin\phi\cdot\sin\theta & \sin\phi\cdot\cos\theta & \cos\phi \end{bmatrix} \begin{bmatrix} u_R \\ u_\theta \\ u_\phi \end{bmatrix}$$

A simple FORTRAN program has been used to calculate velocity fields resulting from the formulae above for a sphere in a 4.8 ft/sec uniform velocity which is the preliminary estimate of the maximum obtainable water velocity in this thesis water tunnel design. The program listing is included as Appendix B. The width and height of the rectangular tunnel are required input to the program, but these parameters have no effect in the case where the image array is one by one images. This case corresponds to flow about a sphere in an infinite free stream. Note that the image array always has same number of images in both

directions in the YZ plane and that the array dimension should be an odd number so the central image is the domain of interest.

As the image array size is increased, the flow fields calculated more resemble flow in a tunnel in that the velocity at a wall location (actually the mid point between the central image and the next nearest image) has lesser components in the Y or Z direction, whichever direction is the normal to the particular wall in question. Larger image array sizes also slow the computations considerably, especially when generating a velocity field at many points. An array size of 21 was deemed optimal since a desk top computer generated results fairly quickly with this value and the numerical error occurred only after three significant digits when compared to results generated with a 1,000 by 1,000 array of images. The computations with such large arrays took an impracticably long time to accomplish and clearly indicated that the effects of image doublets at the large distances involved are negligible. This was expected as the velocity components contain R^3 terms in the denominator. These numerical errors are even less important when considered along with the error introduced with the original assumption of inviscid flow in this analysis. The fact that this potential flow analysis predicts no wake blockage at all is its most serious shortcoming. Nevertheless, the flow parameters predicted on the tunnel

walls on the upstream side of the sphere are expected to be accurate enough to make design decisions for preliminary instrumentation for the water tunnel and for the tunnel test section design itself.

Figure 5a is a plot of the negative of pressure coefficient versus longitudinal position in the tunnel test section predicted by the computer program described above.

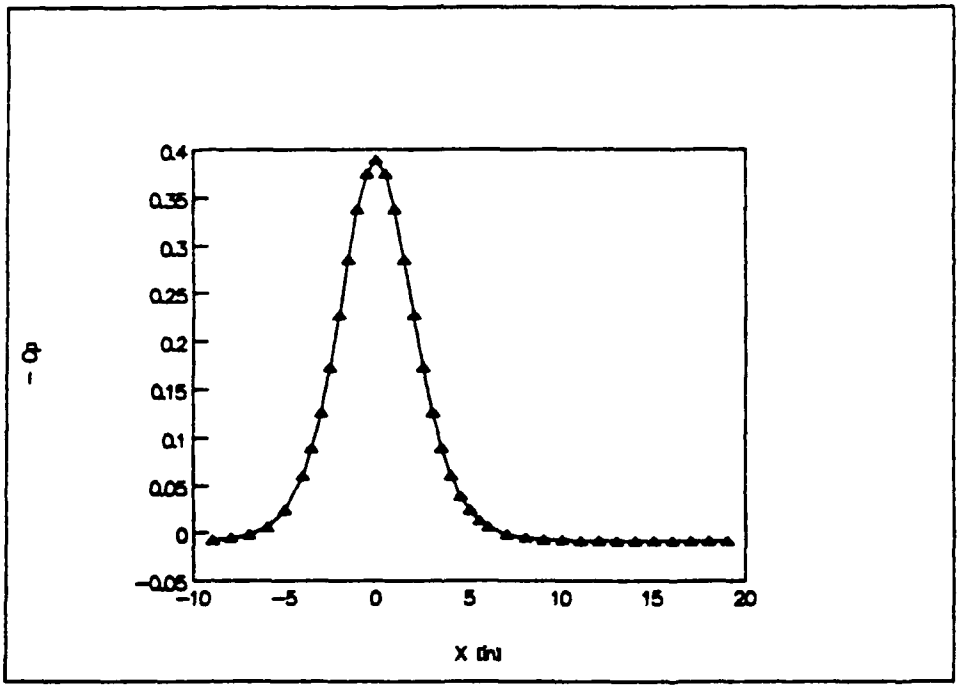

Figure 5a. Pressure Coefficient, Wall Pressure Signature Predicted, Wake Neglected

The usual definition of pressure coefficient as

$$C_p = 1 - \left(\frac{u}{U}\right)^2$$

where u = local velocity

U = free stream velocity

is used in this analysis. The markers on the plot indicate the locations of static pressure ports along the centerline of the test section windows. The overall shape of the plot is the same as the shape of the symmetric part of the plot in Figure 1. Recall that the anti-symmetric part of a wall pressure signature is that attributed to wake blockage. The magnitude of the predicted wall pressure signature is on the same order as some of those reported by Hackett [16] for a sphere model which spans half of the height of a 30" by 43" wind tunnel, in subcritical flow with a Reynold's number about 220,000.

The previous analysis can be improved by the addition of the velocity contribution to the flow of a Rankine oval to simulate the wake blockage effect. This is done by placing a point source on the downstream x-axis at its intersection with the model sphere surface. A point sink is placed on the positive x-axis far downstream. The velocity potential for a point source at the origin is [21]

$$\Phi(\bar{r}) = \frac{q}{4\pi\bar{r}}$$

which leads to the velocity components induced by the source

at any other point given in cartesian coordinates as [21]

$$u_x(x,y,z) = \frac{q}{4\pi} \frac{x}{\left(x^2 + y^2 + z^2\right)^{3/2}}$$

$$u_x(x,y,z) = \frac{q}{4\pi} \frac{y}{\left(x^2 + y^2 + z^2\right)^{3/2}}$$

$$u_x(x,y,z) = \frac{q}{4\pi} \frac{z}{\left(x^2 + y^2 + z^2\right)^{3/2}}$$

where q = source strength (negative value for a sink)

The FORTRAN program in Appendix B includes the effect of sources and sinks of any specified strength placed along the x-axis which should be interpreted as the centerline of a rectangular tunnel. In this analysis, however, only a source on the downstream side of the sphere model and a sink far downstream are used.

The resulting wall pressure signature from a doublet, a Rankine oval as just described, and a uniform flow is shown in Figure 5b. The source and sink strength are taken as equal to the doublet strength which in this particular case produces a wake diameter consistent with flow separation from a five inch sphere at approximately 140^0 from the upstream stagnation point. Note that the effect of adding this Rankine oval has produced little effect on the wall pressure signature upstream of the doublet (the sphere

model) and little effect on the peak value of pressure coefficient on the wall.

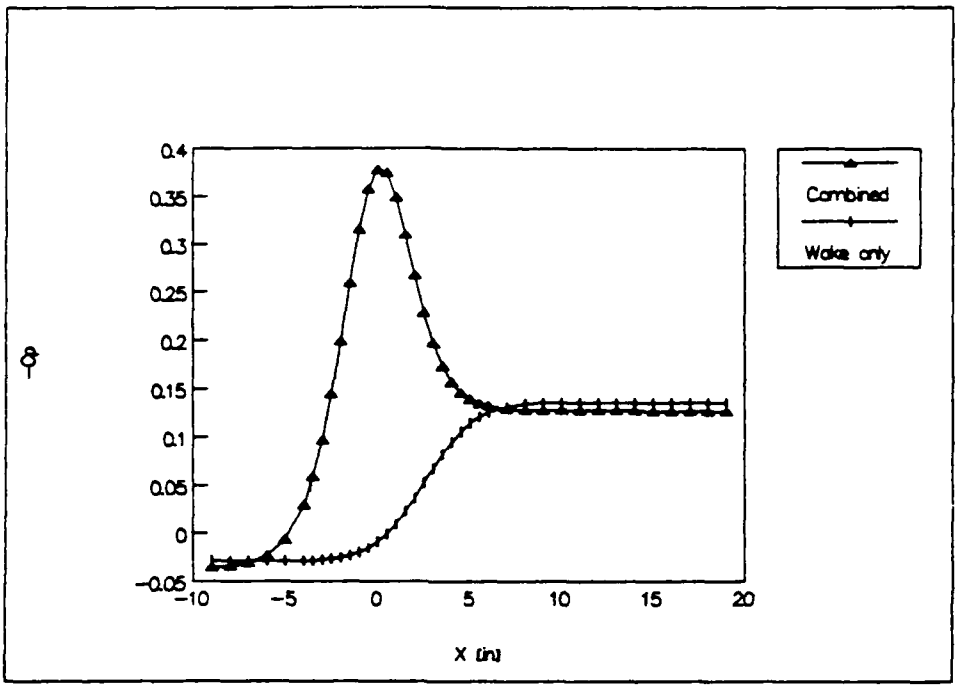

Figure 5b. Pressure Coefficient, Wall Pressure Signature Predicted, Wake Included

Figure 6 contains the same information as Figure 5, but pressure is shown in units of inches of water. This indicates the largest expected magnitude of wall pressure likely in this water tunnel design since it assumes a five inch sphere model centered in the ten inch test section and a water velocity of 4.8 ft/sec.

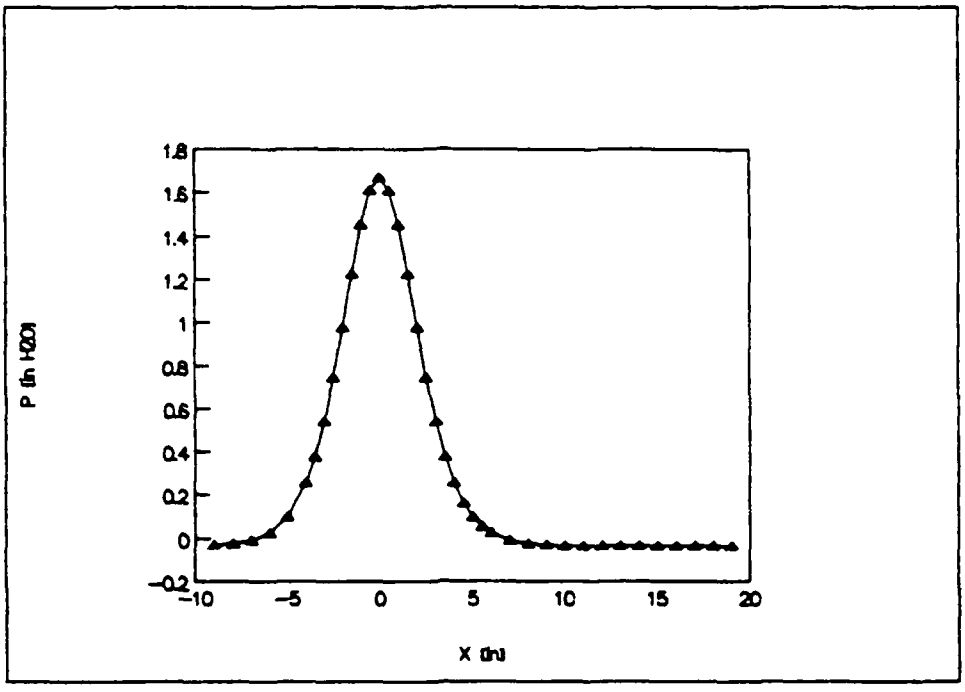

Figure 6. Predicted Wall Pressure Signature from Five Inch Sphere Model, Wake Neglected

In order to benefit from additional wall pressure data points, it is necessary to be able to measure pressure accurately enough to resolve the difference in pressure between two closely spaced static pressure taps. Obviously, pressure taps can be spaced closely in regions of large pressure differentials while, conversely, closely spaced pressure readings of essentially the same pressure over a region of low pressure differential yield information which could have been gained with fewer data points. Indeed, there is a danger that pressure taps in the form of small holes drilled into the tunnel walls can interfere with the flow and therefore cause error in the measured pressure on

other pressure taps further downstream. This risk increases with additional closely spaced pressure taps.

Figure 7a shows the expected difference in pressure between adjacent static pressure ports for the previously described example of a half tunnel span sphere model.

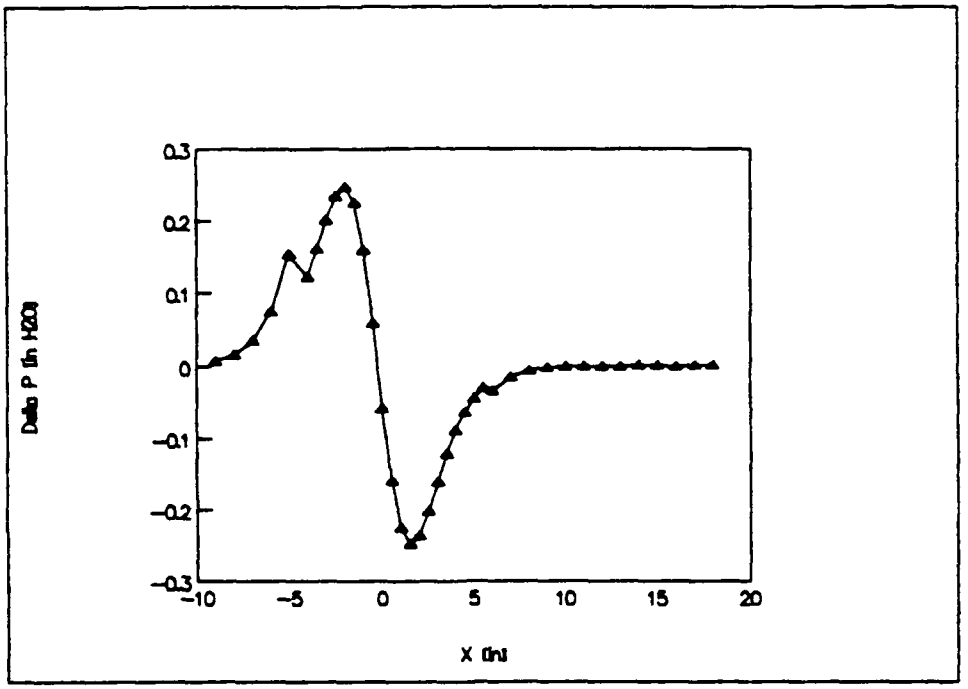

Figure 7a. Pressure Differences Along Window Centerline, Wake Neglected

For this figure, the pressure ports are located along the centerline of a tunnel wall and spaced one inch apart except for a region near the sphere model where the spacing is one-half inch. One pair of acrylic test section windows has been modified to this configuration. The small discontinuities in the otherwise smooth curve in Figure 7 are due to the transition point from one inch port spacing

to one-half inch port spacing. Note that this is not a plot of $\partial p/\partial x$ versus x which would be a smooth curve throughout but is a plot of pressure differences calculated from point to point with some variation in the point spacing. The conclusion drawn from this figure is that pressure differences must be measured to an accuracy of 0.001 inches of water which is one order of magnitude smaller than the smallest pressure difference predicted near the sphere model location to accurately represent a wall pressure signature similar in magnitude to that shown in Figure 6. The need for accuracy in pressure measurement increases with smaller models and with lower flow velocities.

Figure 7b shows the same information as Figure 7a except that the effect of the wake simulated by a Rankine oval is included. The pressure differences shown on the upstream portions of both curves are essentially the same while the downstream portion of Figure 7b shows a smaller peak pressure difference. Including the wake effect in the analysis does not substantially change the accuracy required of the wall pressure signature measuring instruments.

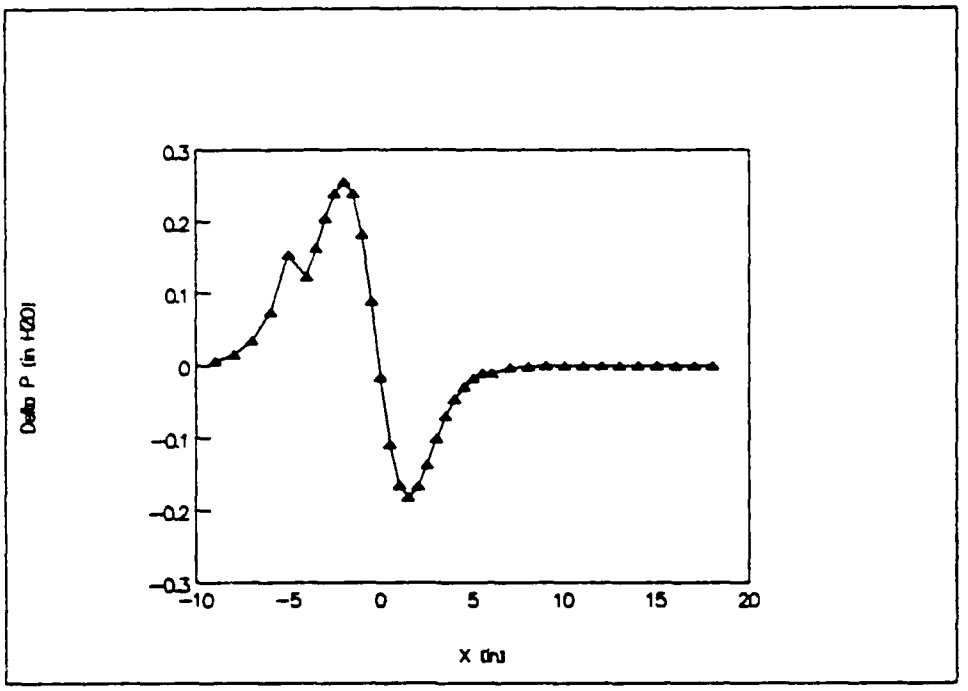

Figure 7b. Pressure Differences Along Window Centerline, Wake Included

All of the preceding analysis concerned pressure measurements taken along the centerline in the flow direction of a test section wall or window. As shown in Figure 8a which is a contour plot of the negative of pressure coefficient over an entire test section window, this is exactly where the largest pressure gradients are located.

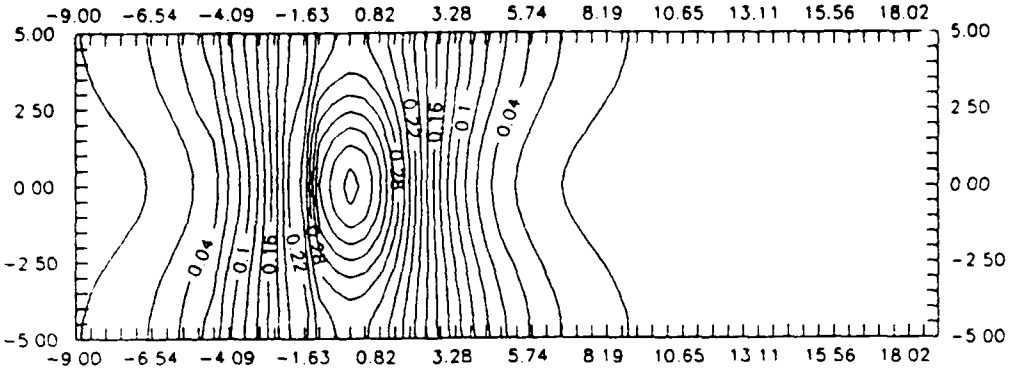

Figure 8a. Pressure Coefficient on Test Section Wall, Wake Neglected

It is also apparent from Figure 8a that not much variation of pressure exists perpendicular to the flow direction on the wall except at x = 0. If it were desired to add more pressure ports to the existing array along the window centerline it seems that the most useful configuration would be ports spaced along a single line perpendicular to the flow and centered on the model location. The total array of ports would then form a cross centered on the model. Figure 8b shows that this same configuration is indicated even when wake effects are included in the analysis. The most important difference between Figure 8a and Figure 8b is that the pressure coefficient downstream of the model location is larger in Figure 8b while the contours in Figure 8a are symmetric about the sphere location at x=0.

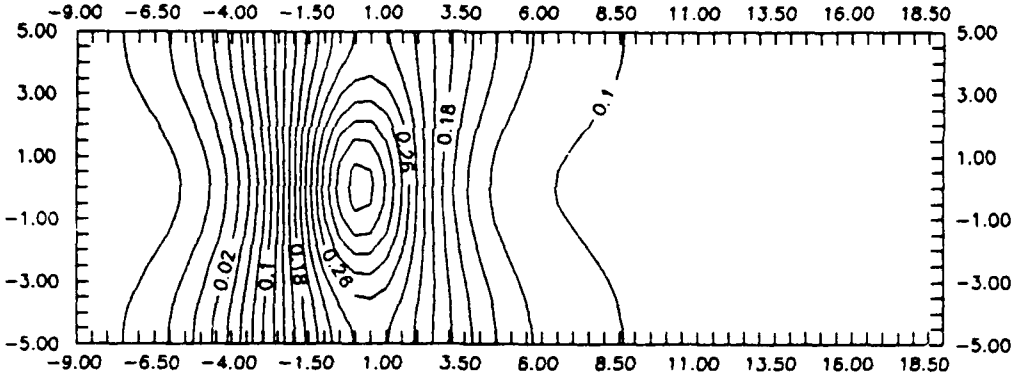

Figure 8b. Pressure Coefficient on Test Section Wall, Wake Included

To illustrate the difference in flow fields obtained in the wall constrained cases just considered and the unconstrained case, contour plots of the negative of pressure coefficient along a plane of the same dimensions and the same distance from the sphere are included as Figure 9a and Figure 9b.

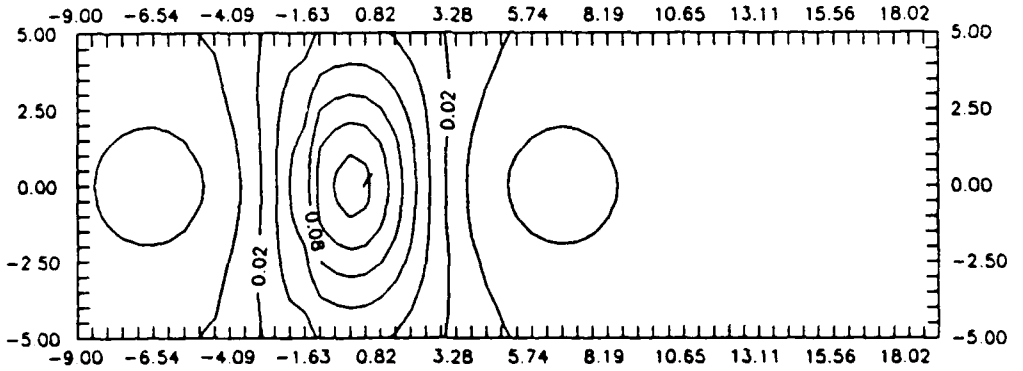

Figure 9a. Free Stream Pressure Coefficient Contours, Wake Neglected

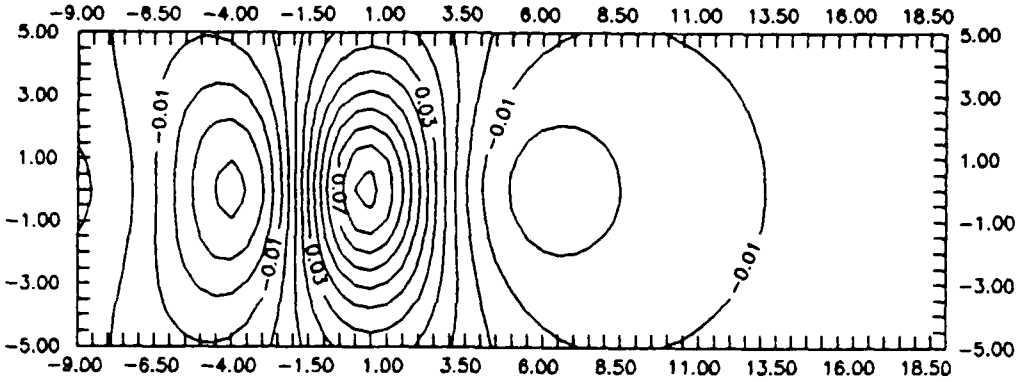

Figure 9b. Free Stream Pressure Coefficient Contours, Wake Included

For this unconstrained flow case, the overall pressure coefficient and the pressure gradients are smaller. Also the region where the pressure coefficient changes sign (which indicates flow velocity lower than free stream velocity in this case) is closer to the model location. The maximum pressure gradient is still along a line in the direction of the flow.

Note that Figures 8b and 9b contain the information necessary to calculate tunnel corrections to unconstrained stream values for the given model. Suppose that experimental data corresponding to the case predicted in Figure 8b was available and that it was desired to correct this data to calculate the pressure expected in an unconstrained flow. Then it would be necessary to take the difference in the velocity fields corresponding to Figures 8b and 9b, and add this difference to the velocity

field measured in the experiment. The technique just described does not consider the effects of boundary layer growth along tunnel walls, or the effects of tunnel wall confinement on wake and vortex trajectories.

The result of this flow analysis is that the geometry of the test section design is shown to be likely to yield measurable wall pressure signatures with a simple spherical model centered in the tunnel. The analysis also predicts the nature of the experimental data to be taken in the preliminary research conducted in this water tunnel assuming that close to uniform flow is achieved with this tunnel design.

IV. DESIGN OF WATER TUNNEL

Primary Requirements

The primary performance requirements for a water tunnel test section for this study are that uniform flow be provided at a high enough velocity so that wall pressure signatures can be measured conveniently. It is also desirable to change as little as possible the existing test rig in test cell 23 on the first floor of building 18 since the experiment now in place will continue to be useful for some time.

Description of Present Facility

The experiment presently installed in the water tunnel is the Multi-Ducted Inlet Combustor [34]. A block diagram of the water flow used in this experiment is included in Figure 10.

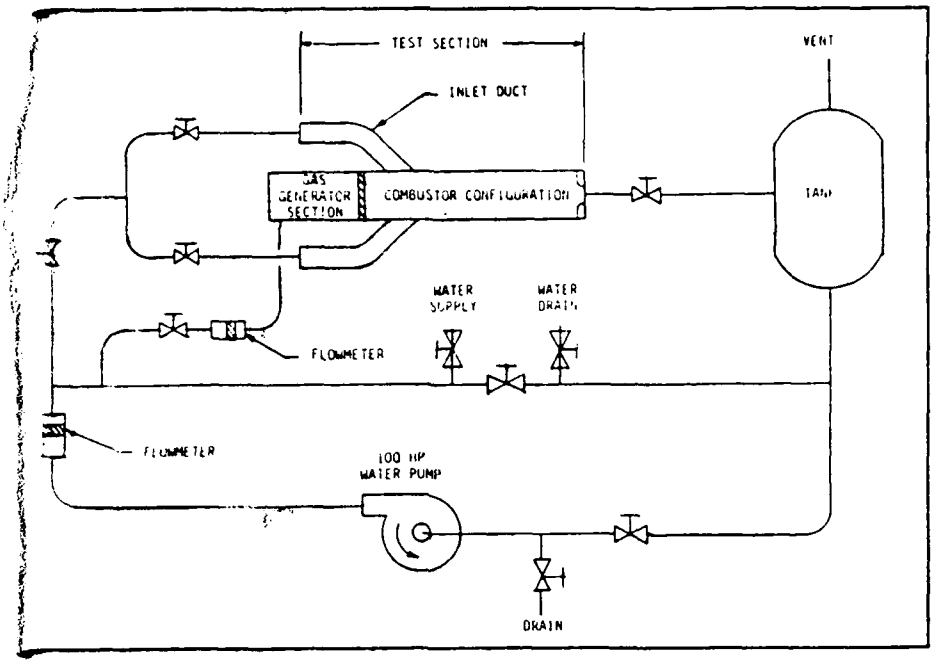

[34]

Figure 10. Flow Diagram

The existing test rig is known as the six inch water tunnel because of the inside diameter of the combustor model in the test section of the present experiment and because most of the plumbing supplying water flow between the pump and the test fixture is nominal six inch diameter Polyvinyl Chloride (PVC) Schedule 80, Type II pipe. The actual inside diameter of this variety of PVC pipe is 5.709". The centrifugal water pump is located in the basement of building 18 and is powered by a direct drive 100 horsepower electric motor. This pump and motor are rated as being able to provide a flow rate of 1500 gallons per minute [34]. Assuming uniform flow in the PVC plumbing, this

corresponds to a water velocity of 18.8 feet per second. Using this velocity and taking the water temperature as 60^{0}F, which is the lowest temperature the tunnel is likely to experience, a Reynolds number of 733,000 is obtained based on the pipe diameter. Obviously, this is much greater than Reynolds upper critical number of 4,000 for usual piping installations [35] and fully developed turbulent flow is expected in the PVC plumbing at all times.

The water supply is routed through a water softener located next to the pump and motor, and valves are provided to either manually fill the test rig quickly or automatically maintain a desired water level. It is sometimes desired to leave the tunnel drain slightly open and have the water supply automatically maintain the level with fresh water since this keeps the water temperature lower than it would be otherwise. Continuous operation of the tunnel can easily cause the water temperature to rise to 120^{o} F or more. The PVC and Acrylic construction of most of the test rig could withstand somewhat higher temperatures, 150^{o} F or more, and operator safety is not much of a concern at this temperature, but the increase in vapor pressure of water with temperature will cause cavitation in low pressure regions of the test section flow.

In the test cell, the PVC plumbing providing water flow from the pump is supported within an adjustable steel rack which is 20 feet long, 2.5 feet wide and about three

feet high. The test section and instrumentation is mounted on top of this rack at about five feet above floor level. Immediately downstream of the experiment is a large steel settling chamber about five feet in diameter and six feet high. The settling chamber receives all water flow from the experiment before routing the water back to the pump. This chamber also has a six inch diameter stack extending from the top which is kept nearly full during tunnel operation for the purpose of maintaining a high water pressure in the test section. With the stack full, the static pressure in the test section is about 60" of water or 2.2 psig depending on the exact height at the location in question in the test section.

Modifications to Present Facility

Installation of the 10 inch square test section requires that the present test section be disassembled and removed. The existing supporting rack remains necessary, but many of the adjustable support brackets need to be moved and new brackets built. An extension to the support rack is needed as the new test rig is about seven feet longer than the present one. The PVC water supply pipe must also be extended about seven feet at the upstream end of the test section. At the downstream end of the test section, the stagnation tank requires no modification. No modification of the water flow controls are envisioned at this time other

than moving the six inch butterfly shutoff valve at the upstream end of the test section to accommodate the extension in length. It must be possible to reinstall the Multi-Ducted Inlet Combustor model with minimal modifications to the existing interface fixtures related to the extension in length of the support rack.

Design of Ten Inch Square Water Tunnel

As previously mentioned, the primary requirements for this water tunnel are that uniform flow be provided at a high enough velocity to be able to conveniently measure pressure differences due to solid and wake blockage at closely spaced stations along the tunnel walls. This velocity is required to provide a Reynolds number comparable to those obtained in the Air Force Institute of Technology (AFIT) 14" low speed wind tunnel. These considerations lead to the smallest possible test cross sectional area. Opposing this consideration is a secondary requirement that models of a convenient size, and possibly the identical models used in other AFIT test facilities such as the planned 14" square wind tunnel in Building 95, fit in this water tunnel.

Test Section. A 10" square test section was chosen which will provide a water flow velocity of 4.81 feet per second assuming uniform flow. Preliminary calculations indicate that a Reynolds number range of 329,000 to 658,000

may be obtained by controlling the water temperature from 60^0F to 120^0F. These figures assume that the full 1,500 gallons per minute flow rate is achievable, and the characteristic length is taken to be the test width of ten inches. A technique currently used in the facility for temperature control consists of running the tunnel at high speed to raise the temperature from internal friction, and draining water from the tunnel while replenishing with cold tap water to lower the temperature. The increased occurrence of cavitation at higher temperatures is unfortunate because it will often be desired to run experiments at the highest possible Reynolds number. The decrease in viscosity with higher temperature will both directly raise the Reynolds number and may decrease pipe friction loses which will allow greater velocity also raising the Reynolds number. The technique of running water tunnels at elevated temperatures to produce a high Reynold's number is well known and a description of its use is given by Stahl [33]. This range of Reynolds number, assuming an air temperature of 59^0F and based on a characteristic length of 14", would be achieved in the AFIT low-speed wind tunnel at velocities of 44.1 to 88.3 feet per second.

The test section is constructed mainly of 0.62" thick aluminum, bolted together with 10-24 socket head screws and sealed with 0.100" nominal linear O-ring cord. See Figures 18-32 in Appendix A for drawings. The

side walls are acrylic windows which are also bolted in place and sealed with O-ring cord. See figures 33-37. Three pairs of windows have been machined with two sets left unmodified for future use and one set drilled for static pressure taps spaced every one inch down the centerline of the length of the window. The pressure tap spacing is one-half inch in the vicinity of the proposed model location which is 10" downstream from the beginning of the window. This pressure tap spacing scheme was selected based on the expected wall pressure signature from a spherical model, discussed in the previous section of this thesis, which spans one-half of the test section for a cross sectional area blockage ratio of 19.6%. Although the pressure on the windows is only predicted to be between 2.5 to 3.5 psi above atmospheric, this integrates to about 900 pounds force and there was some concern about the ability of the window flange to withstand the load. See Appendix C for a structural analysis which concludes that the design has sufficient strength.

A Pitot tube rake extending the full height of the tunnel (see Figure 38 and 39, Appendix A) is mounted in the tunnel with the fifteen total head probes arrayed vertically. The rake is attached to the tunnel by 0.25" diameter stainless steel rods passing through compression fittings installed in the windows. These compression fittings have had the normal stainless steel ferrules

replaced with nylon ferrules to clamp the rake in any desired horizontal position thus providing the capability to measure dynamic pressure, and therefore velocity, at almost any location in the tunnel cross section. The nylon ferrules do not crimp the stainless steel support rod as would the original stainless steel ferrules, and this provides the capability to change the position of the rake many times before replacement of ferrules and refininshing of support rods is needed.

A permanent total head Pitot probe will be mounted in the PVC supply pipe below the test section. The main purpose of this probe will be to provide a reference pressure for measurements in the test section, but it may also be useful to calibrate the tunnel flow rate.

The first few experiments recommended after the tunnel is completely assembled are to determine the tunnel flow characteristics, to measure the longitudinal pressure drop due to boundary layer growth which decreases the effective cross section, and to measure the velocity profile at the cross section of the proposed model location. The first model planned is be a five inch diameter sphere mounted on a sting which attaches to the acrylic window. Note that none of the preliminary experiments planned involve modification of the aluminum top and bottom test section walls. This is because the acrylic windows have been designed to allow for easy removal and replacement without disassembly of any

other part of the water tunnel. After the initial experiments prove the relative merits of various model mounting schemes, it may be desirable to install permanent pressure ports and model mounts in the top and bottom walls.

Downstream Duct. Usually, a wind tunnel test section will be connected at its downstream end to a diffuser. Many water tunnels have a similar configuration [7]. The purpose for the diffuser is to provide for a relatively slow flow, and therefore low friction losses, everywhere in the typical closed loop tunnel. In this case, a large diameter return loop to the water pump is precluded for a number of considerations relative to this multi-purpose facility. The pump is located in another room and replacing all the six inch PVC plumbing would be expensive and time consuming. Also, the Multi-Ducted Inlet Combustor experiment could not be easily reinstalled after such a modification to the test cell. Finally, the inlet and outlet of the present water pump are only six inches in diameter, and the flow would still have to be reduced to this diameter at the pump or replacement of the pump would be necessary.

Given that the flow must be reduced to pass through six inch PVC plumbing within, at most, a few feet downstream from the test section, the decision was made to not use a diffuser at all, but to build an extension of the 10" square test section which extends downstream for eight feet. See Figures 11 and 40 for drawings of this configuration. This

length was selected as the largest that could be accommodated in the test cell and also as the largest commonly available dimension of 0.75" thick acrylic sheet of which this duct was constructed. This acrylic construction could be a benefit as the flow in the tunnel can be directly viewed over a much longer than typical test length.

An adapter was designed to attach this duct to the PVC plumbing without much concern for the flow characteristics in the adapter. The most likely form of a disturbance in the test section due to this adapter would be from vortices generated near the corners of the adapter interface with the square duct and the strength of the induced velocities would be inversely proportional to distance from the vortices [21]. The adapter is eight feet downstream from the test section; therefore, flow in the test section is not expected to be affected to a measurable degree. See figures 40-47 in Appendix A for drawings.

Upstream Diffuser and Stilling Tank. The purpose of these components is to bring the water flow to as low a velocity as possible immediately before it passes into the test section. Any flow conditioning devices, such as screens to reduce axial velocity differences at a cross section or honeycombs to remove large scale turbulence, will cause less frictional losses when implemented in a relatively slow flow [29:chap 2]. The major design consideration for this diffuser is avoidance of separation

since a separated flow produces a jet of high velocity water in the center of the diffuser, stilling tank and nozzle which makes it impossible to have uniform flow in the test section.

The geometry of the diffuser is a straight cone with a semi-vertex angle of 7^0 which was selected for reasons of both flow performance and ease of fabrication. Kline [22:309] shows that this is about the largest angle at which no stall will occur over a Reynold's number range of 6,000 to 300,000 for flat plane-walled diffusers operating in water. Interestingly, in further research [23] extending this work to other geometries including straight cone diffusers, the same 7^0 semi-vertex angle was shown to be close to the optimal angle for pressure recovery indicating the least possible frictional losses. Gibson [8] compared several diffuser geometries including square, rectangular, and round cross section and straight versus curved diverging boundaries and found that straight cone circular cross section diffusers of about this semi-vertex angle produced the lowest losses of the diffusers tested. Gibson's results also suggest that any performance benefit in a more complicated diffuser design would be small. A more complicated design would probably be longer than the straight cone design to produce the same overall area ratio since the maximum slope in the diffuser is always limited by the same avoidance of separation consideration. The

conclusion is that a more complicated diffuser design would yield little, if any, flow performance benefit and the additional complications involved in design and construction are unwarranted [24].

The area ratio achievable in this design is limited by the available length in the test cell. To produce a 24" inside diameter in the stilling tank with the previously mentioned 7^0 semi-vertex angle, the diffuser must be 73.3" long. This gives an area ratio of 4.2 and a predicted velocity in the stilling tank of 1.14 feet per second. This velocity assumes uniform flow and a pump flow rate of 1,500 gallons per minute. See Figures 12-16 in Appendix A for drawings.

Nozzle. The purpose of the nozzle is to accelerate the flow to the high velocity needed in the test section in a manner producing as uniform a flow as possible. Separated flow is not so much a concern for the nozzle as it is for the diffuser because the pressure gradient in the flow direction will be negative throughout a properly designed nozzle. A complication arises, however, from the fact that the entrance to the nozzle will be circular in cross section while the exit will be square. See Figure 17 in Appendix A for drawings. A description of the nozzle geometry is given in Appendix D.

Instrumentation. To measure wall pressure signatures, it is necessary to measure the static pressure at a large

number of ports on the tunnel walls. The pair of test section windows to be used first have static pressure ports spaced every one inch down the centerline starting at one inch and ending at 29 inches (29 ports) and every one-half inch in the vicinity of the model from 6.5 inches to 15.5 inches (10 additional ports). The reference pressure for these measurements will be either the pressure at the furthest upstream static pressure port or the total pressure in the water supply pipe below the test section since a total pressure probe will already be mounted there to serve as a reference value in measuring velocity profiles in the test section With an axi-symmetric model, it may only be necessary to take measurements along one wall; however, measurements along at least two walls will be needed for a lifting model. Thus the possibility arises that 78 static pressure measurements must be made over a short period of time, and quite possibly more measurements than this for experiments that involve unsteady flow, asymmetric model geometry, or asymmetric model location.

No supplier of a scani-valve suitable for use in water was found and it is doubtful that such a device exists. One reason this is a problem is that pressure transducers capable of resolving the small pressure differences predicted between adjacent static ports in this tunnel design are very expensive, on the order of $1,000 or more each for variable reluctance pressure transducers suitable

for use in water. Without a scani-valve a large number of transducers will be needed to take simultaneous measurements and at this stage of development the risk of selecting an inappropriate transducer precludes such a large expenditure.

It may be possible to use a transducer which is limited to pressure measurements in gases by designing a trap to keep the transducer input from coming in contact with the water. For example, the transducer can be connected to a pressure port with a long plastic tube which forms a high loop above the highest water level in the test rig. The advantage to this is that such transducers are available for about $150 each. However, such a configuration invites damage to the transducers in case of any deviation from the tunnel operation procedures which would need to be developed to keep water from siphoning into the transducers. Another disadvantage of this scheme is that longer tube length will slow the time response of pressure measurements. Slow response is not so important when measuring steady flow effects, in fact it could help by dampening noise from small scale turbulence, but a slow responding measurement system would limit the type of research that can be undertaken in this facility. Consequently, it was decided to defer the selection of transducers until after preliminary experiments have been completed using manometers as instrumentation.

Another transducer to measure wall pressure signatures which appears to offer both performance and economic

benefits for a water tunnel application and should be investigated is the Piezoelectric Polymer Tactile Sensor Array (PPTSA). PPTSAs are a recent development of an application for piezoelectric polyvinylidene fluoride which results in a pressure sensor array of small size in the form of a polymer film [28,30]. The development has progressed to the point that this sensor film seems to have the pressure sensitivity required to measure a water tunnel wall pressure signature. Also, the water tunnel environment is less severe than that of the robotics application for which the PPTSAs are designed [29]. A larger number of measurements may be made simultaneously than would be practical to attempt with other types of pressure transducers because it is not necessary to drill holes in the tunnel walls for static pressure ports and because an individual transducer element is small. It is envisioned that a large pattern of PPTSAs need to be mounted on the inside of the tunnel walls in direct contact with the flow. Covering even a large area of the water tunnel test section with PPTSAs would cost less than a single linear array of $1,000 per unit variable reluctance pressure transducers assuming that the cost of the associated amplifiers and other support electronics for data collection, required in either case, is about the same.

A Pitot tube rake has been designed and constructed for use in this water tunnel as already discussed in the

description of the test section design. See figures 38-39 in Appendix A for drawings. It is planned that preliminary tunnel flow characterization measurements will be made with the rake mounted ten inches downstream from the edge of the test section window, where the experimental models will eventually be mounted. After these first experiments, the rake can be remounted downstream from the model location and used to provide momentum deficit measurements from which drag force on a model can be calculated without having instrumented the model.

Although this facility has been designed to provide pressure measurements directly, and force measurements indirectly, nothing precludes the use of the flow visualization techniques usually associated with water tunnels [7]. The facility already has in place a dye injection system with automatic controls capable of providing dye pulses as short as 0.01 seconds [34] which provides good results at low flow velocities. A laser/optical dye detector to provide dye concentration time histories is also available. At higher velocities, an air bubble injection system is used which along with a high intensity mercury vapor lamp has provided both normal still photographic and videotape records of flow phenomena.

V. Conclusions and Recommendations

The wall pressure signature method has been shown to be feasible as a water tunnel experimental research project by analysis of the flow around a spherical model in a rectangular tunnel. The results of this analysis have been used to make design decisions concerning a new test section which has been constructed for the Aero Propulsion Laboratory's six inch water tunnel.

Combined with the boundary element method, wall pressure signature measurement in the water tunnel should yield a solution for the flow characteristics at every point in the flow within the tunnel test section. With the flow field known, the resultant force on the model in the flow can be calculated. The pitot tube rake mounted downstream from the model provides a means of measuring the momentum deficit in the flow which can be used to calculate the drag on the model. The pitot tube rake can also be used to provide input to a boundary element method analysis such as the velocity profile across the downstream boundary and the size and location of the viscous wake which defines the shape of portions of the boundary.

Flow visualization techniques should also be used to provide input to the boundary element method. The size and location of separation bubbles and wakes due to a model should be found by injecting dye, or air bubbles as

appropriate, into the flow upstream of the model and moving the dye probe until the dye is observed to be in a streamline which just passes the model or starts to interact with the model boundary layer.

The wall pressure signature method has previously been used to good effect in wind tunnels to correct experimental data for the flow constraining effect of the wind tunnel walls. In a water tunnel, it is expected that a similar method could be developed and applied to flow visualization experiments.

This water tunnel design is also amenable to other types of research involving various internal or external flow. Since the acrylic windows are easily replaceable, test fixtures involving fluid jets impinging on the flow in the test section could be fabricated by passing ducts through the windows. Again, both pressure and flow visualization data can be taken in such investigations. It would also be possible to mount models in the test section which have fluid jets supplied from outside the test section to study the jet interaction with the main flow in the tunnel. The advantage offered by this water tunnel for such purposes is that the steady flow velocity of 4.8 feet per second which should be achievable is rather larger than the steady velocity currently achievable in other local water tunnels.

It is recommended that the first series of experiments run in the water tunnel be aimed at characterizing the flow in the test section at all flow velocities up to full speed. This should include measurement of the wall pressure signature with no model or pitot tube rake present to determine the longitudinal variation of pressure in the test section at various velocities. Next, the pitot tube rake should be used to measure velocity profiles at the cross section where subsequent research will have models mounted. It may also be possible to measure velocity profiles with a flow visualization technique of injecting dye pulses simultaneously at various points in the flow and measuring the dye pulse trajectories over time with either still photography or a videotape system. These velocity profiles should be used to decide what, if any, flow conditioning devices such as screens or honeycombs need to be mounted in the stilling tank upstream from the test section. This is an iterative process where the entire series of measurements should be repeated after each change to the configuration of the tunnel.

Only after the most uniform possible flow at high velocity is established should measurements be attempted with a model. The first model is presently envisioned to be a five inch diameter sphere mounted on a sting support. This model should have several static pressure taps on its surface which are connected to instrumentation through the

sting support which passes through one of the acrylic windows downstream of the model.

The previously described flow characterization measurements should be repeated with only the sting model support installed and then again with the sphere model also installed. The data thus collected should be used to design a data collection system using a more convenient pressure transducer than the manometers which will have been used to this point in the tunnel development.

Other possibilities for instrumentation which should be investigated are hot film anemometers, laser velocimeters, and especially piezoelectric polymer tactile sensor arrays as previously discussed.

Finally, any model designed for either this tunnel or the AFIT 14" low-speed wind tunnel should by considered for use in both facilities. Besides the benefit in model construction economy, both test facilities have advantages for particular tests with the water tunnel being superior for flow visualization studies.

Appendix A - Water Tunnel Component Drawings

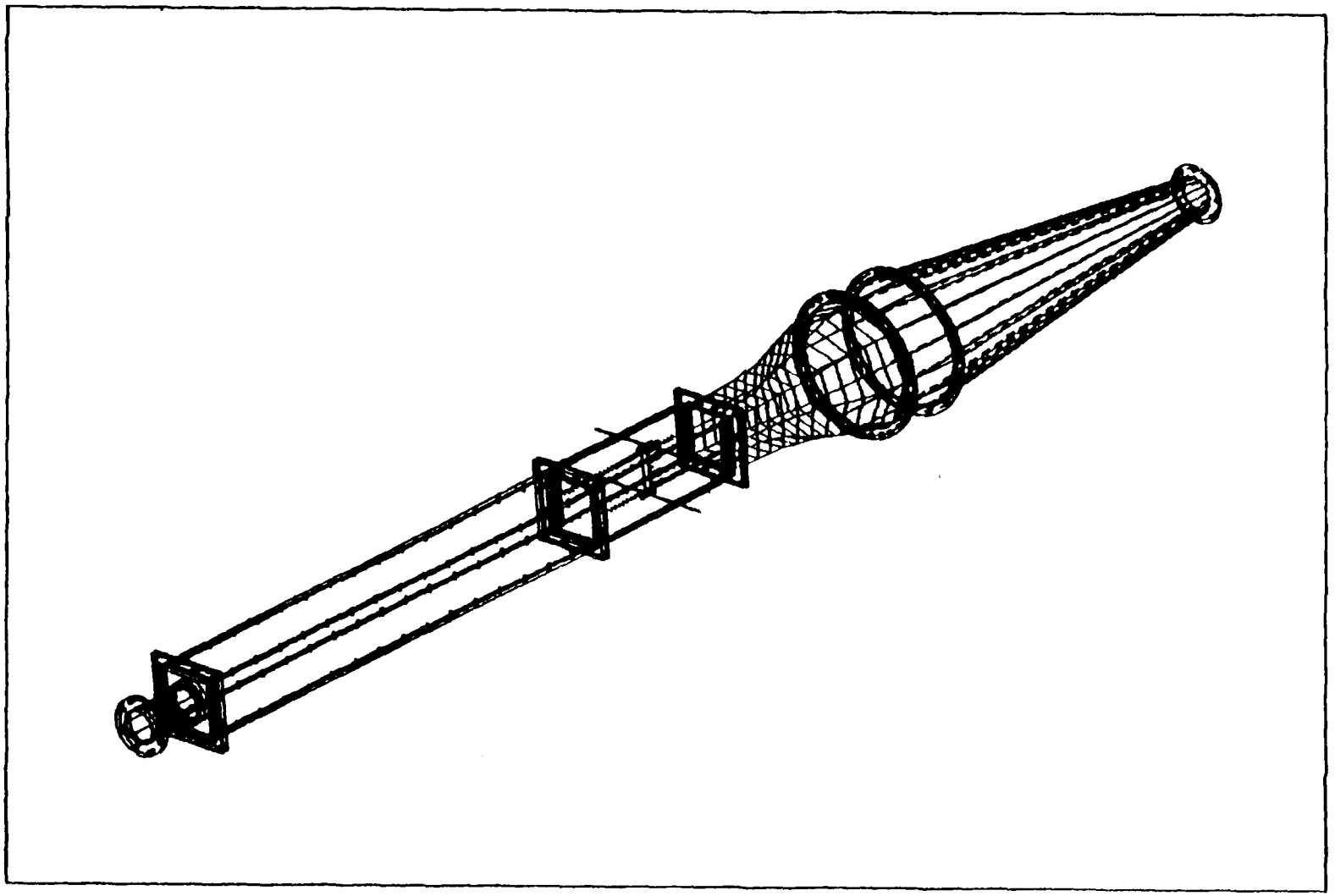

Figure 11. Isometric View, Water Tunnel Assembly

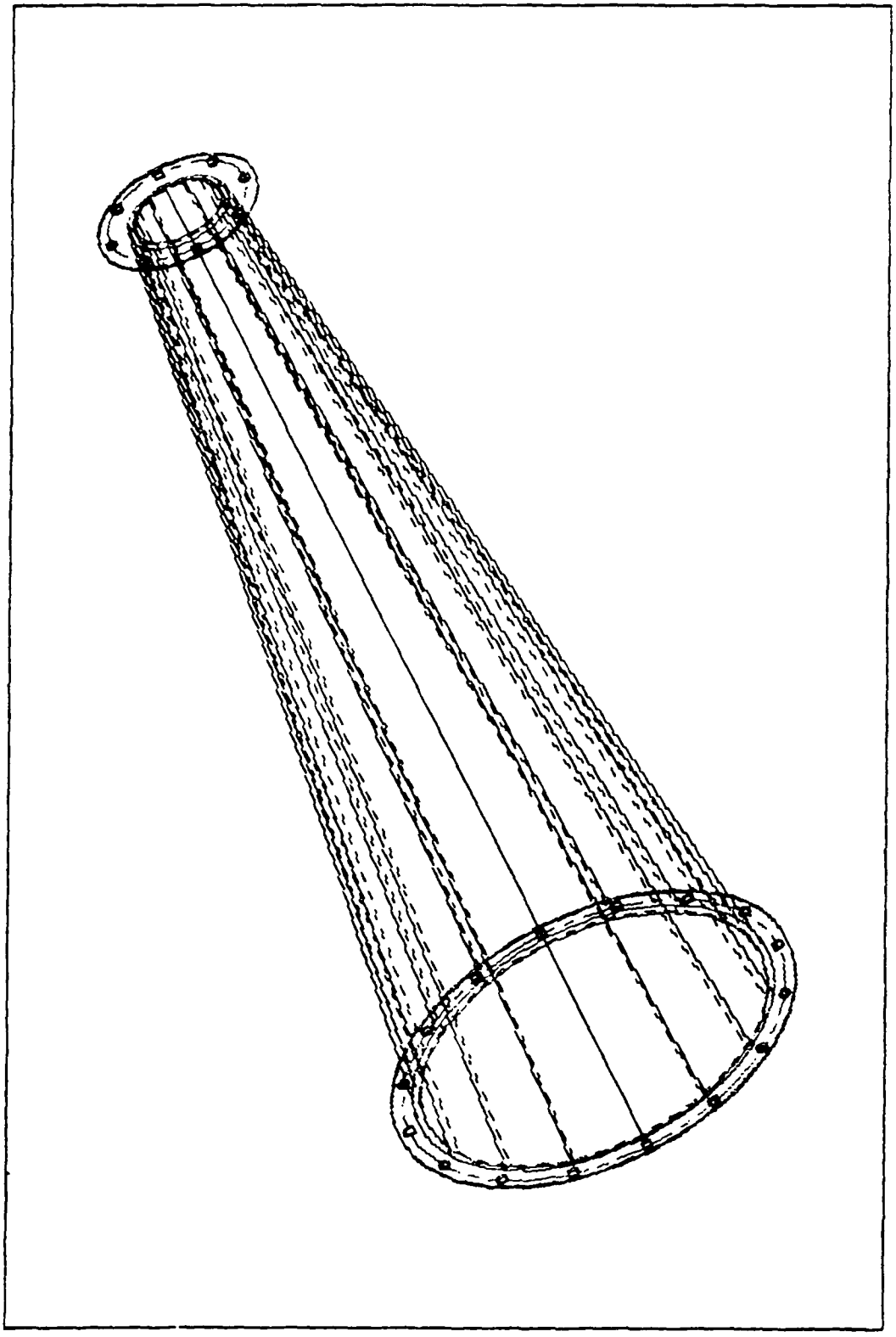

Figure 12. Isometric View, Diffuser

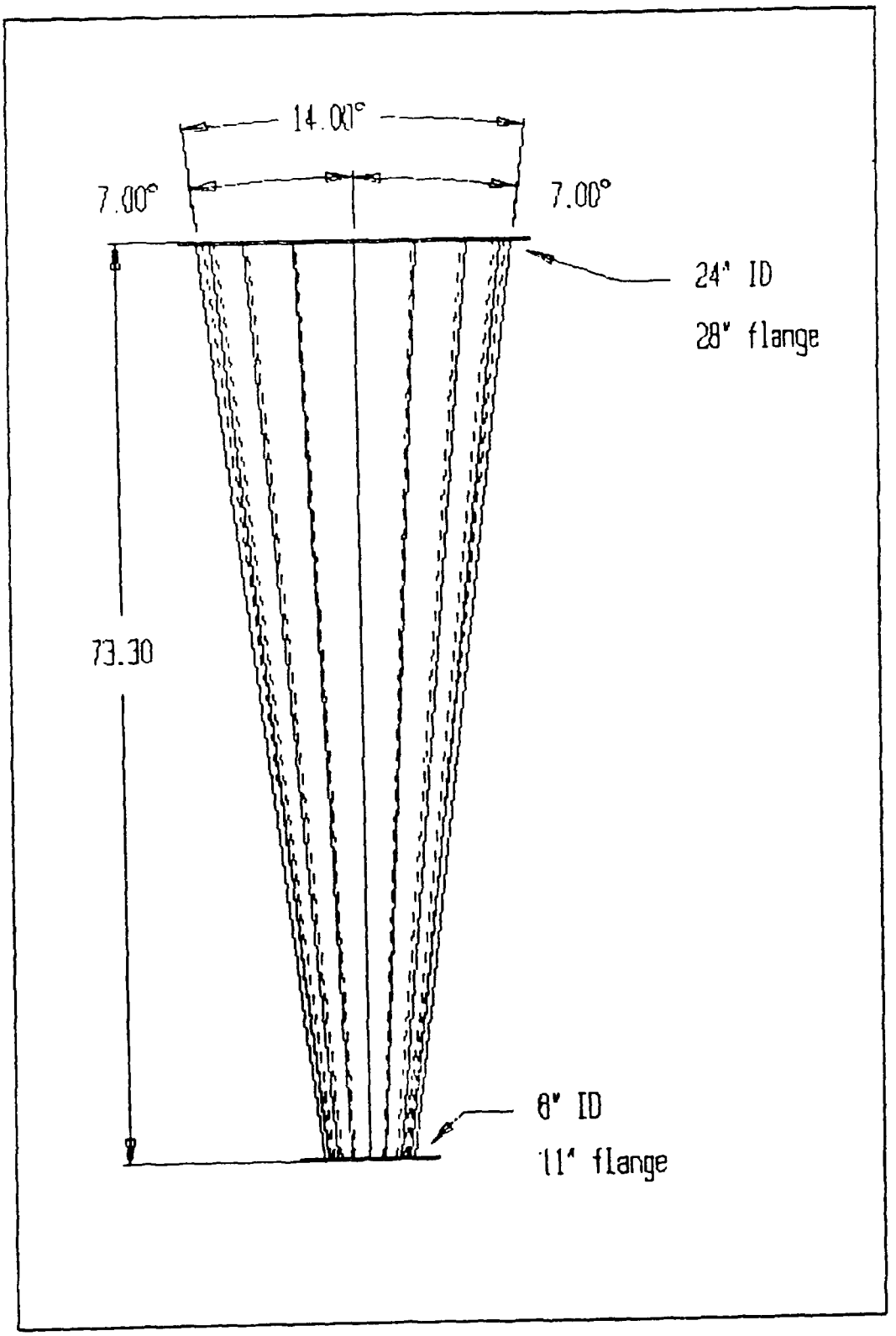

Figure 13. Side View, Diffuser

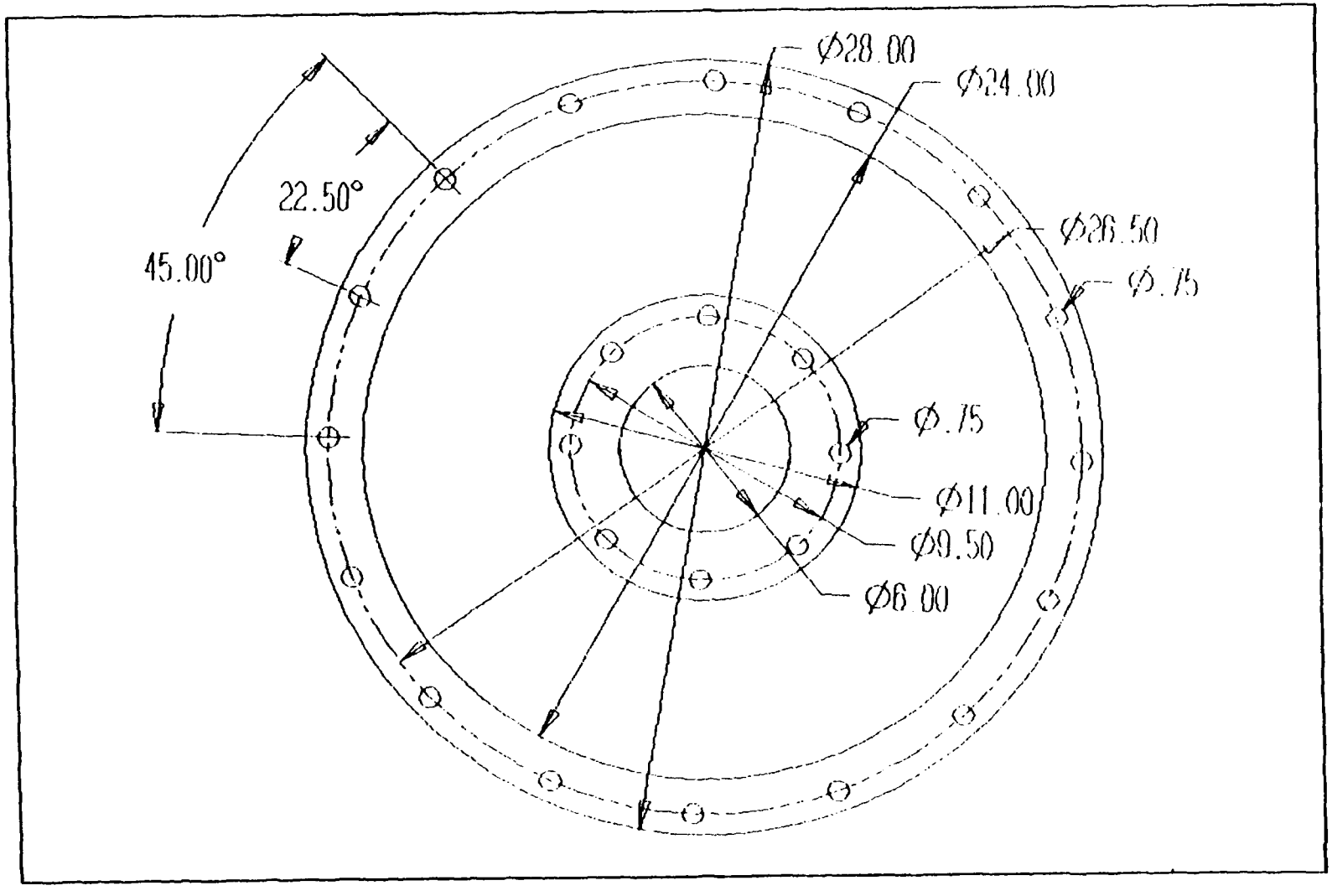

Figure 14. Diffuser Flange Dimensions

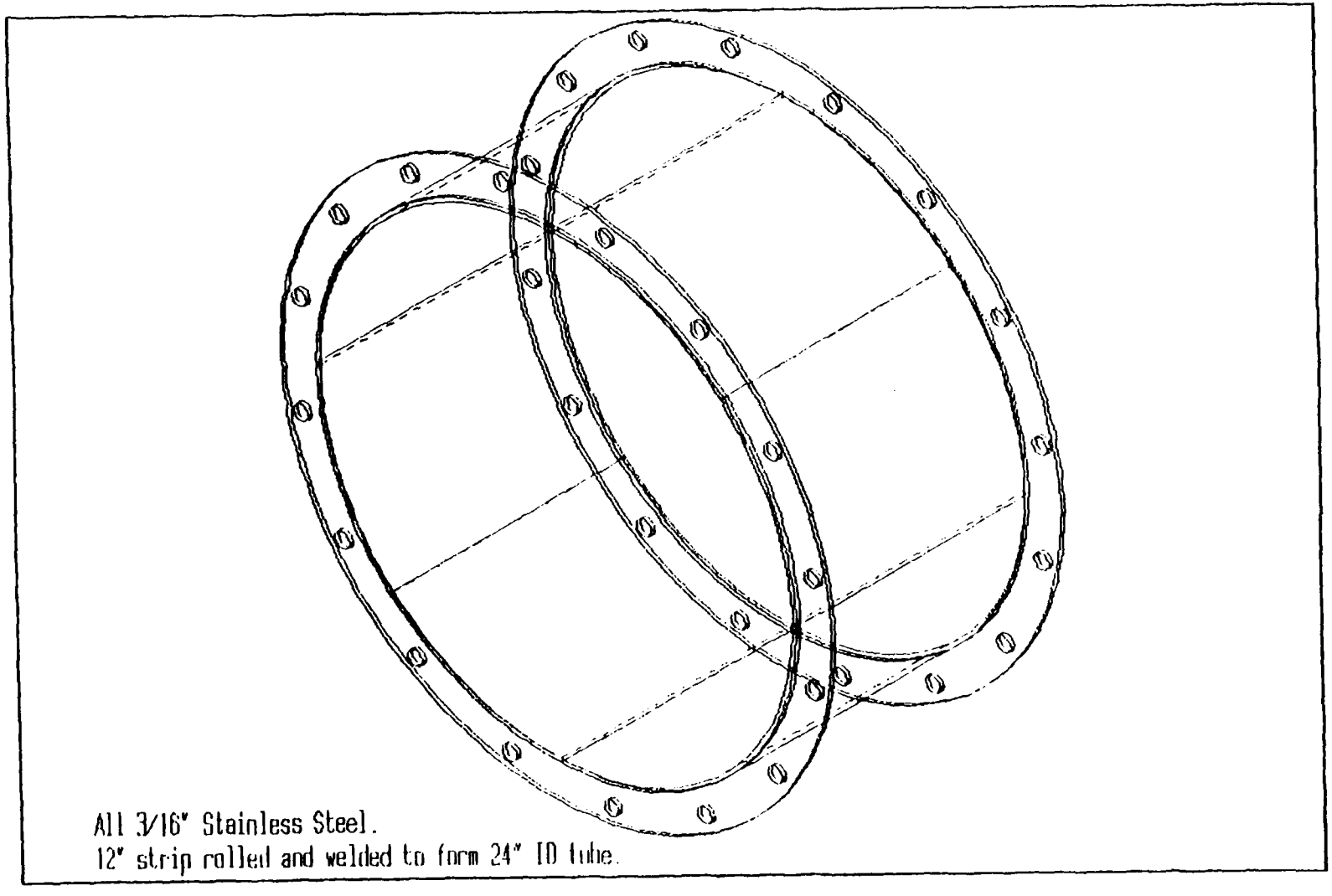

Figure 15. Isometric View, Stilling Tank

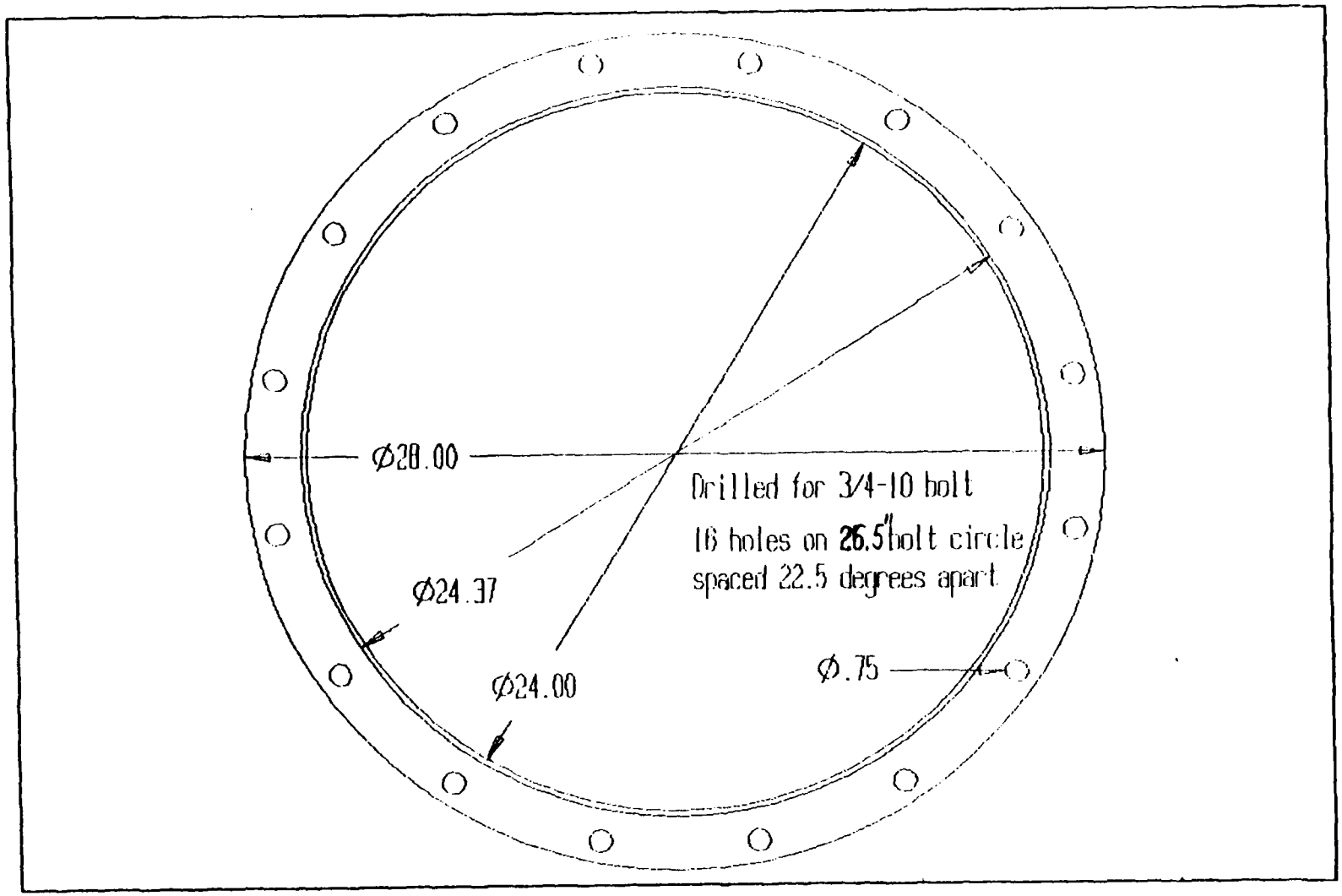

Figure 16. Stilling Tank Flange Dimensions

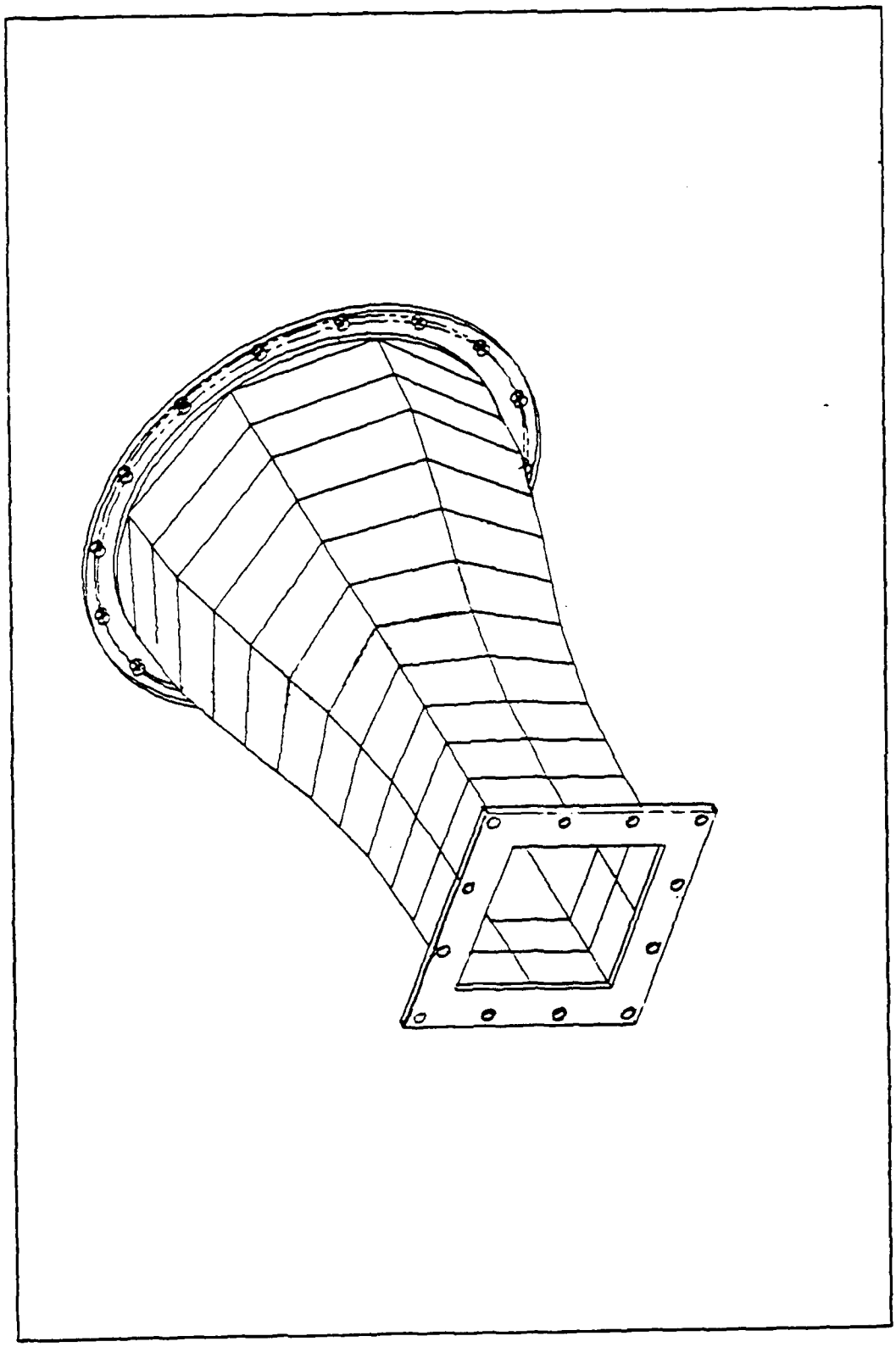

Figure 17. Isometric View, Nozzle

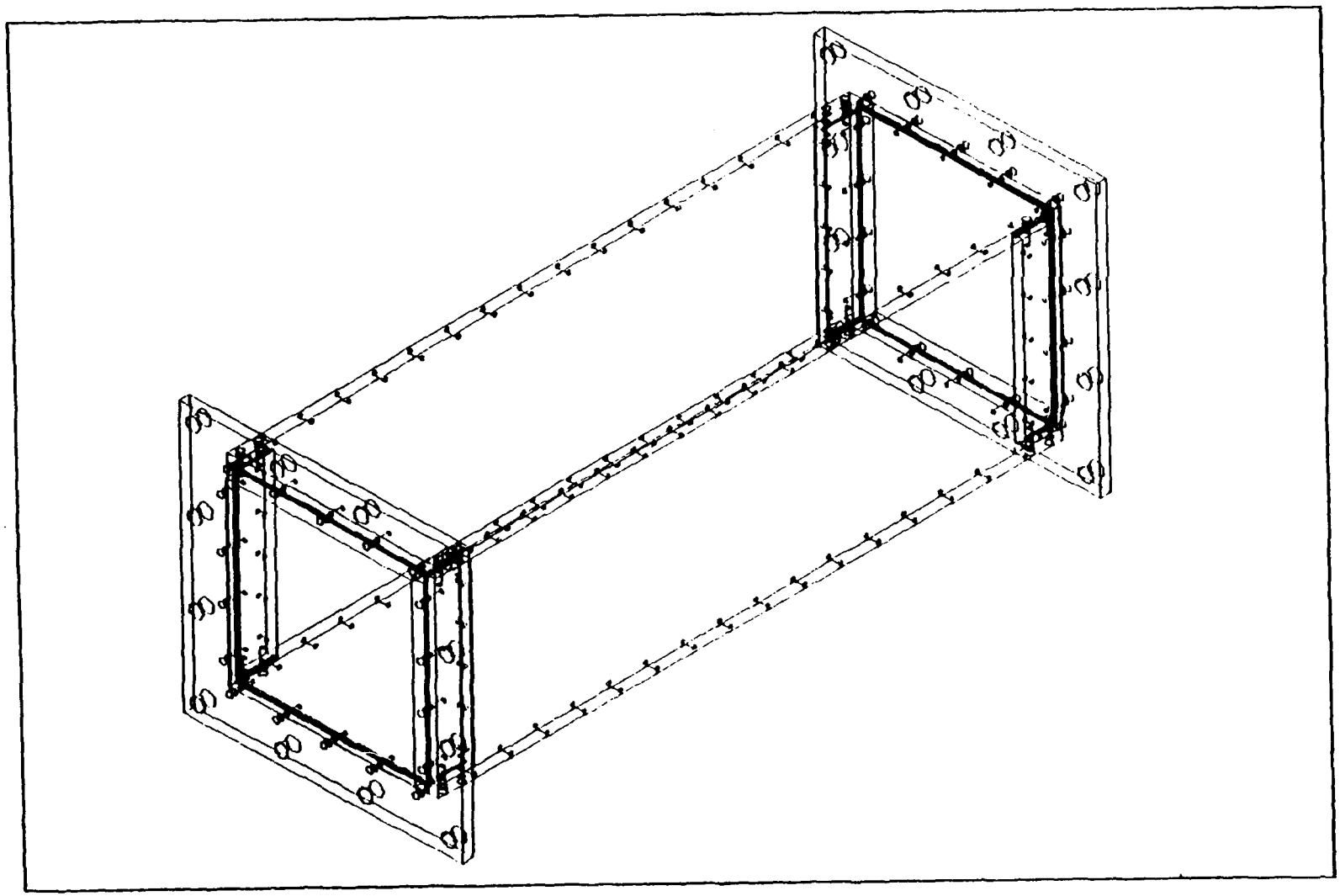

Figure 18. Isometric View, Test Section Assembly

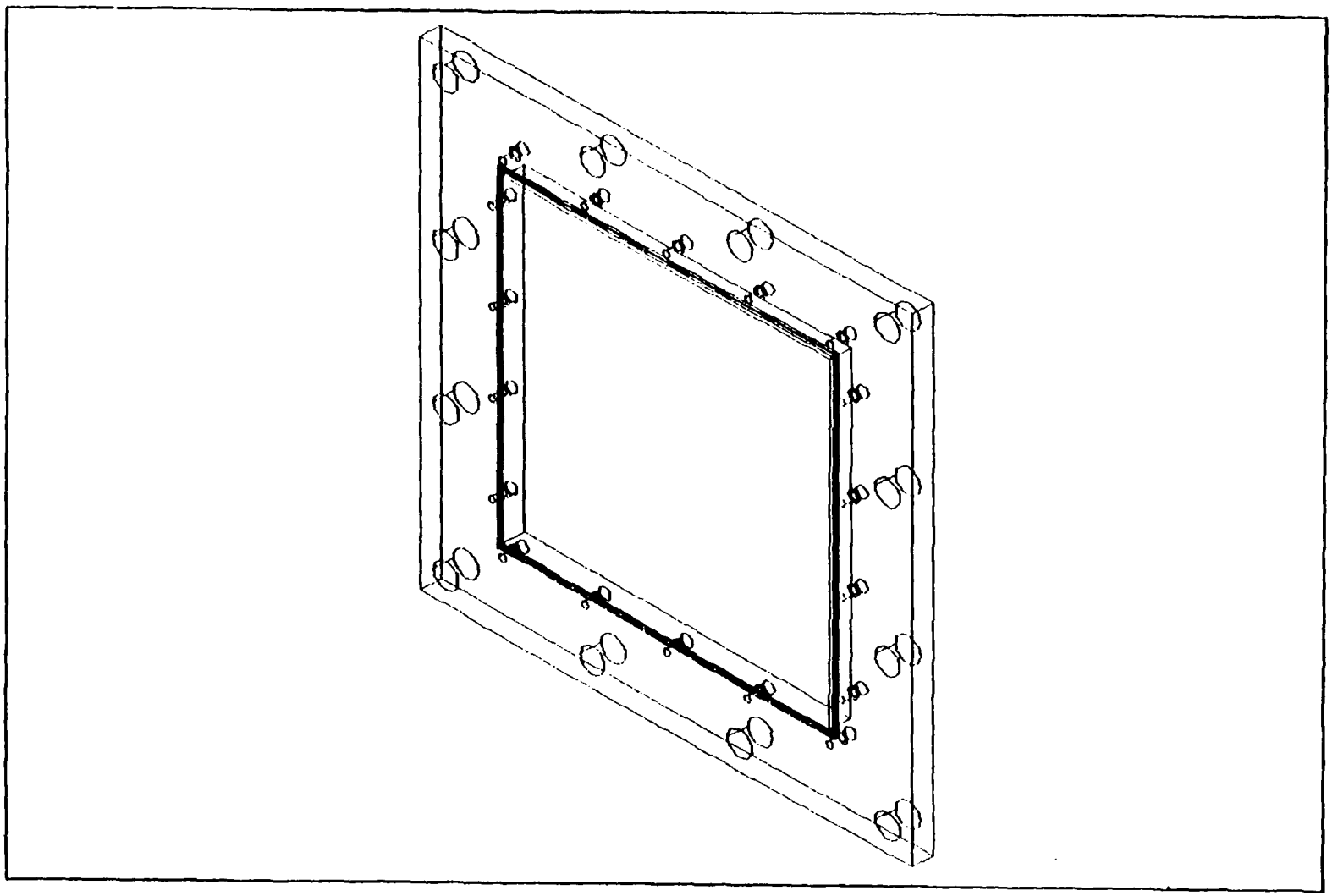

Figure 19. Isometric View, Test Section Flange

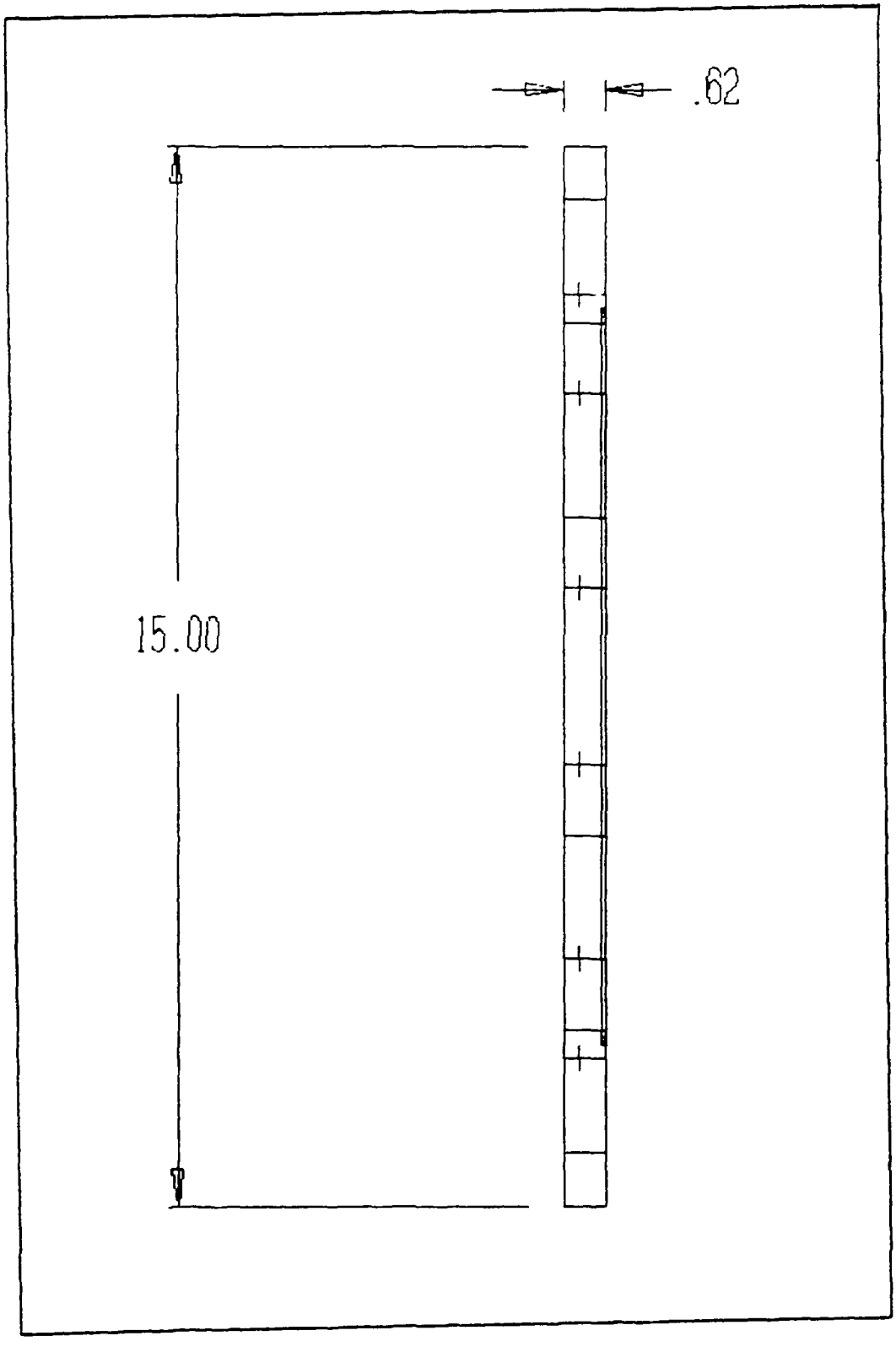

Figure 20. Side View, Test Section Flange

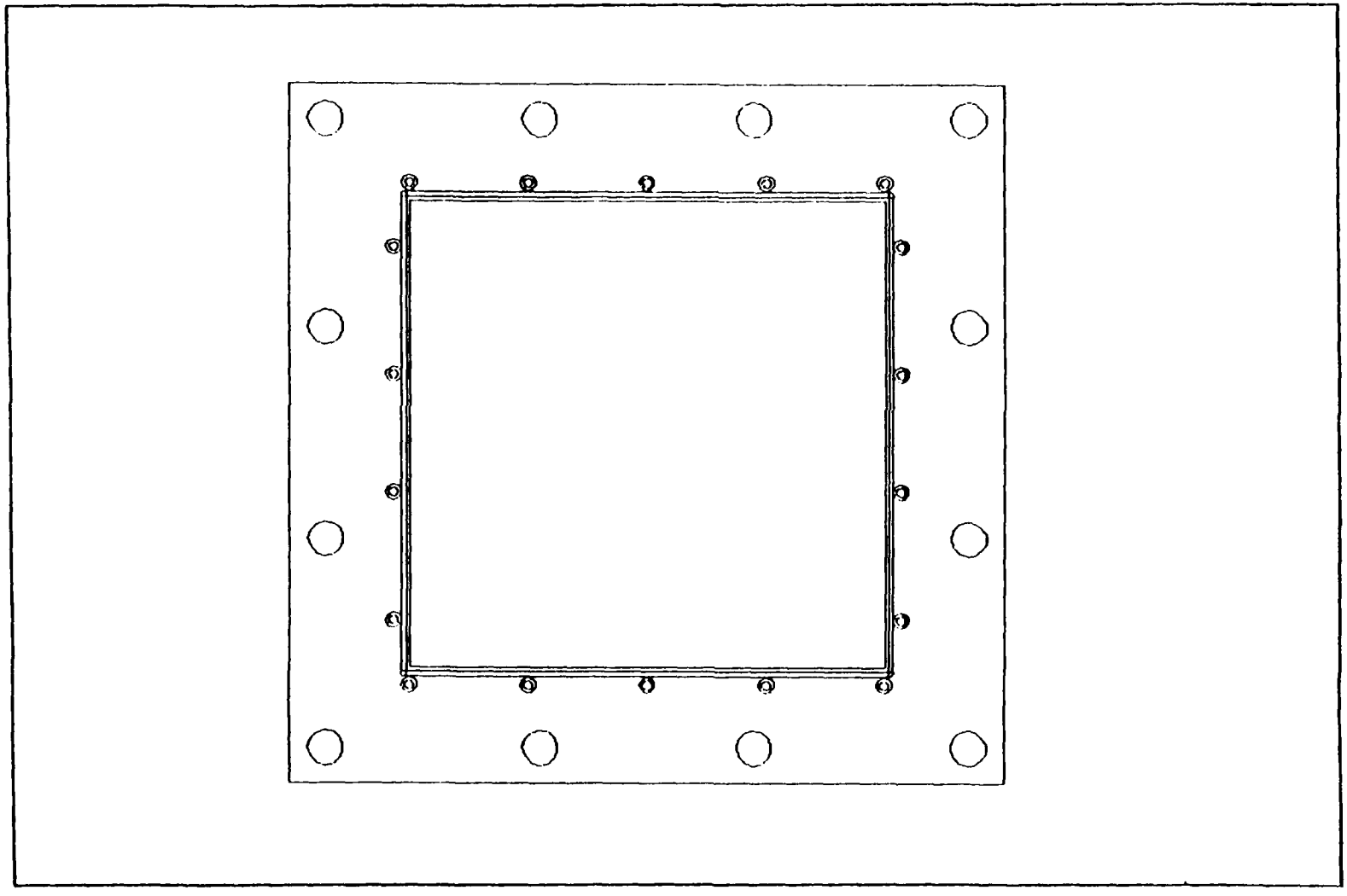

Figure 21. Front View, Test Section Flange, no Dimensions

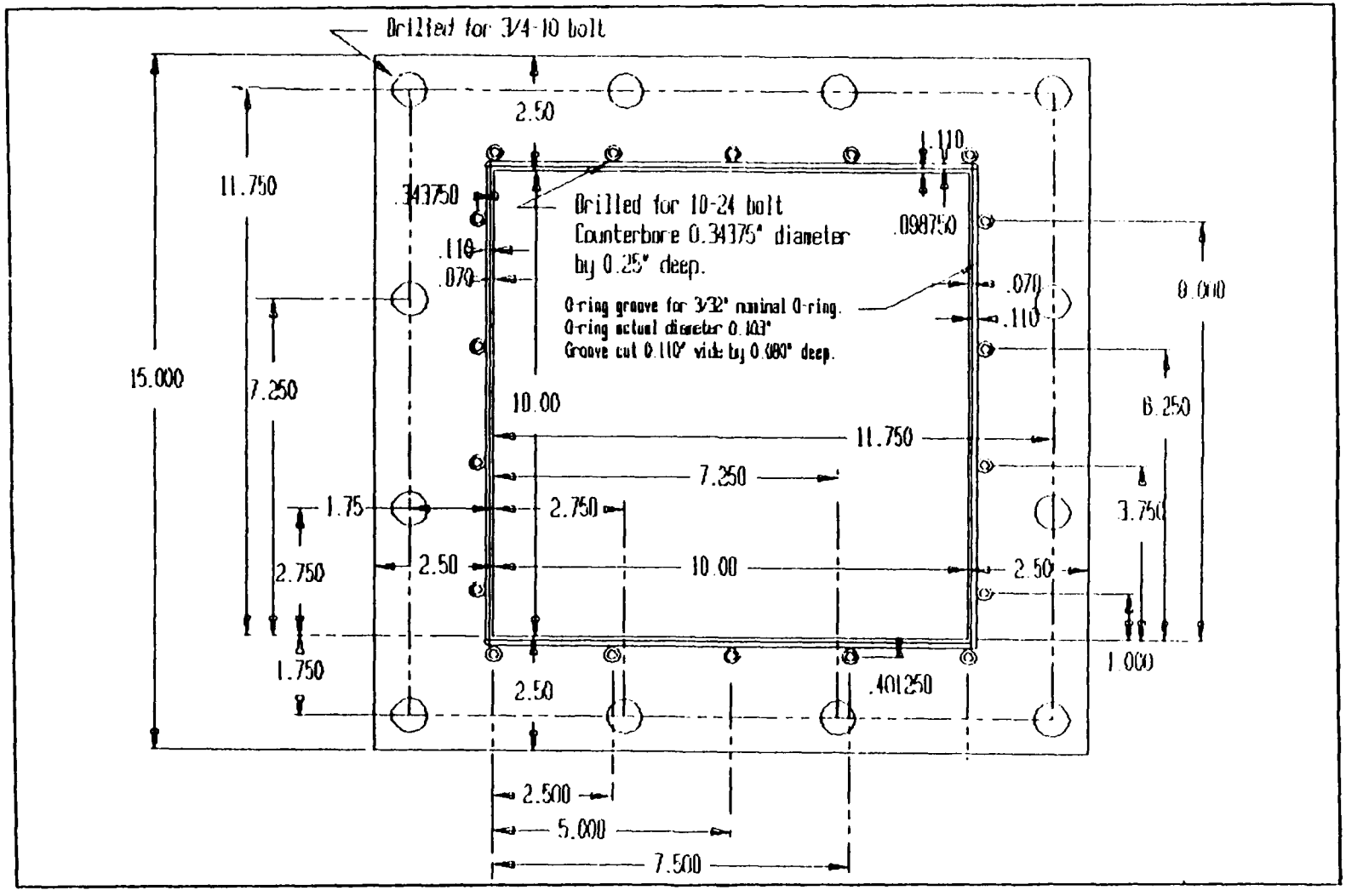

Figure 22. Front View, Test Section Flange, with Dimensions

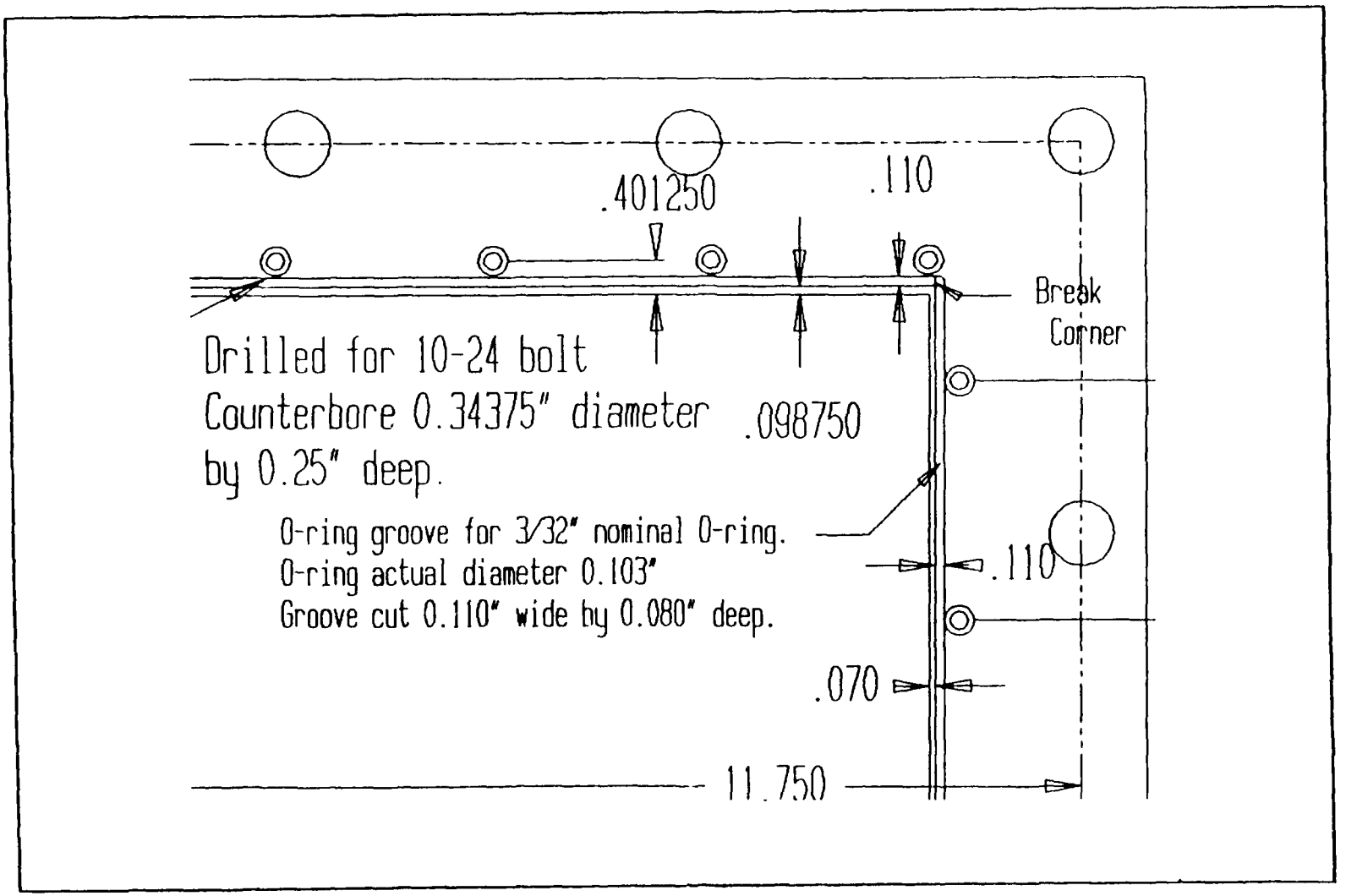

Figure 23. Front View, Details of Test Section Flange

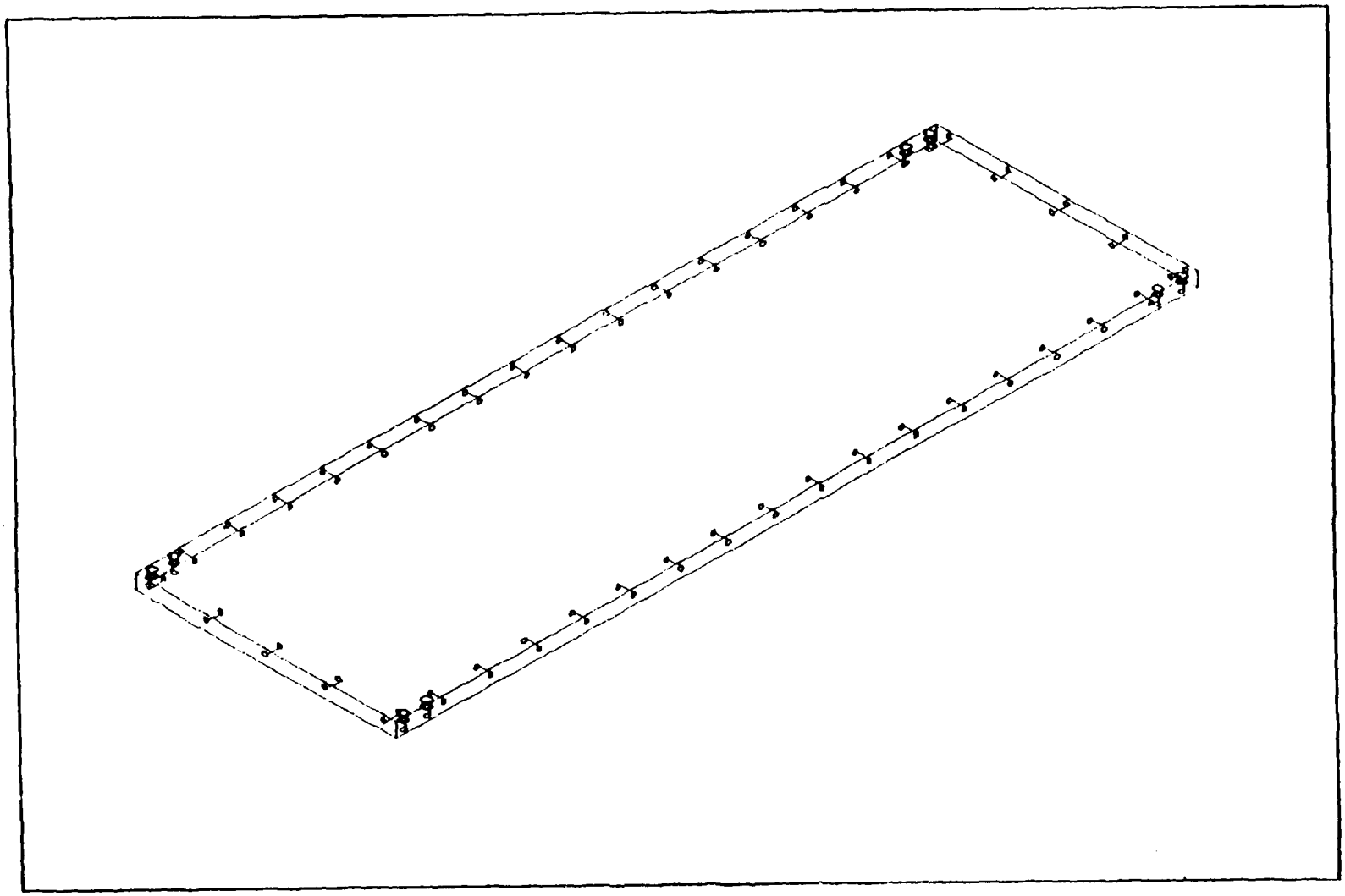

Figure 24. Isometric View, Test Section Ceiling/Floor

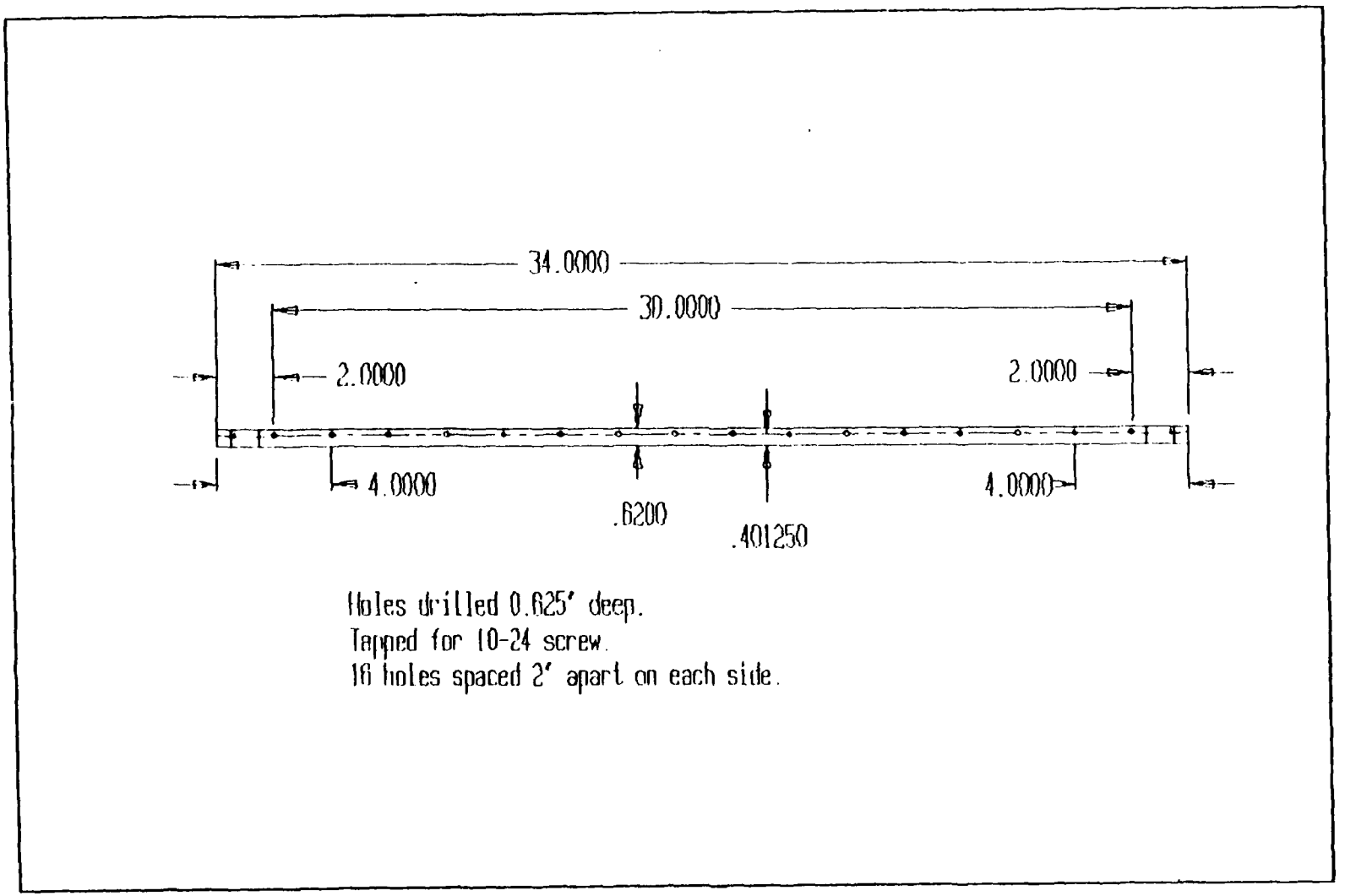

Figure 25. Side View, Test Section Ceiling/Floor

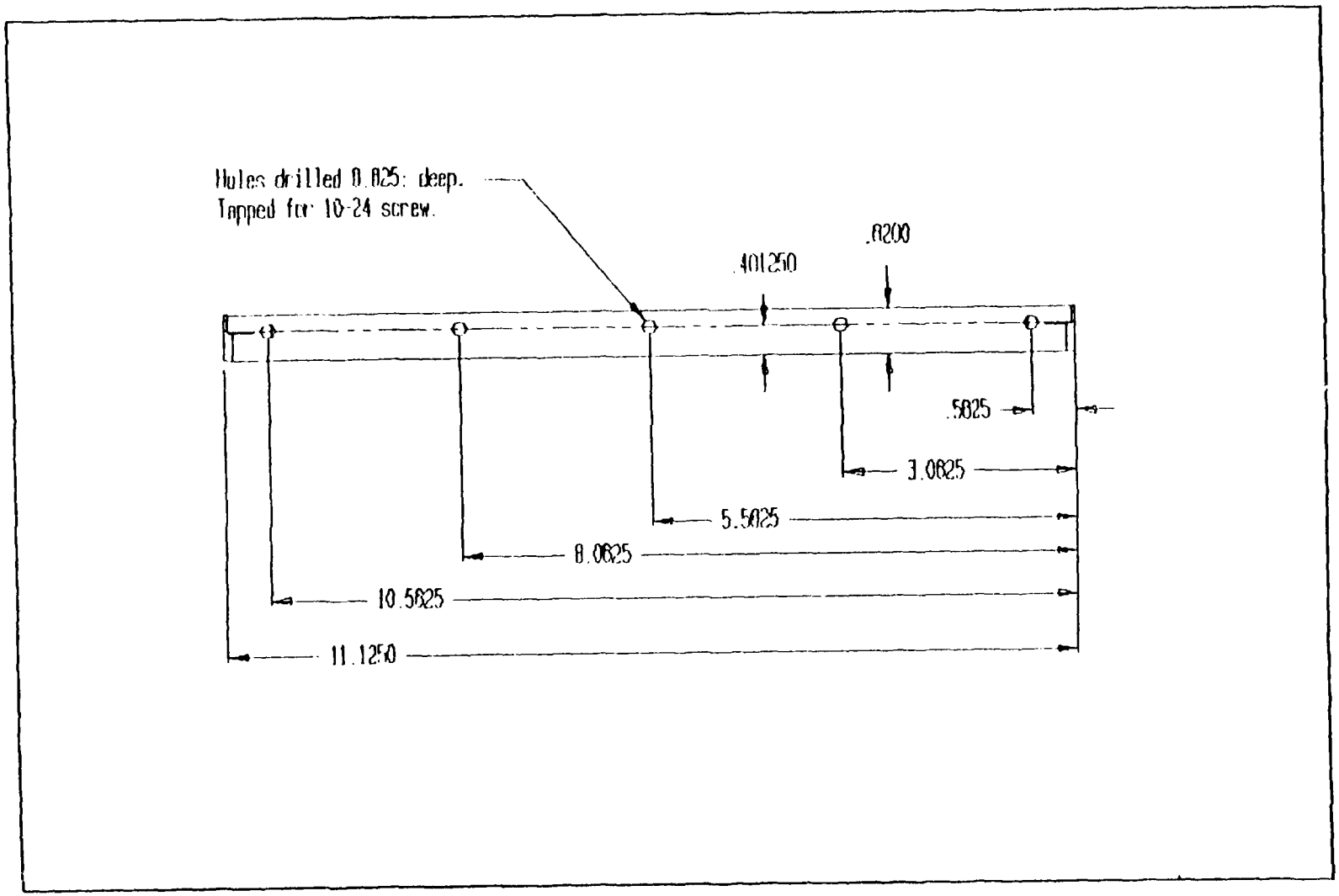

Figure 26. Front View, Test Section Ceiling/Floor

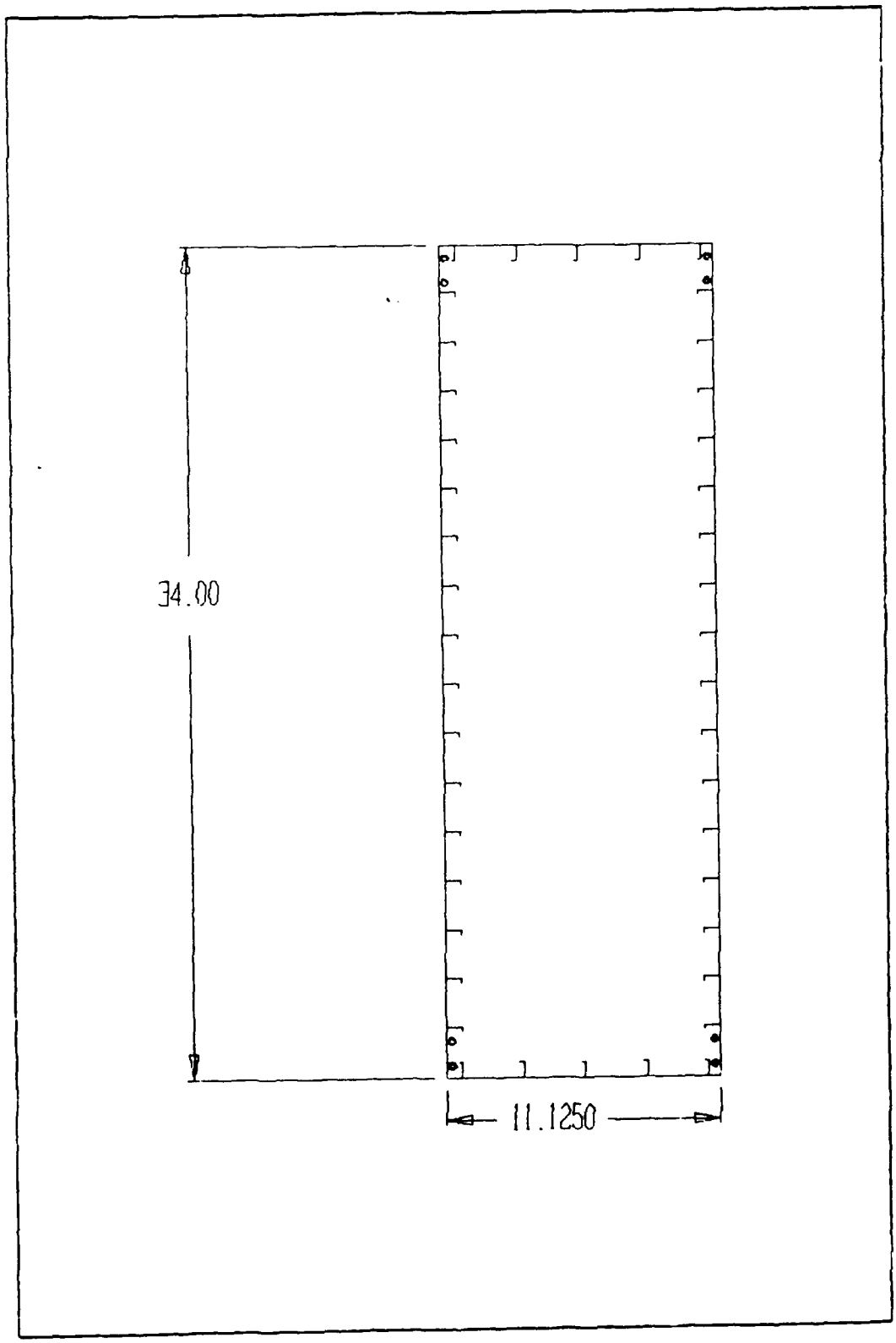

Figure 27. Top View, Test Section Ceiling/Floor

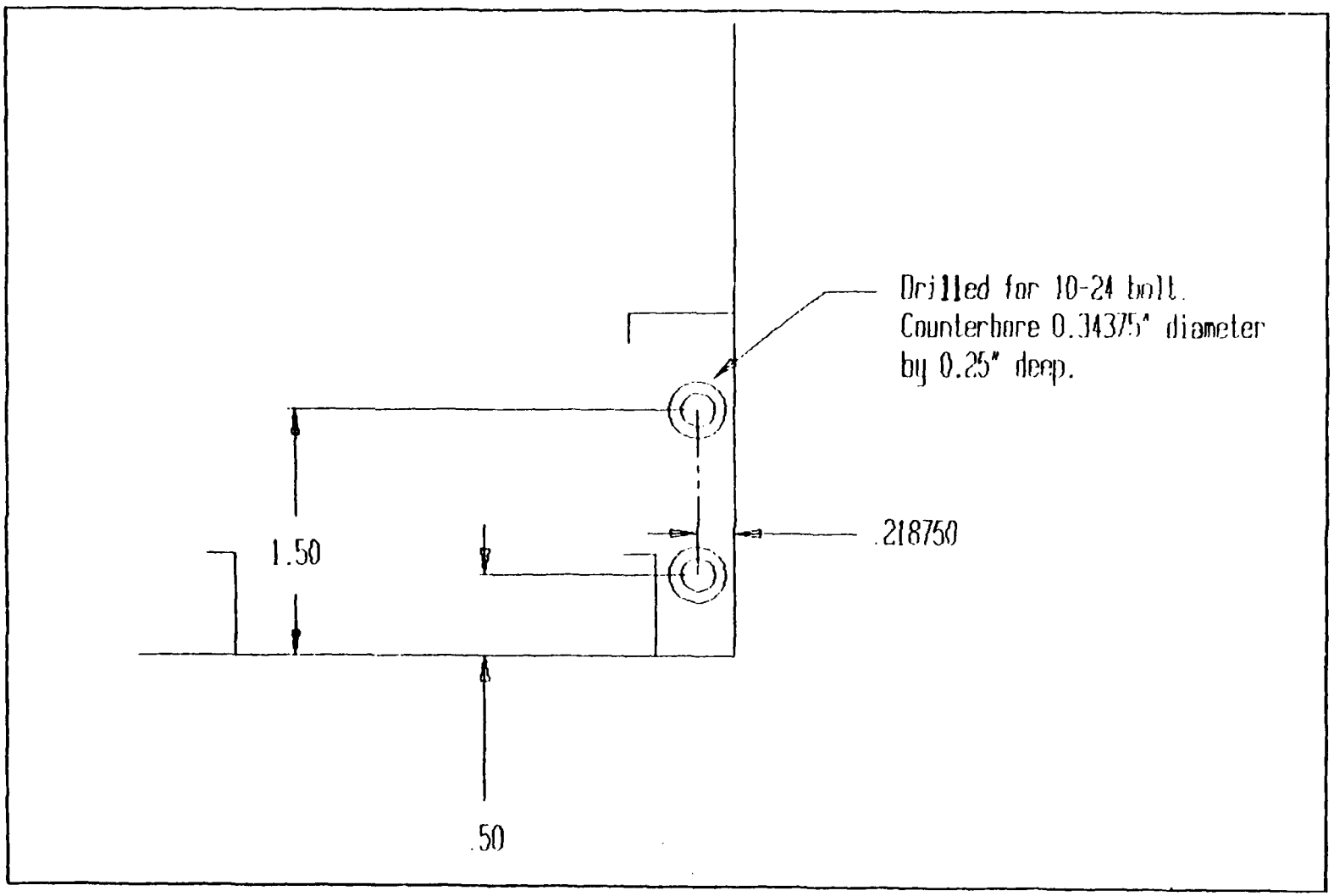

Figure 28. Top View, Detail of Test Section Ceiling/Floor

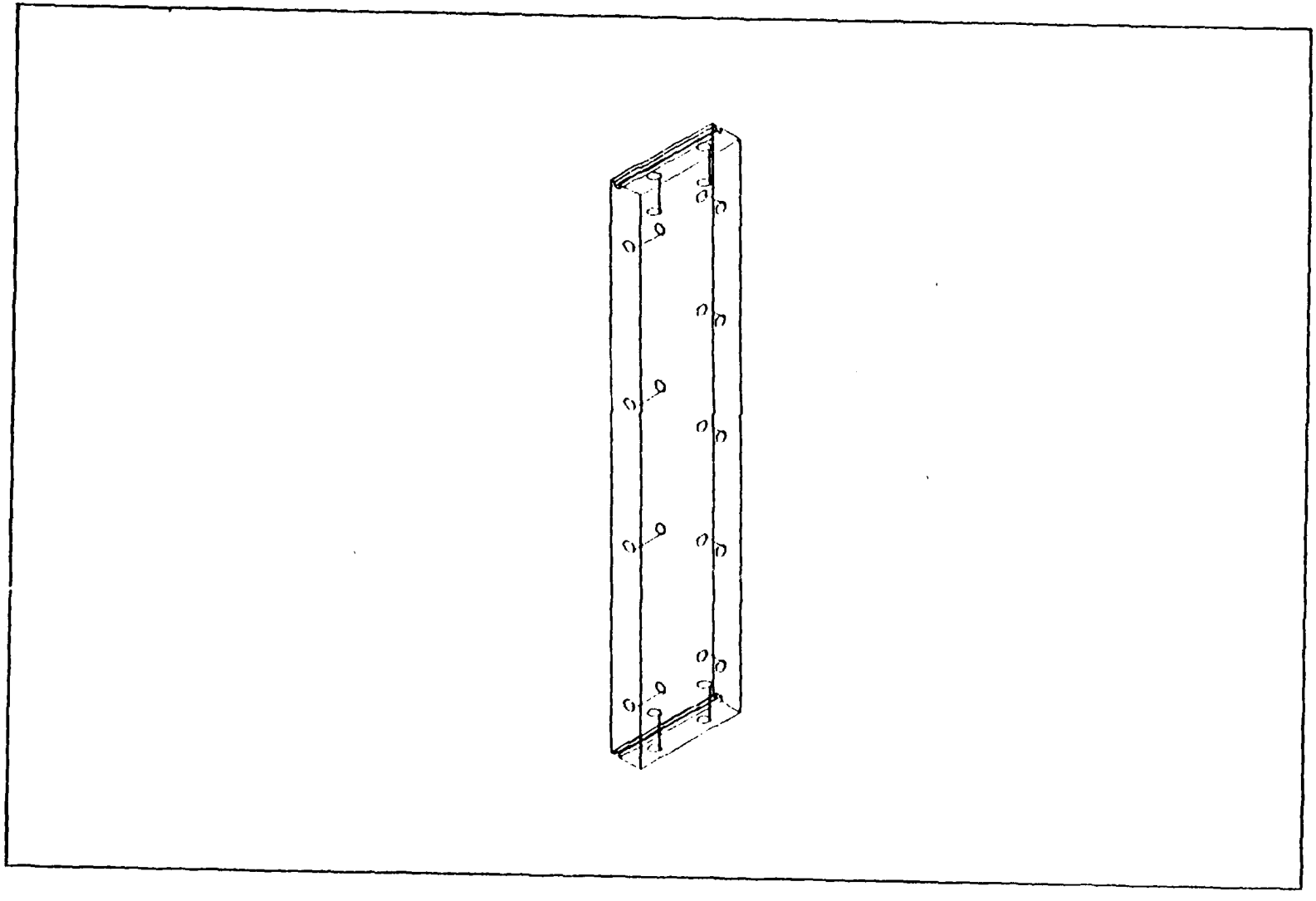

Figure 29. Isometric View, Test Section Corner Brace

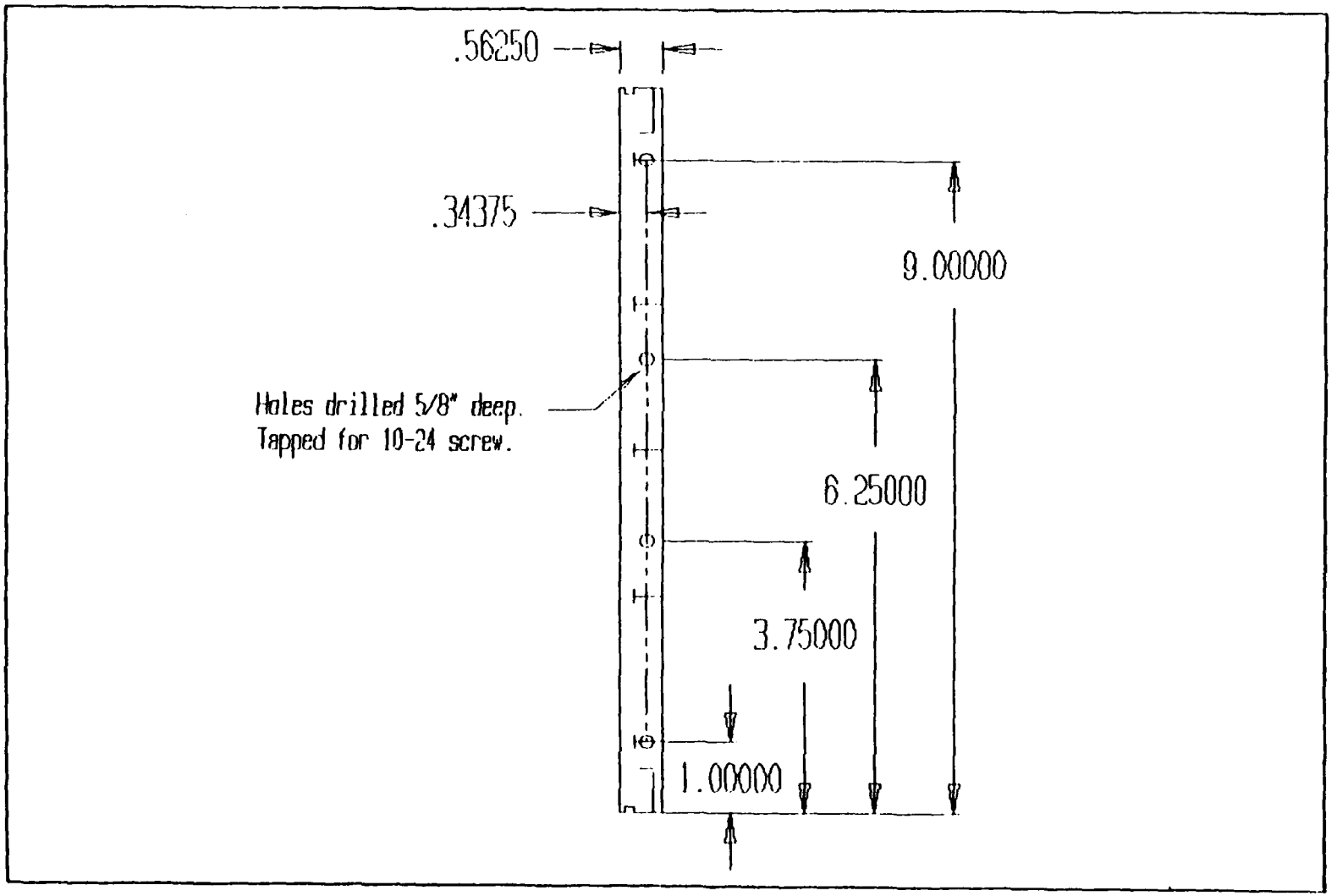

Figure 30. Front View, Test Section Corner Brace

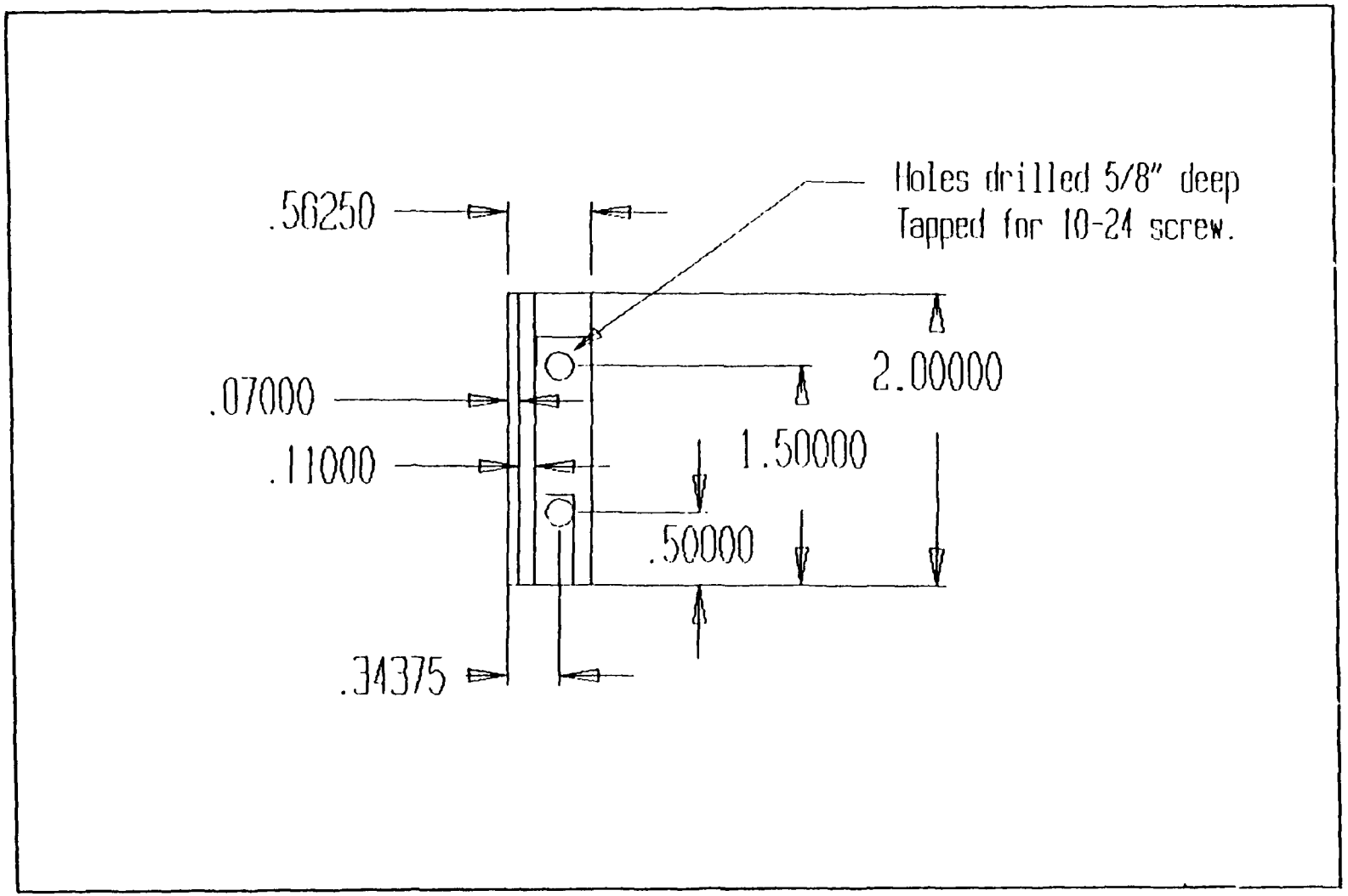

Figure 31. Top View, Test Section Corner Brace

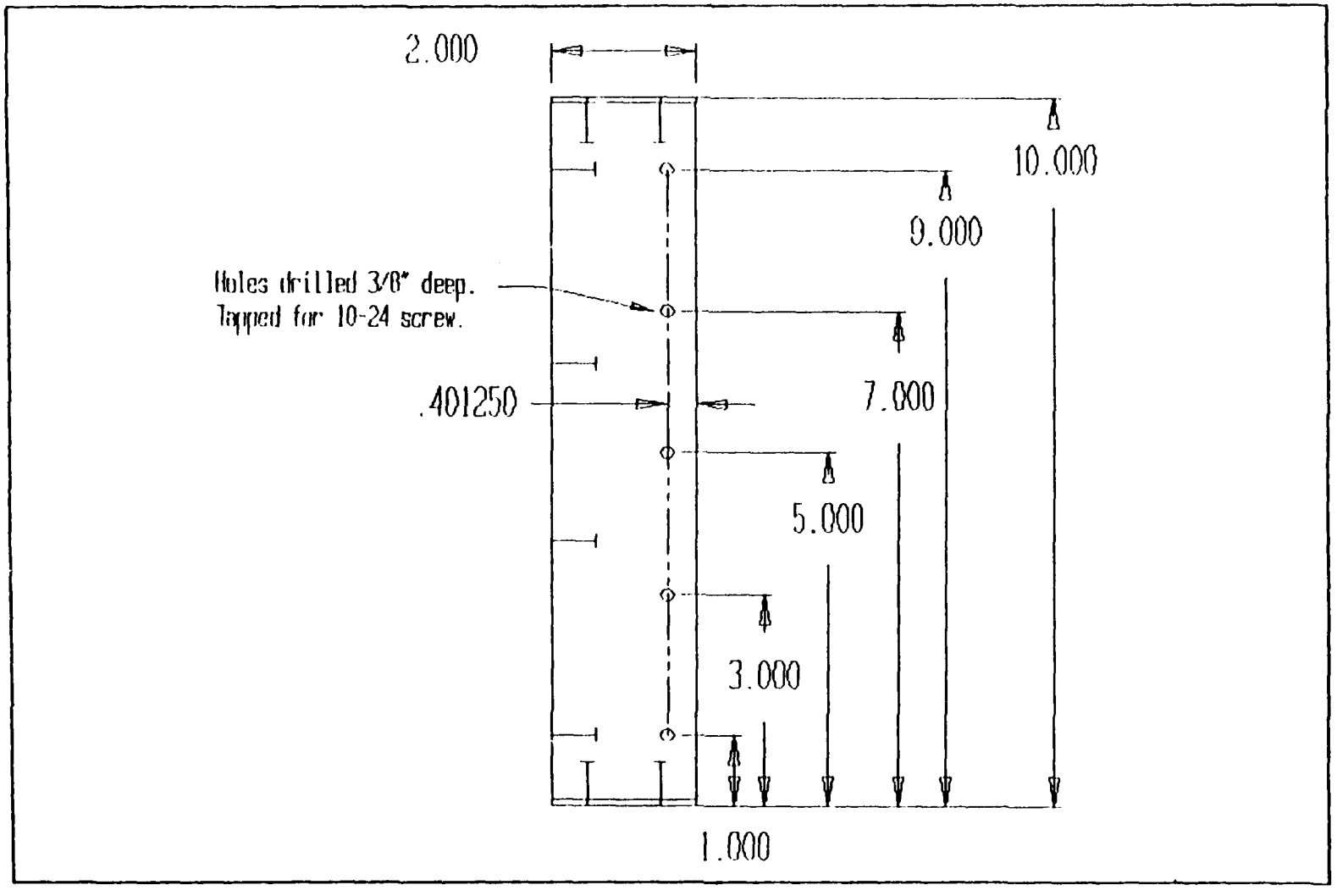

Figure 32. Side View, Test Section Corner Brace

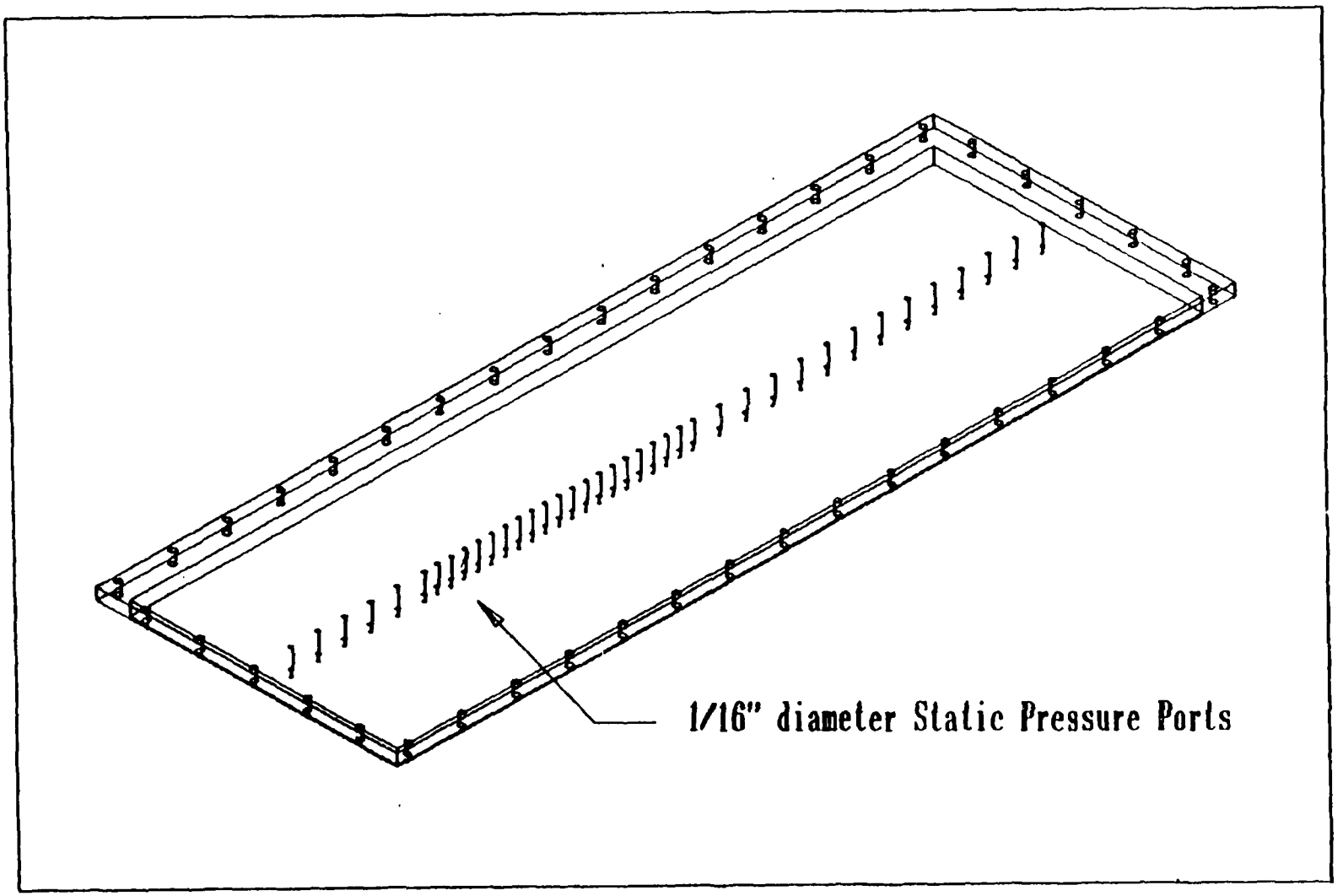

Figure 33. Isometric View, Test Section Acrylic Window

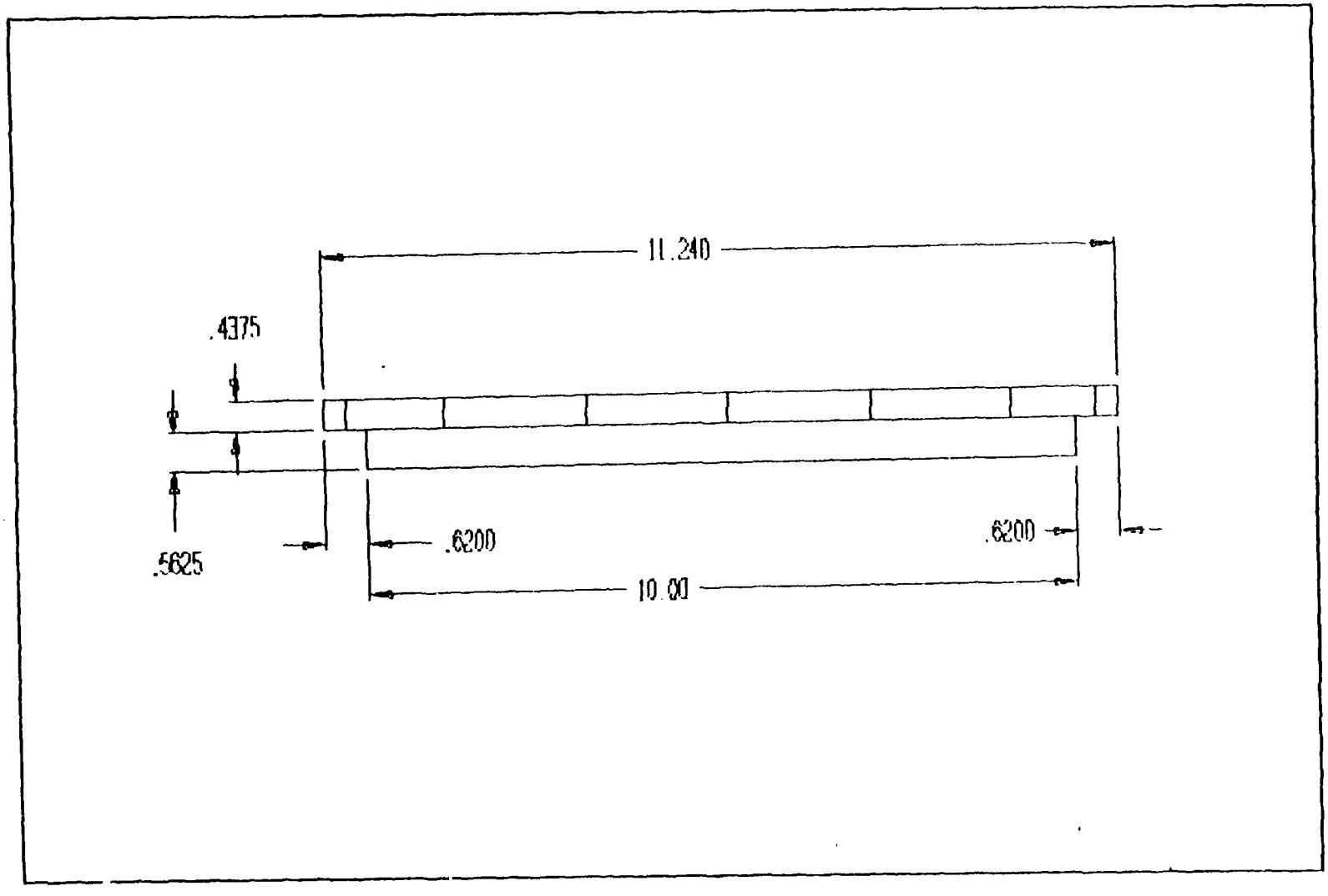

Figure 34. Front View, Test Section Acrylic Window

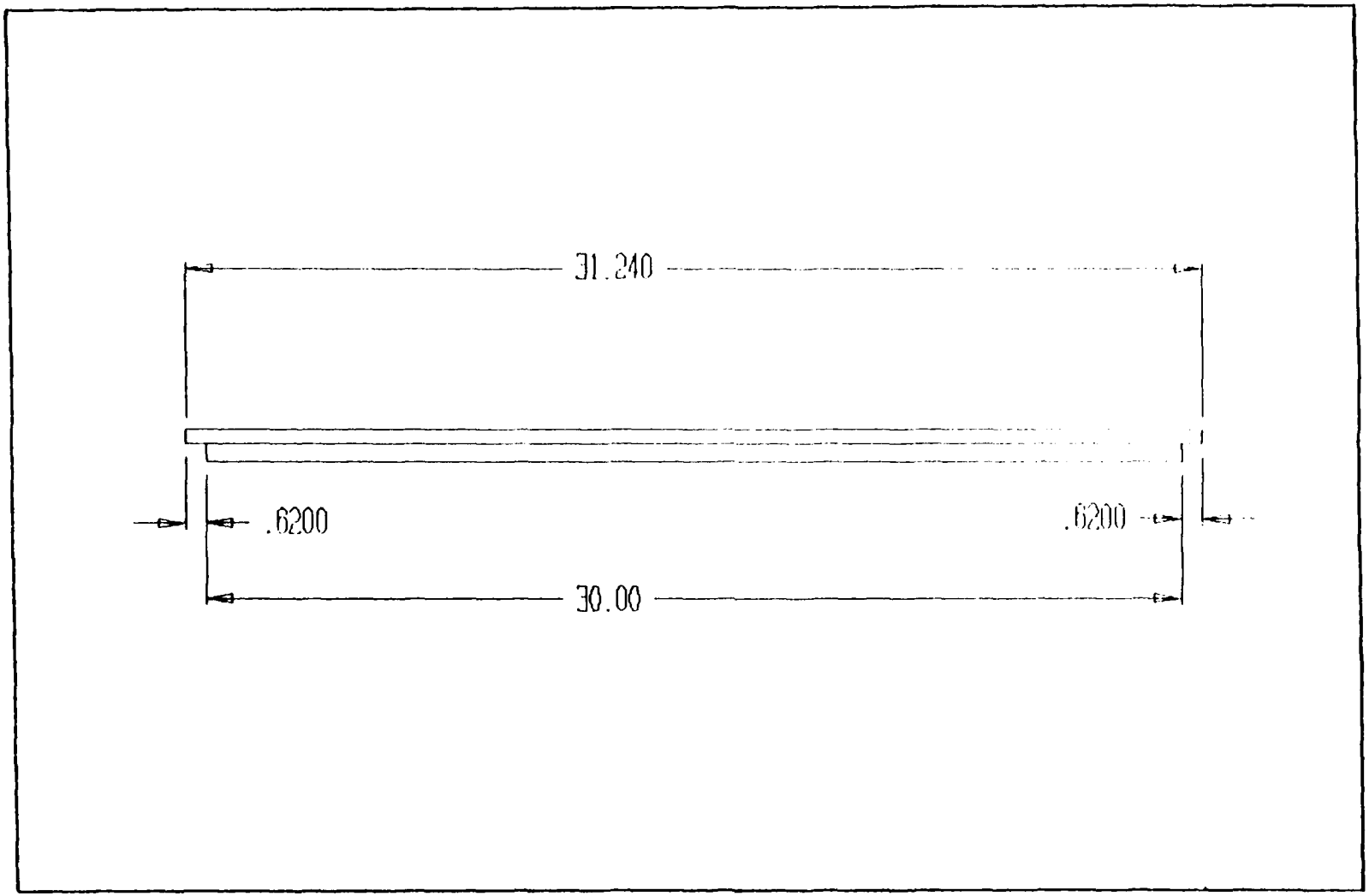

Figure 35. Side View, Test Section Acrylic Window

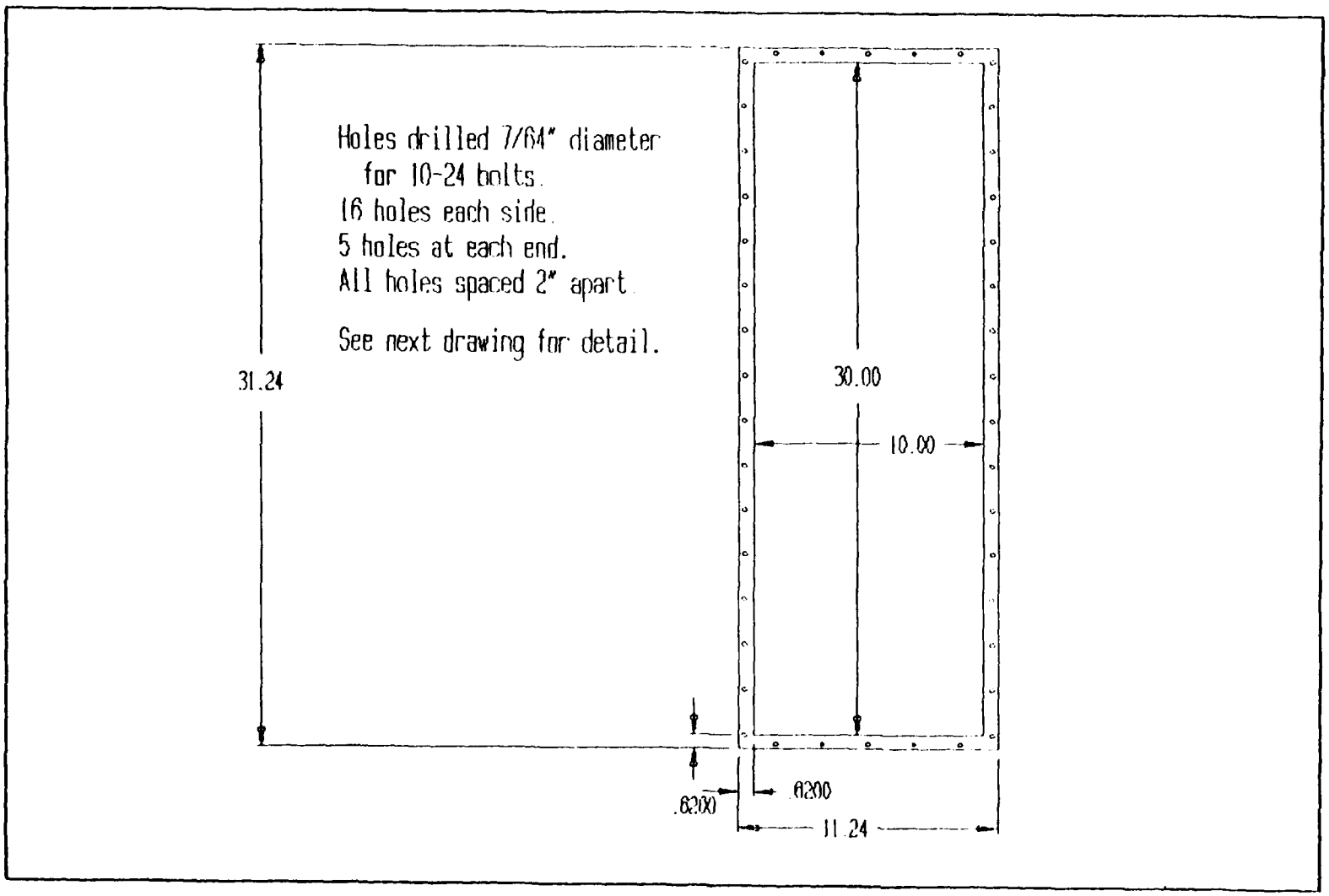

Figure 36. Top View, Test Section Acrylic Window

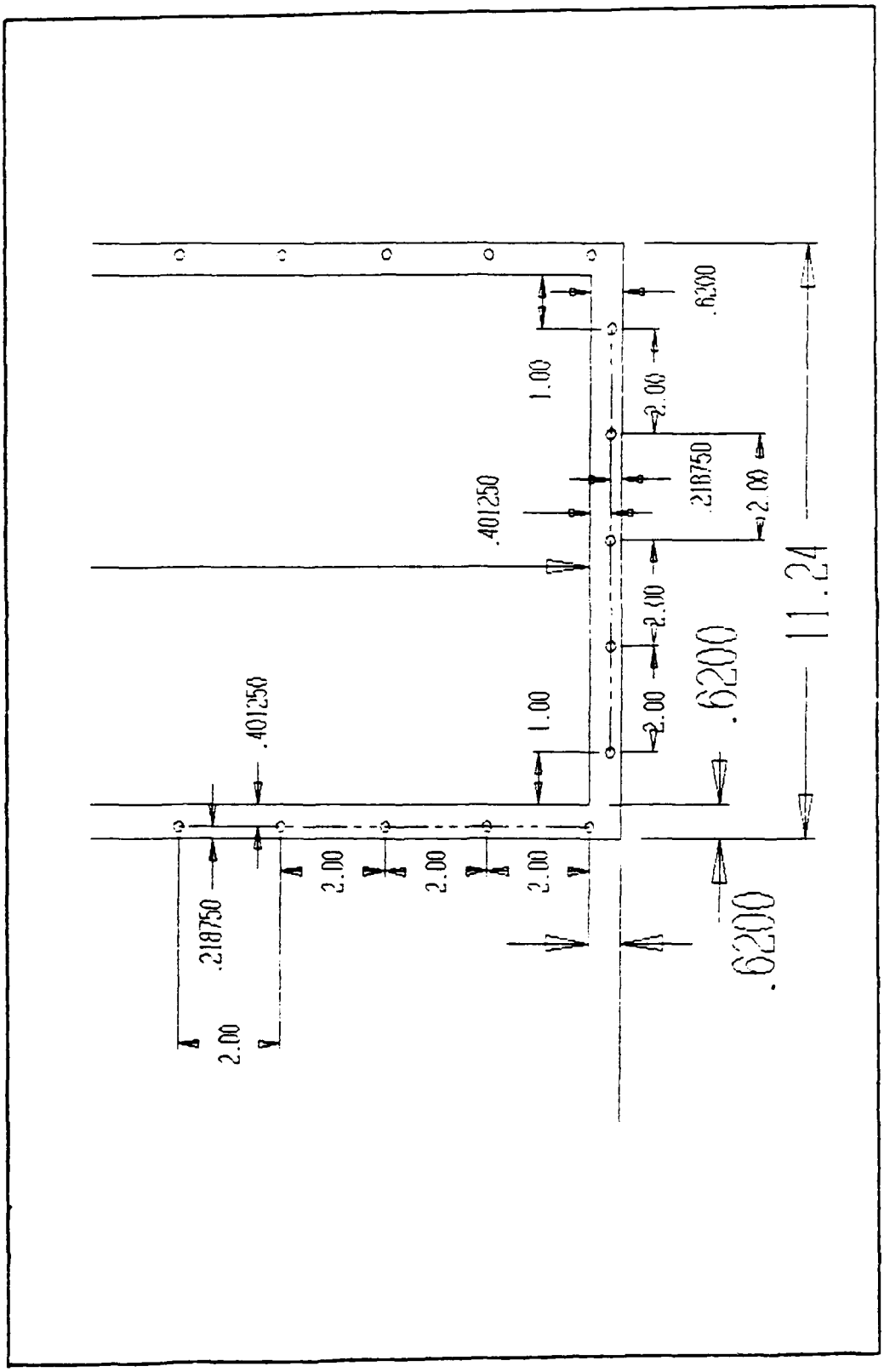

Figure 37. Top View, Detail of Acrylic Window

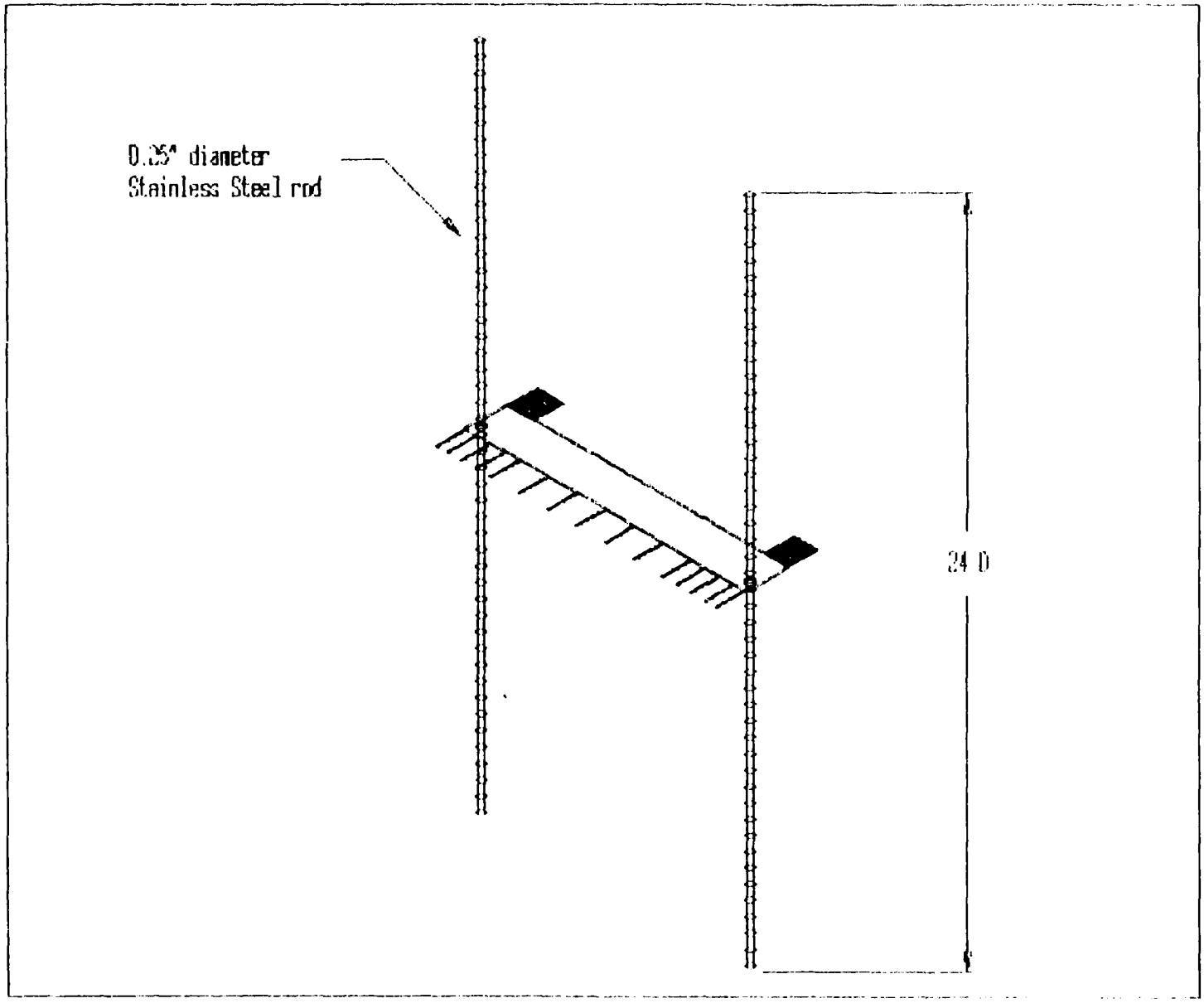

Figure 38. Isometric View, Pitot Tube Rake

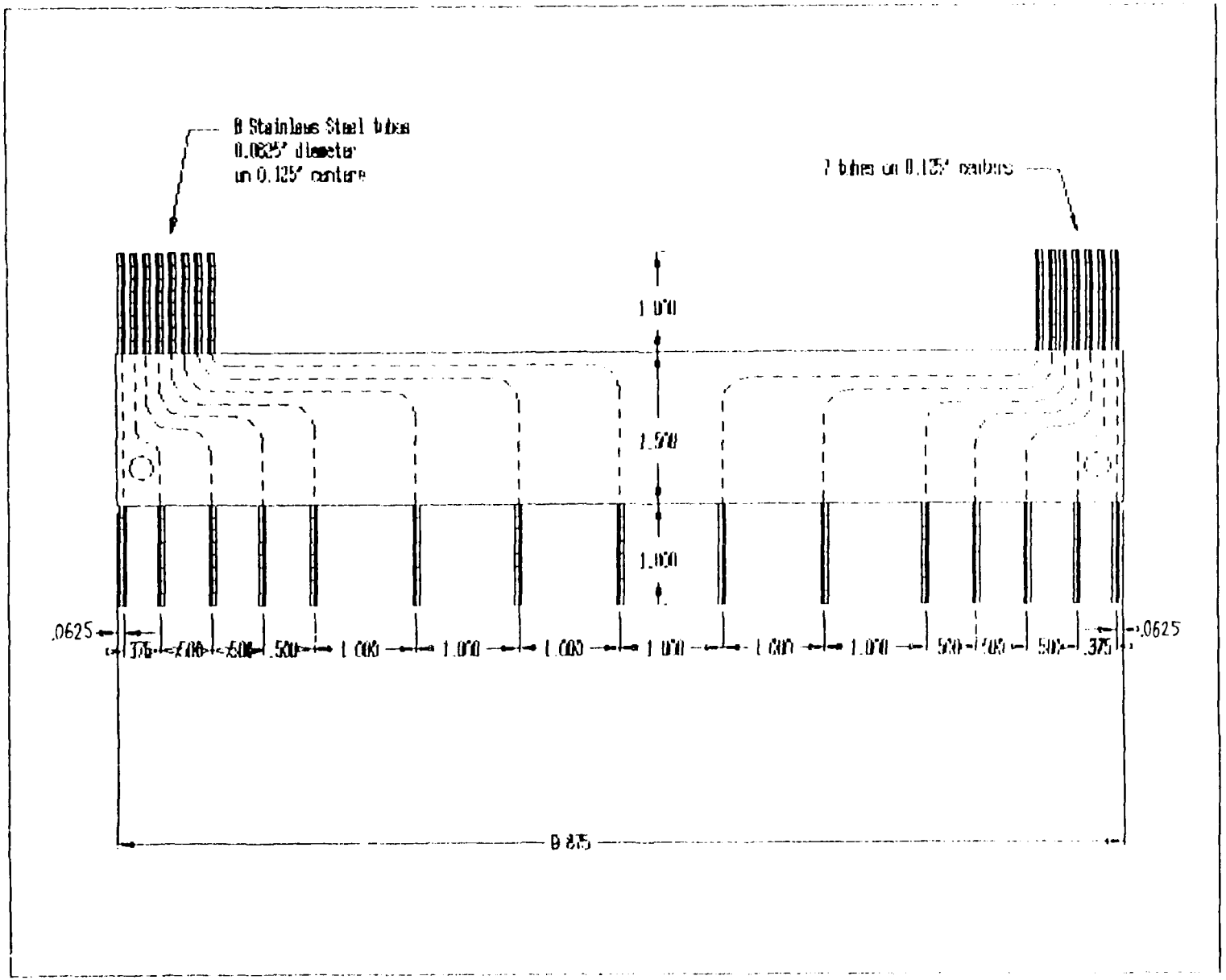

Figure 39. Top View, Pitot Tube Rake

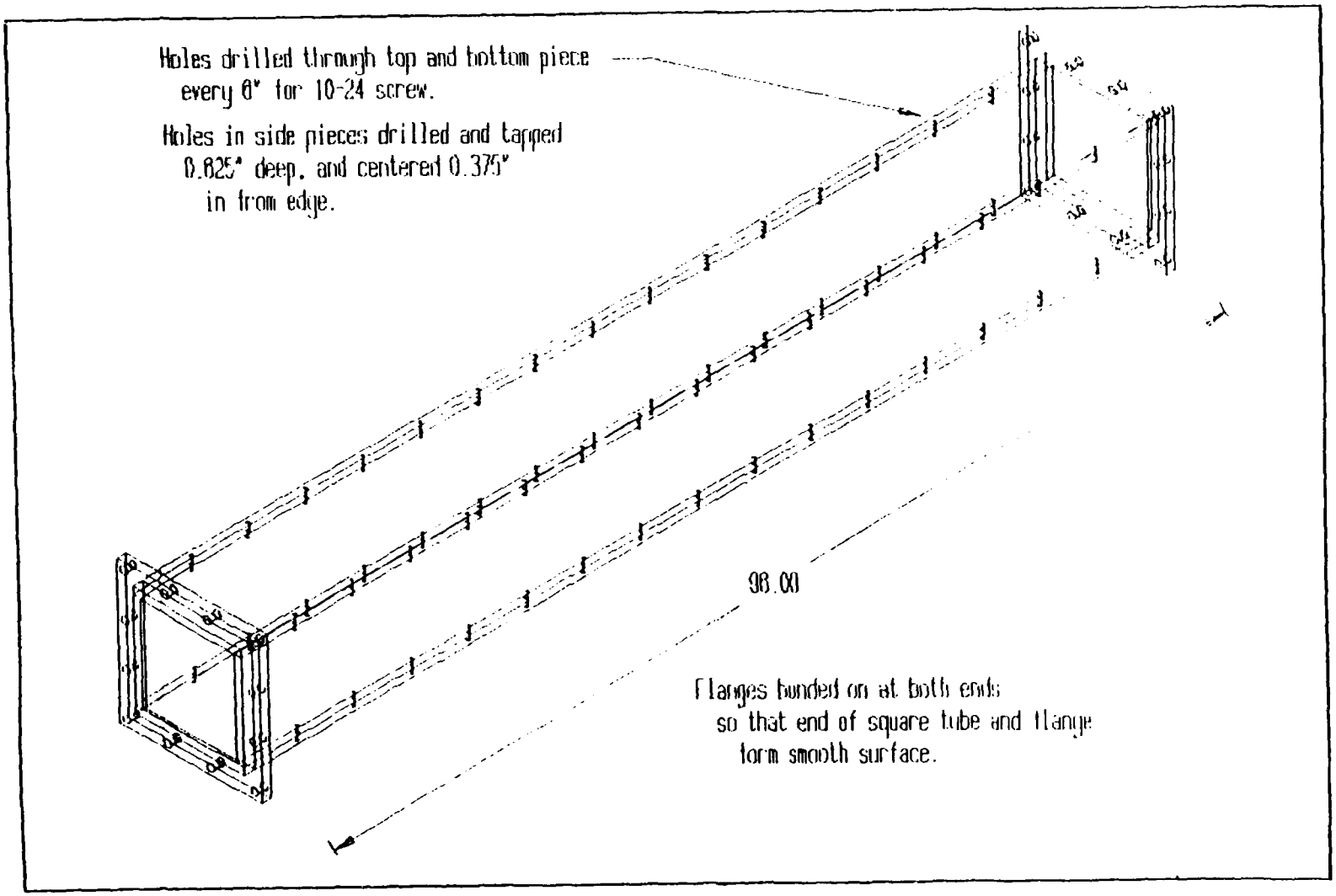

Figure 40. Isometric View, Downstream Square Duct

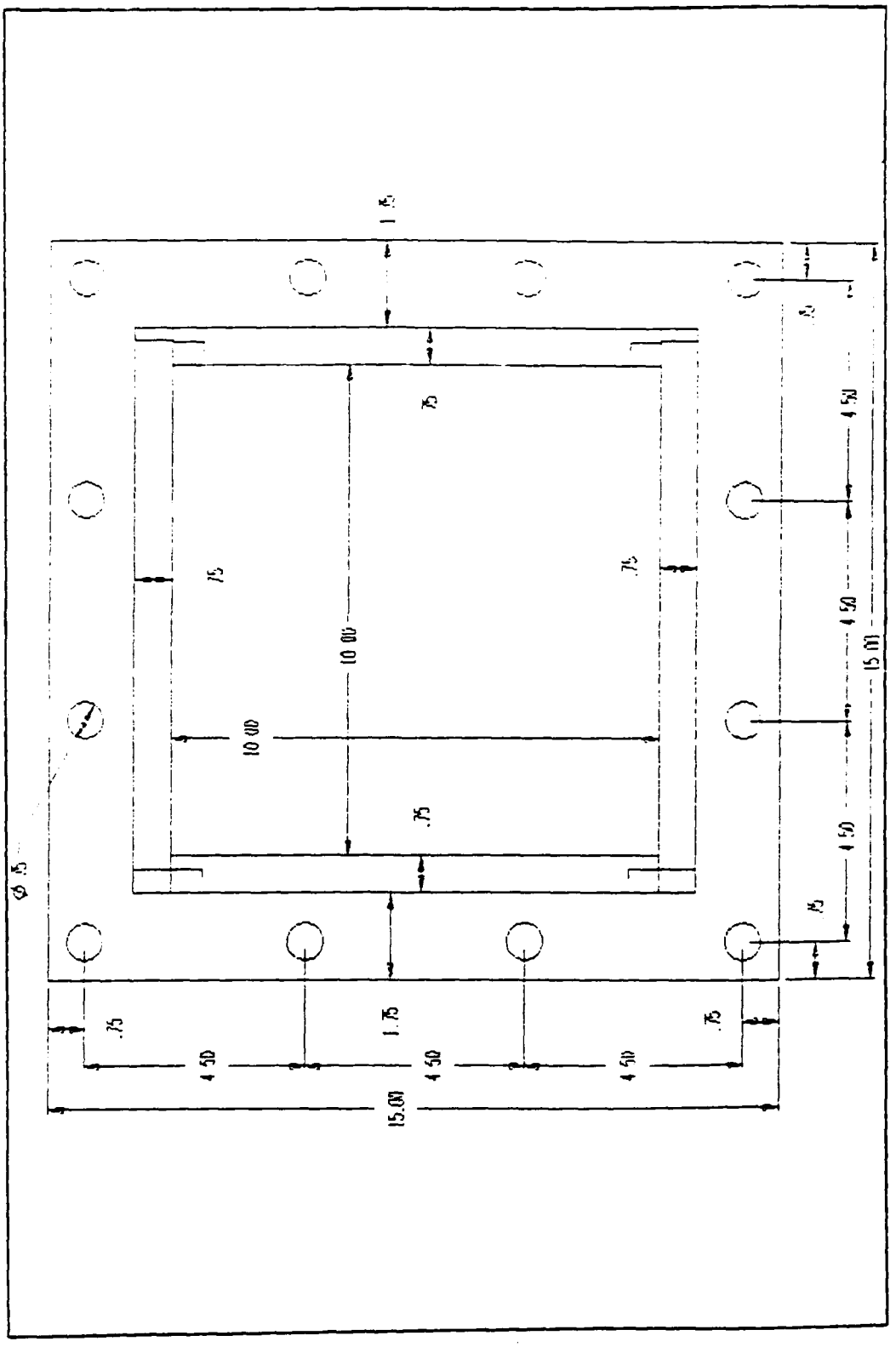

Figure 41. Front View, Downstream Square Duct Flange

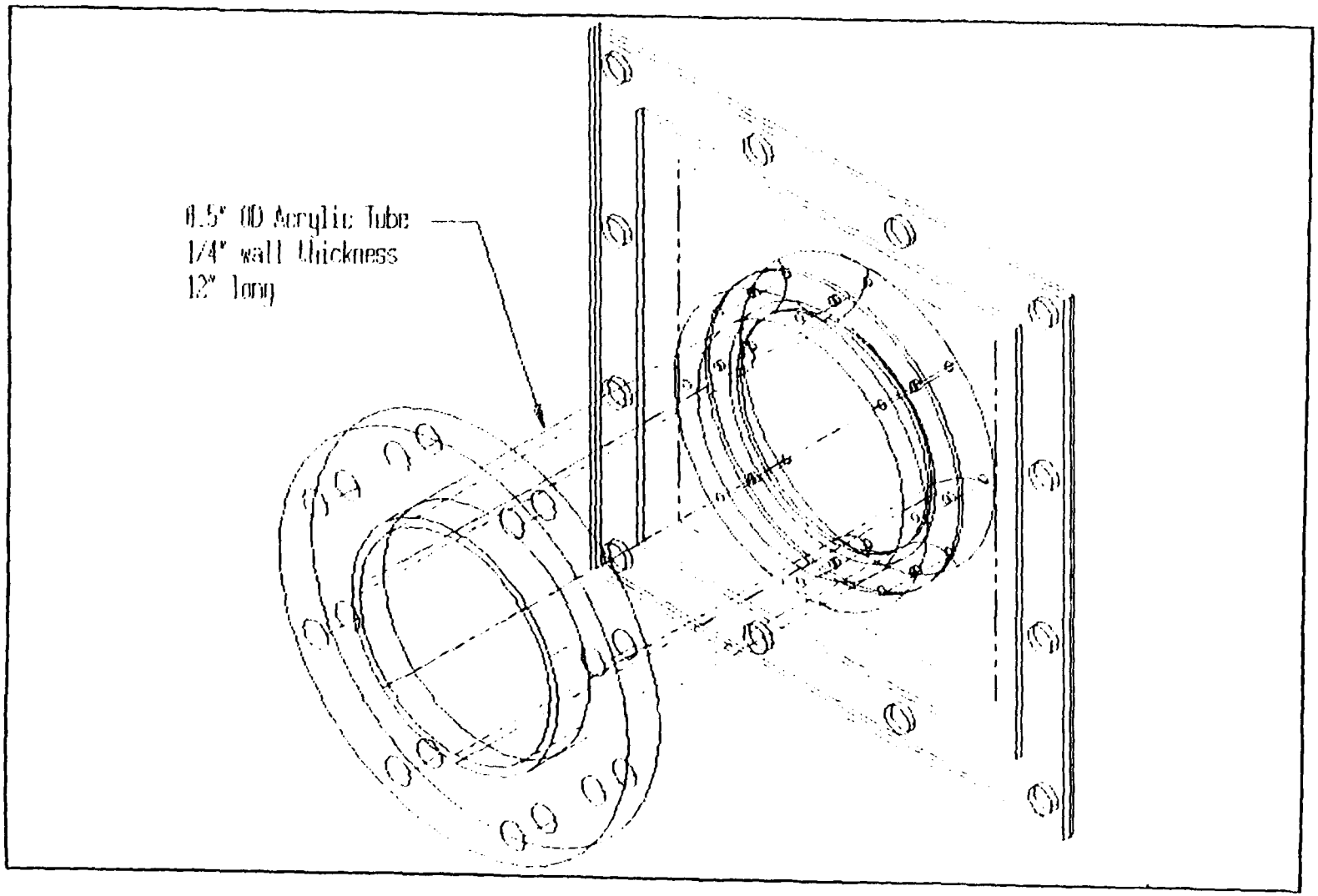

Figure 42. Isometric View, Adapter Assembly

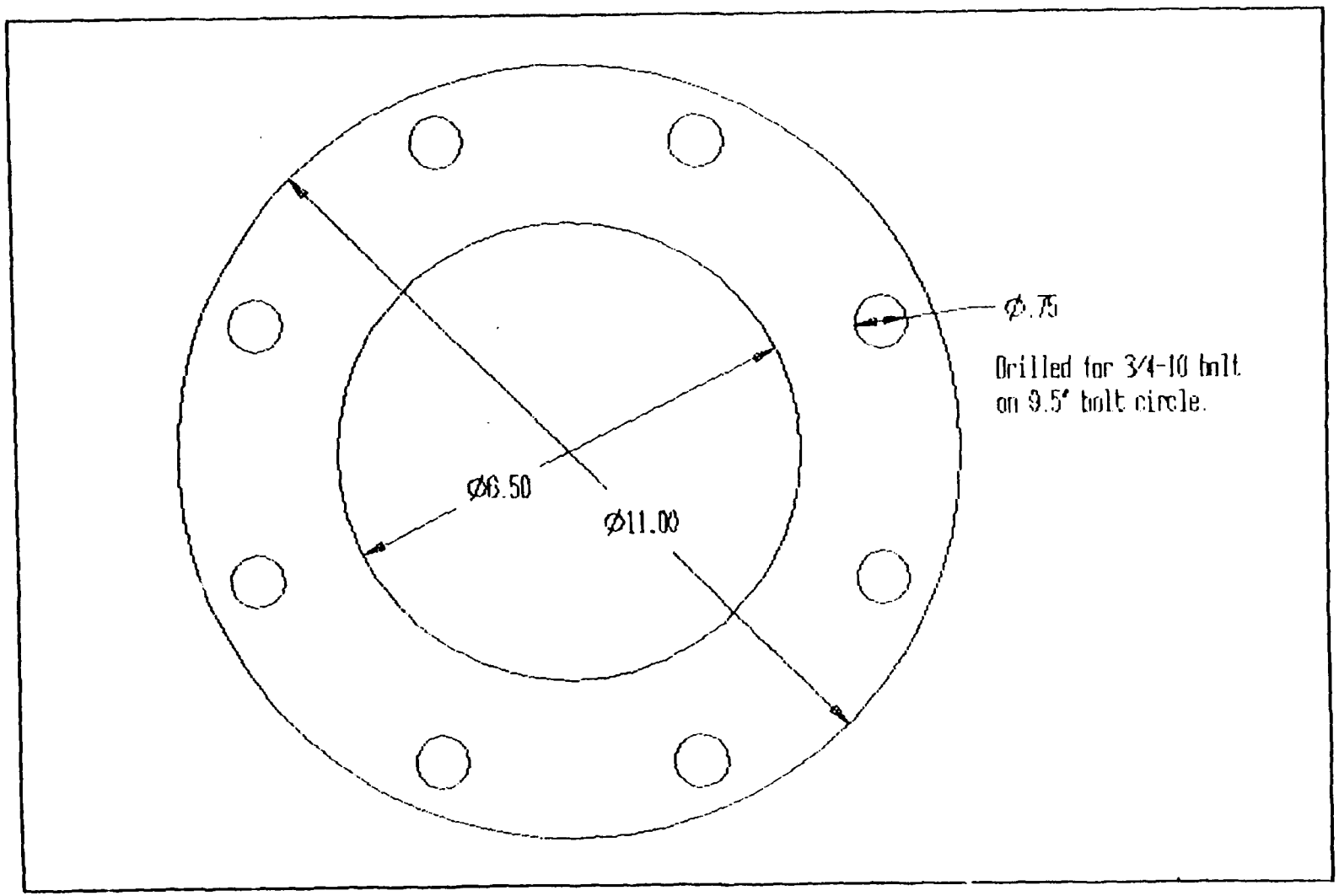

Figure 43. Front View, Adapter Large Round Flange

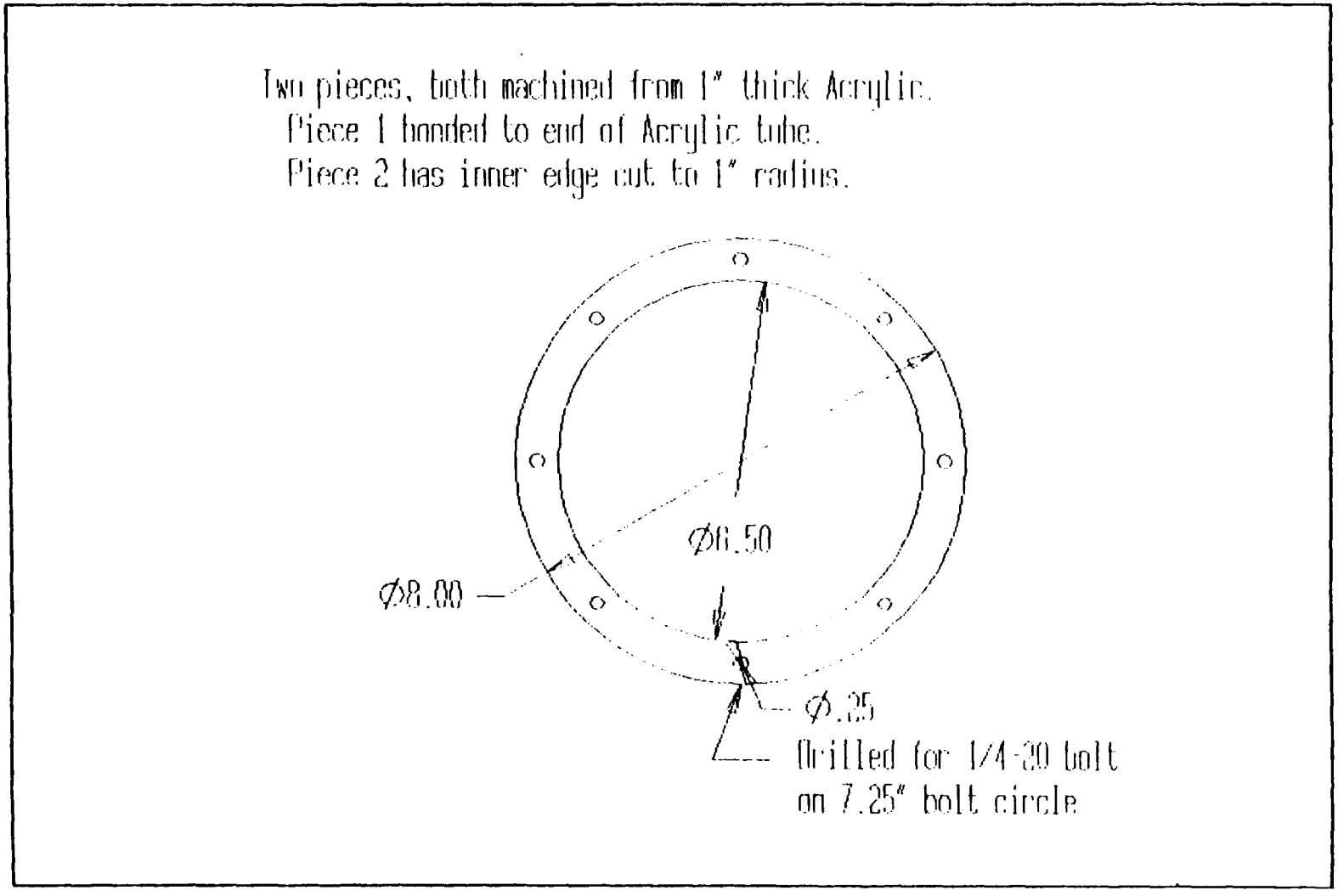

Figure 44. Front View, Adapter Small Round Flange

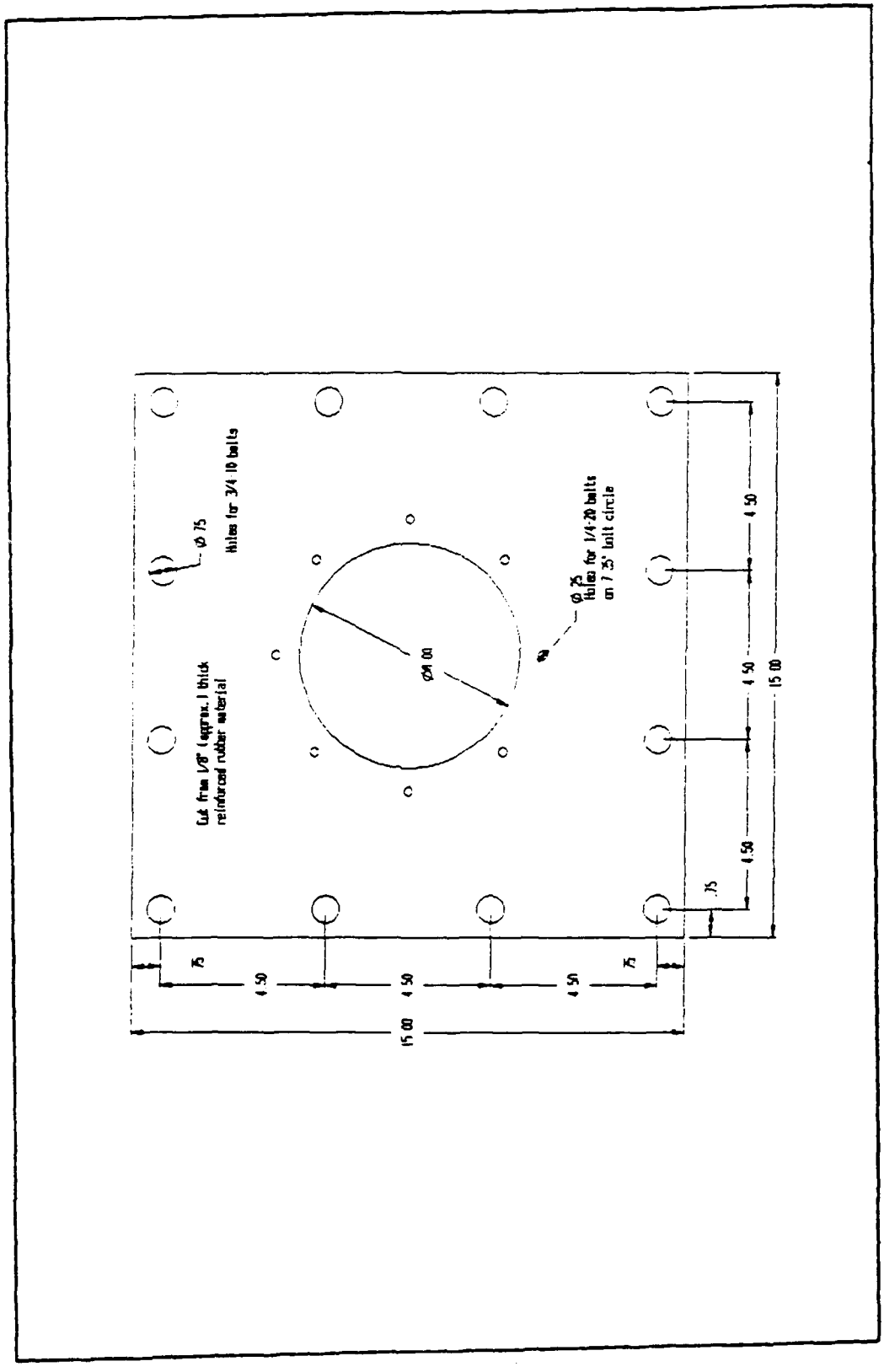

Figure 45. Front View, Adapter Reinforced Rubber Diaphragm

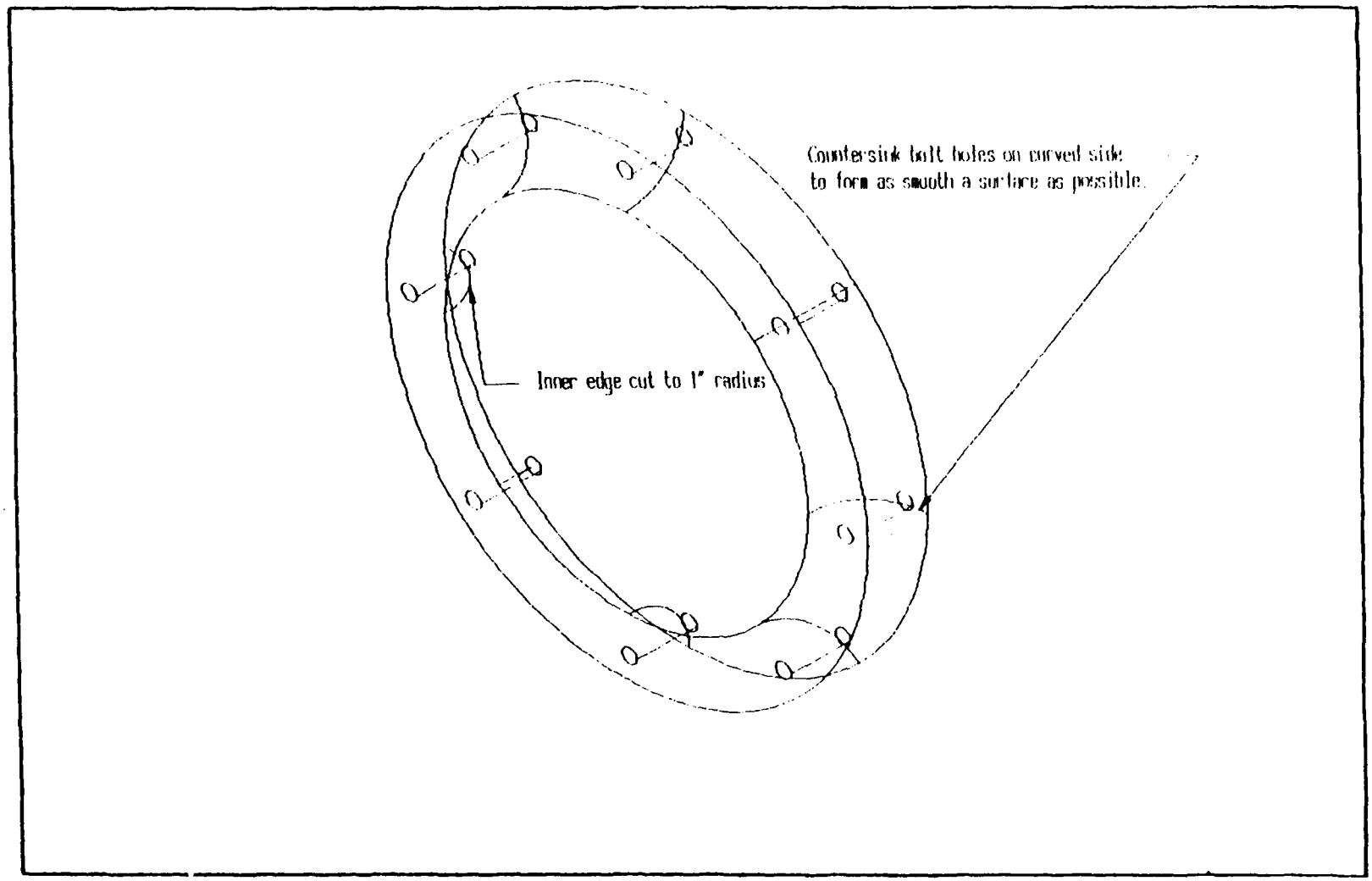

Figure 46. Isometric View, Adapter Round Diaphragm Clamp

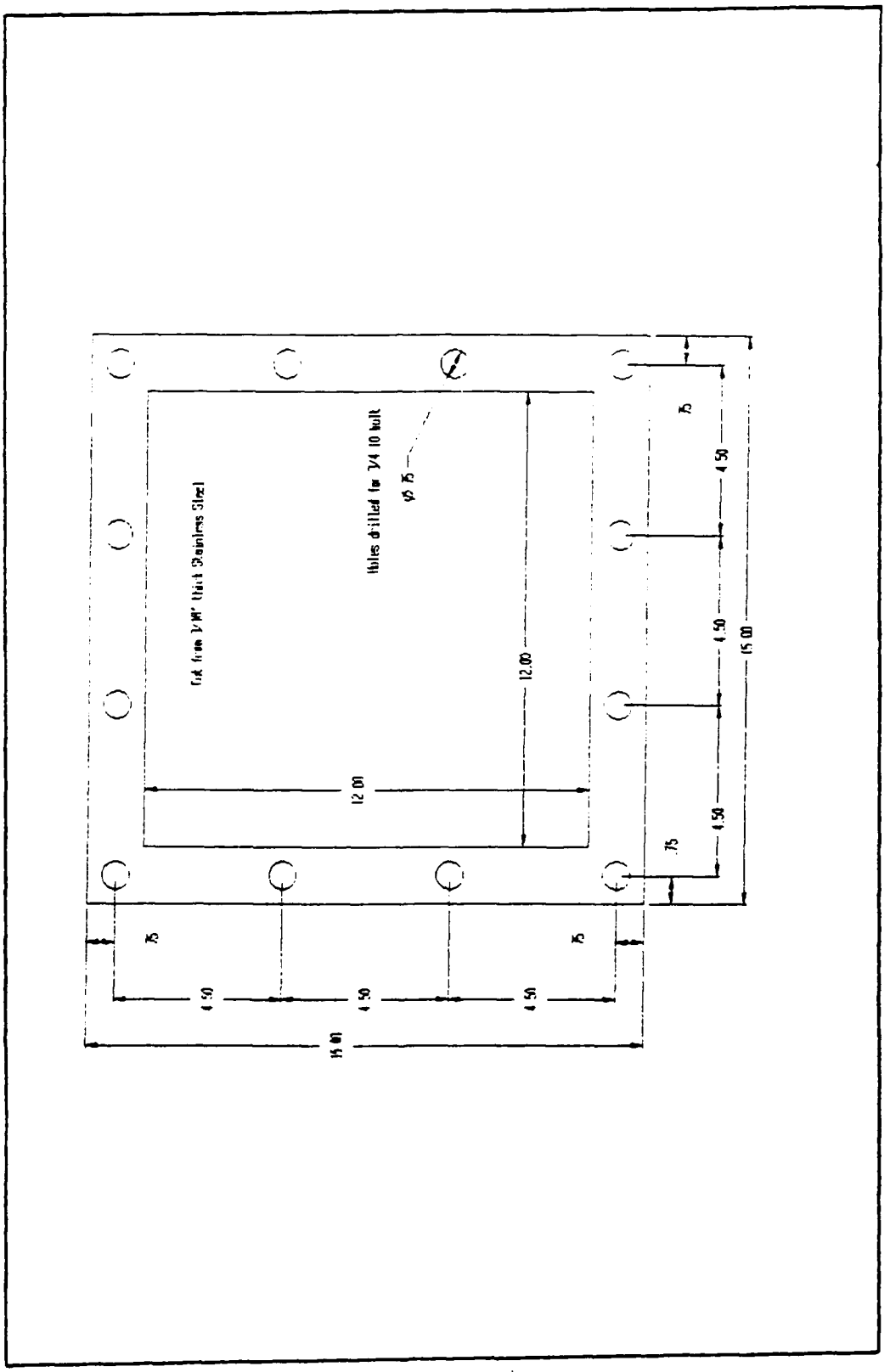

Figure 47. Front View, Adapter Square Diaphragm Clamp

Appendix B - FORTRAN Program for Calculation of Velocity Field Around Sphere in Rectangular Tunnel

```
C*************************************************************
C
C Calculate Velocity at points around a Sphere
C   in a Rectangular Tunnel, Velocity due to:
C     -Uniform Stream
C     -Doublet Potential Flow (Karamcheti, p. 339-340)
C     -Doublet Images (Pope, p. 348)
C     -Sources and Sinks on Centerline (Karamcheti, p. 322)
C INPUT:  N  size of doublet image array NxN
C   N=1 corresponds to infinite field (no tunnel effect)
C         B    Tunnel width [ft]
C         H    Tunnel height [ft]
C         D    Diameter of sphere [ft]
C         U    Free stream velocity [ft/sec]
C         P    number of points
C         X(1...p), Y(1...p),Z(1...p) coordinates of points
C         mu   Strength of Doublet
C         xsrc Location of Sources and Sinks
C         qsrc Strength of Sources and Sinks
C*************************************************************

      integer P
      real mu
      parameter( pi= 3.141592654 )
      dimension xd(201),yd(201),zd(201)
      dimension x(2000),y(2000),z(2000),Vx(2000),Vy(2000)
      dimension Vz(2000), xsrc(100),qsrc(100)
      character*20 infiln,outfil
      logical dblt,src

      write(*,*) ' Enter Input File Name'
      read(*,6) infiln
 6    format(A20)
      write(*,*) ' Enter Output File Name'
      read(*,6) outfil
      print*,' Use doublet at x=0? [ .T. or .F. ]'
      read*,dblt
      print*,' Enter Number of Sources and Sinks'
      read*,nsrc
      if (nsrc .gt. 0) then
       print*,'? Location [inch], Negative is Upstream'
       print*,' '
       print*,'? Strength [Multiple of Doublet Strength]'
       print*,'   Positive for Source, Negative for Sink'
       endif
      do 110 i=1,nsrc
```

```
            print*,' Enter Location',i
            read*,xsrc(i)
            xsrc(i) = xsrc(i)/12.0
            print*,' Enter Strength',i
            read*,qsrc(i)
 110        continue
      open(7,file=infiln,status='old')
      read(7,1) N,B,H,D,U
  1   format(I3,4(1x,F10.6))

C     Read coordinates of points in tunnel
      read(7,*) P
      read(7,2) (x(i),y(i),z(i),i=1,p)
      close(7)
      print*,'Images:',N,'Width,Height:',B,H,'Diameter:',
     +         D,'Uinf:',U
  2   format(3F11.6)

C     Generate Grid points for Doublet and Doublet Images
      open(8,file=outfil,status='new')
      write(8,1) N,B,H,D,U
      do 10 i=1,n
            xd(i)= 0
            yd(i)= B* (i-int(n/2)-1)
            zd(i)= H* (i-int(n/2)-1)
  10  continue

      mu= U*2*pi*(D/2)**3
      write(*,*) '"mu:"',mu
      write(*,*) '"p:"',p

      write(8,*) '"Velocity [ft/sec] at P(x,y,z)"'
      write(8,3) '"P"','"x"','"y"','"z"','"Vx"','"Vy"',
     +           '"Vz"','"V"'
  3   format(A4,7(A10))
C     Calculate Velocity at the p points
      do 20 i=1,p
         Vx(i)= U
         Vy(i)= 0
         Vz(i)= 0
         do 30 k=1,N
           do 40 j=1,N
             rx= x(i)
             ry= y(i) - yd(j)
             rz= z(i) - zd(k)
             rho2= ry**2 + rz**2
             R= sqrt(rx**2 + ry**2 + rz**2)
             if ( (R.lt.1.0e-03) .or.
     +          ( (rx-xsrc(m))**2+rho2).lt.1.0e-03 ) then
               Vx(i)= 0
               Vy(i)= 0
               Vz(i)= 0
```

```
                goto 30
                end if
C             Add Doublet effect for Sphere
                if (dblt) then
                  Vx(i)= Vx(i)+mu*(rho2/2-rx**2)/(2*pi*R**5)
                  Vy(i)= Vy(i)-3*mu*rx*ry/(4*pi*R**5)
                  Vz(i)= Vz(i)-3*mu*rx*rz/(4*pi*R**5)
                  endif
C             Add Sink and Source effects for wake
                do 100 m=1,nsrc
                  qvel= mu*qsrc(m)/(4.0*pi)/
     +                    ( (rx-xsrc(m))**2 + rho2 )**1.5
                  Vx(i)= Vx(i)+ qvel* (rx-xsrc(m))
                  Vy(i)= Vy(i)+ qvel* ry
                  Vz(i)= Vz(i)+ qvel* rz
 100              continue
 40             continue
 30           continue
            V= sqrt(Vx(i)**2 + Vy(i)**2 + Vz(i)**2)
            write(8,4) i,x(i)*12.0,y(i)*12.0,z(i)*12.0,
     +          Vx(i),Vy(i),Vz(i),V
            write(*,5) '+record ',i,' of ',p,'written'
 4          format(I4,7(1x,F10.6))
 5          format(A8,I4,A4,I4,A7)
 20         continue
          close(8)
          stop
          END
```

Appendix C - Acrylic Window Structural Analysis

The material chosen for the side walls of the water tunnel test section is acrylic sheet of nominal one inch thickness. This material is a thermoplastic also known as polymethylmethacrylate or by the trade names lucite and plexiglas. Acrylic has the following physical properties [5] relative to its use in this research facility:

Table 1. Physical Properties of Acrylic Plastic

Tensile Strength	7,000 - 11,000 psi
Compressive Strength	11,000 - 17,000 psi
Young's Modulus	350,000 - 500,000 psi
Specific Gravity	1.17 - 1.20

Poisson's ratio was not reported for this material so a value of 0.3 was assumed. The minimum reported value of 350,000 psi for Young's modulus is used in the following analysis.

Preliminary analysis was performed using formulae for the stress and deflection of a thin plate under a pressure load on one side [32:386,393]. The configuration, loading, and boundary conditions of the acrylic window did not quite fit any of the limited number of cases for which formulas were provided so the NISA II PC [6] finite elements analysis computer program was used to provide a more refined analysis.

Reference 32 provides the following formulae for the case of a uniform thickness plate of aspect ratio three or more under a uniform pressure load on one side. The width of the plate is taken to be the distance between the mounting screw centers. Since the mounting screws are located every two inches around the perimeter of the window, there is some ambiguity involved in calling the boundary conditions either clamped or simply supported.

Case 1.

For a plate which is simply supported along all four sides, the maximum stress is tensile and occurs in the center of the plate on the side opposite the applied pressure.

$$\sigma_{max} = \frac{0.7134\ p\ b^2}{t^2}$$

where σ = stress

p = pressure = 3.5 psi

b = plate width = 10.8 inches

t = plate thickness

The pressure is assumed uniform at 3.5 psi. This is the pressure expected at the bottom of the test section and is a conservative assumption. Another formula from reference 32 shows that this uniform pressure assumption produces a greater maximum stress than if the pressure were assumed to vary linearly across the width of the plate from 2.5 psi to 3.5 psi which is the load actually expected. The maximum

deflection also occurs at the center of the plate and is given by

$$y_{max} = \frac{0.1335\ p\ b^3}{E\ t^3}$$

where y = deflection

E = Young's modulus = 350,000 psi

Case 2

For a plate which is clamped along all four sides, the maximum stress is again tensile and occurs in the center of the longest edge, on the clamped boundary on the same side of the plate as the applied pressure. This stress is given by

$$\sigma_{max} = \frac{0.5\ p\ b^2}{t^2}$$

The maximum deflection is again at the center of the plate and is

$$y_{max} = \frac{0.0284\ p\ b^4}{E\ t^3}$$

Summary of Preliminary Analysis

The nominal one inch thick acrylic plate has an actual minimum thickness of 0.96". Because the thickness varies by as much as 0.040" throughout the plate, the minimum thickness of the flange which supports the window is 0.30".

The following shows the result of evaluating the formulae given above at both thicknesses.

Table 2. Summary of Stress on Thin Acrylic Plate

Boundary	Thickness [inches]	Stress [psi]	Deflection [inches]
simply supported	0.30	3,236	0.673
simply supported	0.96	316	0.021
clamped	0.30	2,268	0.143
clamped	0.96	221	0.004

It is obvious from these results that the window would be sufficiently strong if it were 0.96" thick throughout. Since the window has a 0.30" thick flange along the entire perimeter, however, it is noted that the maximum stress for a 0.30" thick plate is of the same order of magnitude as the maximum allowable stress (7,000 psi). Also, the maximum stress is likely to occur near the edge of the window, which is where the corner of the flange is located, and such a corner is a known stress concentration factor. This indicates that a more rigorous analysis is needed, and a finite element analysis of the window is presented next. The results of the above analysis for the 0.96" thick plate with a clamped boundary are used to validate the

finite element model of the window as explained in the next section.

NISA Finite Element Analysis

The window was modeled using three dimensional solid elements with nodes at each corner and at the midpoints of the edges for a total of twenty nodes per element. Only one-quarter of the window was modeled, and symmetric boundary conditions were applied at the appropriate boundaries. Many of the elements had rather large aspect ratios, but the elements near the edges were nearly square. Even with the large elements and the symmetry technique, this model was near the upper limit of model complexity possible on the personal computer version of NISA available.

The first model used was that of a plain plate, the purpose being to compare results to the preliminary results reported in the previous section. A diagram of the cross section of the model, not to scale, follows.

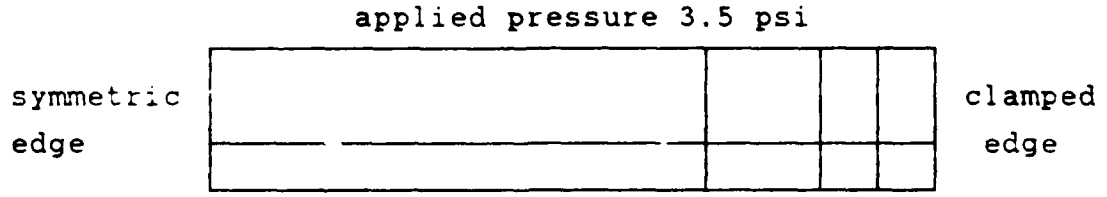

Figure 48. Cross Section of Finite Element Model of Flat Plate

The maximum deflection computed was 0.004" at the

center of the plate which is the same as the estimate in Table 2. The maximum stress was 237 psi tension at the center of the longest edge on the same side of the plate as the applied pressure, and the maximum compressive stress was -262 psi at the side of the plate opposite the applied pressure. The magnitude of these stress values is 7.2% higher and 18.5% higher, respectively, than the corresponding estimates in Table 2 above and in neither case is the computed stress as large as that estimated for the simply supported edge case above. So it seems that the large aspect ratio elements used in the central portion of the finite element model have not seriously degraded the results obtained.

The finite element model for the window is obtained from the plate model by deleting certain elements as can be seen in Figure 49 below. Note that only a cross section of the model is shown, and the model is in fact composed of three dimensional elements. The flange on the long edge can

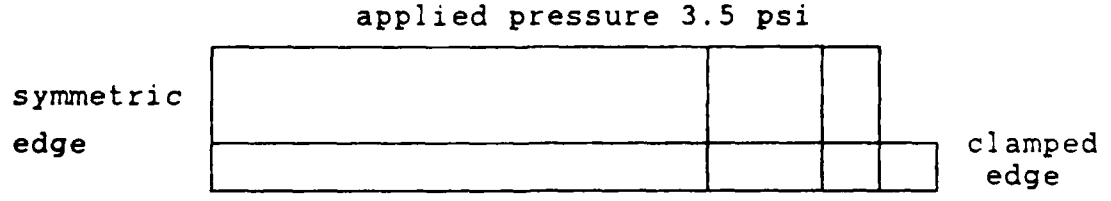

Figure 49. Cross Section of Finite Element Model of Window

be seen in the figure, and while the flange on the short

edge is not shown, it was included in the model.

The maximum deflection for the window model was -0.009". This deformation occurred in the center of the window and was somewhat larger than the deformation of the plate, as expected. The maximum stress occurred at the center of the long edge, as expected, but on the clamped boundary. The tensile stress was 379 psi on the side of the flange closer to the applied pressure and compressive stress was 719 psi on the side opposite the pressure load. In the corner where the flange joins with the thick part of the window, the stress is compressive and at the center of the long edge has a value of 184 psi. Recall that it was expected this corner would be a stress concentration factor and that a large tensile stress would occur at this point. This seems not to have occurred probably because of the rigidity of the thick part of the window which causes mostly a shear stress to be propagated into the flange rather than a bending stress. The deformation at this point is 0.0002" down (referring to Figure 49) and 0.0001" to the right which should not cause any leakage of water around the O-ring seal between the window and the test section frame. Since the allowable stress is at least 7,000 psi, it seems that the window has a safety factor of about 9.7 based on a maximum computed stress of 719 psi.

Appendix D - Nozzle Design

The problem to be addressed in designing a nozzle for this research project is that a relatively slow flow of circular cross section must be accelerated to a fast flow of square cross section which is as uniform as possible. First, the flow in the 24" diameter stilling tank is assumed uniform as is the flow in the 10" square test section. Then, smooth polynomial curves are used to mate the circular cross section to the square cross section.

The polynomials used to define the shape of the nozzle have zero slope in the longitudinal direction at either end of the nozzle and have an inflection point along the length of the nozzle at a specified location. Since the boundaries of the nozzle can be generated by simple polynomials, and are streamlines (actually stream surfaces), it is possible to derive a stream potential and a velocity potential for flow inside the nozzle although this will not be shown in this thesis. According to Professor Larsen [24], this method has often been used to design both internal flow diffusers and nozzles and external flow aircraft fuselage and nacelle parts where some specified shape must be enclosed by a smooth curved surface.

Consider the graph of a smooth curve as shown in Figure 50 where the slope of the curve at $x = 0$ and at $x = L$ is

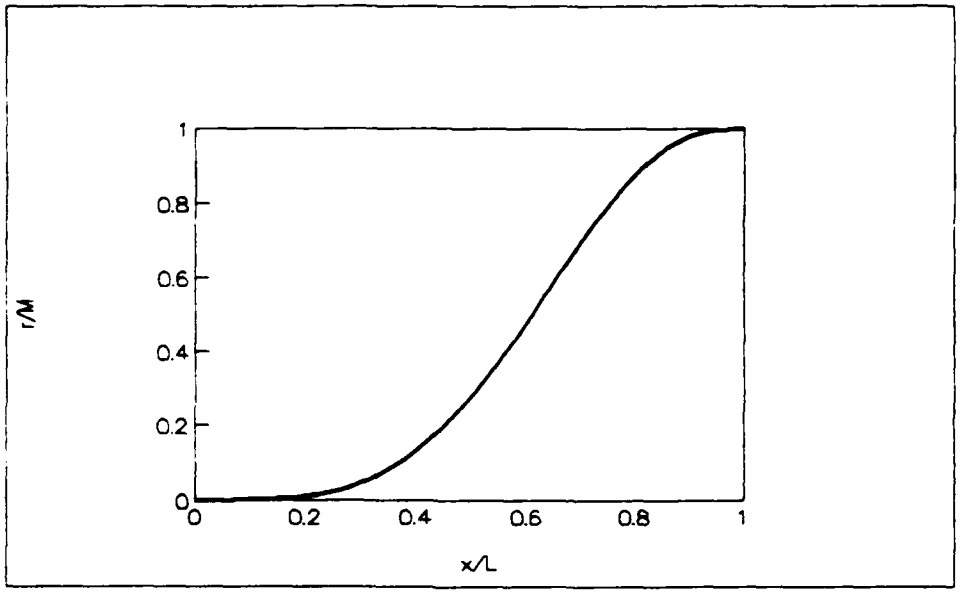

Figure 50. General Longitudinal Section of Nozzle

zero. The curve has an inflection point at $x = x_i$ which is chosen to be about two thirds of the way from the origin to $x = L$. As the abscissa varies from zero to L, the ordinate r varies from zero to M. The dimensions x and r may be non-dimensionalized by L and M respectively as follows

$$\bar{r} = \frac{r}{M}, \quad \bar{x} = \frac{x}{L}$$

Then $\bar{r}$ varies from zero to one as $\bar{x}$ varies from zero to one. The overall length of the nozzle will be 36" but it is convenient to leave the $\bar{x}$ coordinate non-dimensional for now. The derivative of the function describing the curve will have the form

$$\frac{d\bar{r}}{d\bar{x}} = k\bar{x}^{p}(1-\bar{x})^{q} \qquad (1)$$

where q must be an integer in order to keep the remaining analysis simple, and p may be any real number. The constant k will be evaluated later. The second derivative of $\bar{r}(\bar{x})$ will be

$$\frac{d^{2}\bar{r}}{d\bar{x}^{2}} = k\left[p\bar{x}^{p-1}(1-\bar{x})^{q} - \bar{x}^{p}q(1-\bar{x})^{p-1}\right]$$

Now set the second derivative equal to zero and the resulting value of $\bar{x}$ will be $\bar{x}_i$ the value at the inflection point.

$$0 = k\bar{x}^{p-1}(1-\bar{x})^{q-1}\left[p(1-\bar{x}_i) - q\bar{x}_i\right]$$

The roots of this equation at $\bar{x} = 0$ and $\bar{x} = 1$ are not of interest so solve the equation for $\bar{x}_i$ resulting in

$$0 = p(1-\bar{x}_i) - q\bar{x}_i$$

$$\bar{x}_i = \frac{p}{q+p}$$

Since we desire $\bar{x}_i$ to be about two-thirds, and q must be an integer, set q = 2. Then a value of p = 3.5 will give $\bar{x}_i = 0.636$.

Substituting q = 2 into equation (1) and integrating produces

$$\bar{r} = \frac{k}{p+1}\bar{x}^{p+1} - \frac{2k}{p+2}\bar{x}^{p+2} + \frac{k}{p+3}\bar{x}^{p+3} + C$$

where C is a constant of integration. Evaluating the integral between the limits $\bar{x} = 0$ and $\bar{x} = 1$ produces C = 0, k = 80.4375, and finally

$$\bar{r} = \frac{r}{M} = 80.4375\left(\frac{\bar{x}^{4.5}}{4.5} - \frac{\bar{x}^{5.5}}{2.75} + \frac{\bar{x}^{6.5}}{6.5}\right) \qquad (2)$$

Equation (2), with the addition of a constant to locate the starting point of the curve on the square end of the nozzle and adjustment of the constant M to place the end point of the curve on the twelve inch radius of the round end of the nozzle, can be used to generate any longitudinal templates describing the radius of the nozzle as a function of x or $\bar{x}$.

Considering the cross sections of the nozzle obtained in the YZ plane, when x is held constant, then

$$\left(\frac{y}{a}\right)^n + \left(\frac{z}{b}\right)^n = 1$$

which is the equation for a generalized ellipse which becomes rectangular as n is increased from two to infinity. This analysis would be valid for a nozzle which varies from an ellipse to a rectangle, but it becomes a bit simpler at this point if a and b are taken to be equal which leads to a shape which is square rather than rectangular and circular rather than elliptical. Note that a and b which are respectively the y-axis and z-axis intercept values of the generalized circle are constants in a given yz plane, but they are not constant with variation in $\bar{x}$. This is also the

case for the exponent n which is constant in a given YZ plane and varies only with $\bar{x}$. The equation for the generalized circle is then

$$\left(\frac{y}{E(\bar{x})}\right)^{n(\bar{x})} + \left(\frac{z}{B(\bar{x})}\right)^{n(\bar{x})} = 1 \qquad (3)$$

Equation (2) is used to produce $B(\bar{x})$ by taking M = (12-5) and adding a constant term of 5 giving

$$B(\bar{x}) = 563.0625\left(\frac{\bar{x}^{4.5}}{4.5} - \frac{\bar{x}^{5.5}}{2.75} + \frac{\bar{x}^{6.5}}{6.5}\right) + 5 \qquad (4)$$

It only remains to find an expression for $n(\bar{x})$ to be able to generate the coordinates for arbitrary points on the nozzle surface.

Along the shoulder line of the nozzle which is a curve that starts at the corner of the square end and follows the surface to the edge of the circular end at a constant angle $\theta=45^0$, a simple relationship exists between y and z. For the case of a generalized ellipse, y = (a/b)z and in this case

$$y = \left(\frac{B(\bar{x})}{B(\bar{x})}\right) z_s = z_s \qquad (5)$$

where z_s = z coordinate of a point on nozzle shoulder Note that z_s is another function of $\bar{x}$ which will be produced by adjustments to equation (2) and yields

$$z_s(\bar{x}) = 280.347321\left(\frac{\bar{x}^{4.5}}{4.5} - \frac{\bar{x}^{5.5}}{2.75} + \frac{\bar{x}^{6.5}}{6.5}\right) + 5 \qquad (6)$$

Substituting equation (5) into equation (3) gives

$$\left(\frac{z_s(\bar{x})}{B(\bar{x})}\right)^{n(\bar{x})} + \left(\frac{z_s(\bar{x})}{B(\bar{x})}\right)^{n(\bar{x})} = 1$$

which can be solved for $n(\bar{x})$ yielding

$$n(\bar{x}) = \frac{\log(1/2)}{\log\left(\frac{z_s(\bar{x})}{B(\bar{x})}\right)} \qquad (7)$$

Finally, the equation which generates templates of the nozzle at any cross section in the yz plane is obtained by solving equation (4) for y which gives

$$y = B(\bar{x}) \cdot \sqrt[n(\bar{x})]{1 - \left(\frac{z}{B(\bar{x})}\right)^{n(\bar{x})}} \qquad (8)$$

For a fixed $\bar{x}$, the value of $B(\bar{x})$ is given by equation (4) and the value of $n(\bar{x})$ is given by equations (6) and (7). Substituting these values into equation (9) provides $y = y(z)$ at a fixed cross section. Figure 51 shows a few of these cross sections for evenly spaced values of $\bar{x}$ between 1/6 and 5/6.

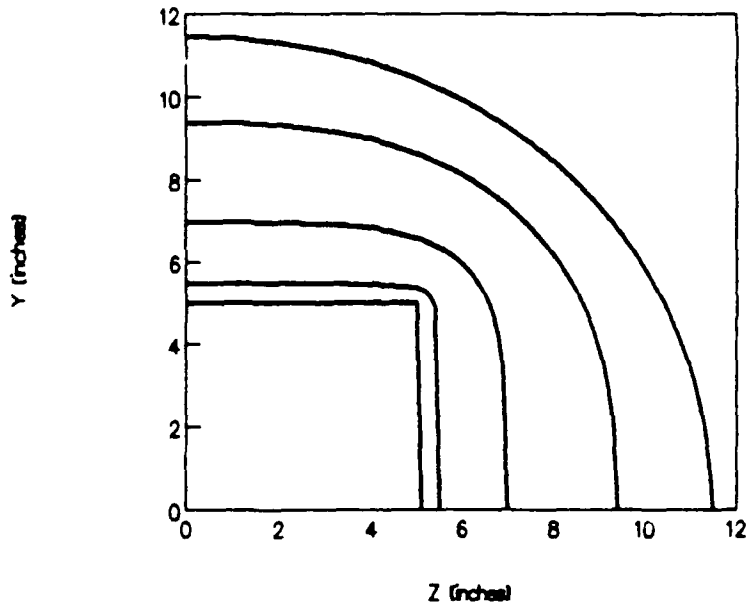

Figure 51. Cross Sections of Nozzle at Evenly Spaced Longitudinal Stations

Recall that Equation (2) can be adjusted to describe longitudinal templates for this nozzle. These template curves will lie in any plane which contains the center line of the nozzle. It can be shown that these curves will be of the form

$$R(\bar{x}) = \frac{B(\bar{x})}{\cos\theta}\left[\frac{1}{1+\tan^{n(x)}\theta}\right]^{1/n(\bar{x})} \qquad (9)$$

where $R(x)$ = radius from center line of nozzle

θ = angle in the YZ plane away from y-axis or z-axis

$B(x)$ and $n(x)$ will be developed next

The angle θ in equation (9) should only be allowed to vary between 0^0 and 45^0. This causes no great difficulties as the nozzle symmetry can be exploited so that a set of templates which covers one-eighth of the nozzle can be used on the other octants as well.

Equation (9) is also be used to find the maximum slope in the nozzle. The nozzle designed for this research project has a maximum slope of 23.03^0 which occurs at four locations corresponding to θ = 0 (the y-axis and z-axis) and is at the same longitudinal location as the inflection point. The nozzle length is 36" so when $\bar{x}_i = 0.636$, and note that the inflection point occurs at $\bar{x}_i = 0.636$ no matter what the angle θ is, then x = (0.636)(36") = 22.9".

Since an adverse pressure gradient in the flow direction is not expected in a nozzle as it is in a diffuser, the maximum slope of 23.03^0 is not expected to cause any stalled regions in the nozzle. If this technique is used to design any diffusers for future modifications to this research facility, it is important to note that this design procedure provides no benefit as far as designing diffusers with large flow turning angles which are any less likely to experience separated flow. This process is presented solely as a technique to mate a round cross section flow with a square cross section flow.

Bibliography

1. Ashill, P.R. and Keating, R.F.A. "Calculation of Tunnel Wall Interference from Wall-Pressure Measurements," Aeronautical Journal, 92-911:36-53 (January 1988)

2. Ashill, P.R. and Weeks, D.J. "A Method for Determining Wall Interference Corrections in Solid-Wall Tunnels from Measurements of Static Pressure at the Walls," AGARD Conference Proceedings CP-335:Paper 1 (May 1982)

3. Ashill, R.P. and Keating, R.F.A. Calculation of Tunnel Wall Interference From Wall-Pressure Measurements, Royal Aircraft Establishment Technical Report 85086, 1985.

4. Brebbia, C.A. The Boundary Element Method for Engineers, (Second Revised Edition). Plymouth, UK: Pentech Press Limited, 1984.

5. Clauser et al. The Encyclopedia of Engineering Materials and Processes. New York: Reinhold Publishing Corporation, 1963.963.

6. Engineering Mechanics Research Corporation. NISA II PC Users' Manual, Release 86.6. Troy, Michigan: August 1986.

7. Erickson, G.E. Vortex Flow Correlation. Technical Report AFWAL-TR-80-3143, January 1981.

8. Gibson, A.H. "On the Flow of Water Through Pipes and Passages Having Converging or Diverging Boundaries," Proceedings of the Royal Society of London, Series A 83:366-378 (1910)

9. Gipson, G.S. Topics in Engineering, Volume 2, Boundary Element Fundamentals - Basic Concepts and Recent Developments in the Poisson Equation. Boston: Computational Mechanics Publications, 1987.

10. Hackett, J.E. Living with Solid-Walled Wind Tunnels. AIAA Paper 82-0583, 1982.

11. Hackett, J.E. and Boles, R.A. Highlift Testing in Closed Wind Tunnels. AIAA Paper 74-641, July 1974.

12. Hackett, J.E. et al. Determination of Wind Tunnel Constraints by a Unified Wall Pressure Signature Method. Part I: Applications to Winged Configurations. NASA Contractor Report, CR-166,186, June 1981.

13. Hackett, J.E. and Wilsden, D.J. "Determination of Low Speed Wake Blockage Corrections via Tunnel Wall Static Pressure Measurements," AGARD Conference Proceedings CP-174:Paper 22-1. October 1975.

14. Hackett, J.E. and Wilsden, D.J. Estimation of Tunnel Blockage from Wall Pressure Signatures: A Review of Recent Work at Lockheed-Georgia. AIAA Paper 78-828, April 1978.

15. Hackett, J.E. et al. Estimation of Tunnel Blockage from Wall Pressure Signatures, a Review and Data Correlation. NASA Contract Report CR-152,224, March 1979.

16. Hackett, J.E. et al. A Review of the Wall Pressure Signature and Other Tunnel Constraint Correction Methods for High Angle-of Attack Tests. Paper Presented to AGARD Fluid Dynamics Panel Subcommittee on Wind Tunnels and Testing Techniques, Round Table Discussion on Wind Tunnel Corrections for High Angle-of -Attack Models: Munich, Federal Republic of Germany, 8 May 1980.

17. Heysen, H.H. General Theory of Wall Interference for Static Stability Tests in Closed Rectangular Test Sections and in Ground Effect. NASA Technical Report TR R-364, 1971.

18. Heysen, H.H. Rapid Estimation of Wind-Tunnel Corrections with Application to Wind-Tunnels and Model Design. NASA Technical Report TD D-6416, 1971

19. Heysen, H.H. Use of Superposition in Digital Computers to Obtain Wind-Tunnel Interference Factors for Arbitrary Configurations, with Reference to V/STOL Models. NASA Technical Report TR R-302, 1969.

20. Joppa, R.G. Wind Tunnel Interference Factors for High-Lift Wings in Closed Wind Tunnels. NASA Contractor Report CR-2191, 1973.

21. Karamcheti, K. Principles of Ideal-Fluid Aerodynamics. Malabar, Florida: Robert E. Krieger Publishing Company, Incorporated, 1980.

22. Kline, S.J. "On the Nature of Stall," Journal of Basic Engineering 81:305-320 (September 1959)

23. Kline, S.J. et al. "Optimum Design of Straight-Walled Diffusers," Journal of Basic Engineering 81:321-331 (September 1959)

24. Larsen, H.C., Professor Emeritus of Aerospace Vehicle Design, School of Engineering, Air Force Institute of Technology, Wright-Patterson AFB, Ohio. Personal Interviews, 13 June through 30 September 1988.

25. Maskell, E.C. A Theory of the Blockage Effects on Bluff Bodies and Stalled Wings in a Closed Wind Tunnel. Air Research Committee (United Kingdom), Reports & Memoranda Number 3400, 1963.

26. Moses, D.F. "Wind Tunnel Wall Corrections Deduced by Iterating from Measured Wall Static Pressure'" AIAA Journal 21:1667-1673 (December 1983)42

27. Newman, P.A. and Barnwell, R.W. Wind Tunnel Wall Interference/Correction. NASA Conference Publication CP-2319, January 1983.38

28. Pirolo, Capt D.G. Piezoelectric Polymer Tactile Sensor Arrays for Robotics. MS Thesis, AFIT/GE/ENG/87D-52. School of Engineering, Air Force Institute of Technology (AU), Wright-Patterson AFB, OH, December 1987.

29. Rae, W.H. Jr. and Pope, A. Low-Speed Wind Tunnel Testing (Second Edition). New York: John Wiley & Sons, Incorporated, 1984.

30. Reston, Capt R.R. Robotic Tactile Sensor Fabricated from Piezoelectric Polyvinylidene Flouride Films. MS Thesis, AFIT/GE/ENG/88D-41. School of Engineering, Air Force Institute of Technology (AU), Wright-Patterson AFB, OH, December 1988.

31. Rauscher, M. Introduction to Aeronautical Dynamics. New York: John Wiley & Sons, Incorporated, 1953.

32. Roark, R.J. and Young, W.C. Formulas for Stress and Strain (Fifth Edition). New York: McGraw-Hill Book Company, 1975.

33. Stahl, W.H. Variable-Temperature Water Tunnel for High Reynolds Numbers. AIAA Paper 85-0051, January 1985.

34. Streby, G.D. Multi-Ducted Inlet Combustor Research and Development Interim Technical Report, August 1981 to August 1982. Contract F33615-82-C-2074 (SB5448-82-C-0518), Air Force Wright Aeronautical Laboratories, Aero Propulsion Laboratory, Technical Report AFWAL-TR-82-2101, October 1982.48

35. Streeter, V.L. and Wylie, E.B. Fluid Mechanics, (Seventh Edition). New York: McGraw-Hill Book Company, 1979.

36. Walker, A.S. and Wiseman, N.P. The Pressure Signature Method for Blockage Corrections, and Its Application to the Industrial Wind Tunnel. BS Thesis, BU-263. Department of Aeronautical Engineering, University of Bristol, June 1981.

37. Zhou, C. Integral Method of Wall Interference Correction in Low-Speed Wind Tunnels. NASA Technical Translation of "Disu Fendong Dongbi Ganrao Xiuzheng Di Jifen Fangfa," Kongqi Lixue Xuebao, Number 2:1-8 (June 1985). NASA-TT-20055, April 1987.

VITA

Kurt A. Lautenbach [redacted] He received an Associate in Applied Science degree in Mental Health and Social Services from Philadelphia Community College in March 1977 and a Bachelor of Science in Chemistry from Saint Joseph's University, Philadelphia in May 1980. He was commissioned through Officer Training School at Lackland Air Force Base, Texas on 15 July 1981 and assigned to the Air Force Institute of Technology for the Undergraduate Engineering Conversion Program where he earned a Bachelor of Science in Aeronautical Engineering in March 1983. He was then assigned to Air Force Systems Command, Electronic Systems Division at Hanscom Air Force Base, Massachusetts where he worked in the Jam-Resistant Voice Communications Systems Program Office first as an Aircraft Integration Project Officer and eventually as HAVE QUICK II High Power Amplifier Program Manager. He entered the Air Force Institute of Technology in the Graduate Aeronautical Engineering Program in June 1987.

[redacted]

UNCLASSIFIED
SECURITY CLASSIFICATION OF THIS PAGE

REPORT DOCUMENTATION PAGE

Form Approved
OMB No. 0704-0188

1a. REPORT SECURITY CLASSIFICATION UNCLASSIFIED	1b. RESTRICTIVE MARKINGS
2a. SECURITY CLASSIFICATION AUTHORITY	3. DISTRIBUTION / AVAILABILITY OF REPORT Approved for public release; distribution unlimited
2b. DECLASSIFICATION / DOWNGRADING SCHEDULE	
4. PERFORMING ORGANIZATION REPORT NUMBER(S) AFIT/GAE/AA/88D-20	5. MONITORING ORGANIZATION REPORT NUMBER(S)
6a. NAME OF PERFORMING ORGANIZATION School of Engineering 6b. OFFICE SYMBOL (If applicable) AFIT/ENY	7a. NAME OF MONITORING ORGANIZATION
6c. ADDRESS (City, State, and ZIP Code) Air Force Institute of Technology Wright-Patterson AFB, OH 45433-6583	7b. ADDRESS (City, State, and ZIP Code) 12 Jan 1989
8a. NAME OF FUNDING / SPONSORING ORGANIZATION 8b. OFFICE SYMBOL (If applicable)	9. PROCUREMENT INSTRUMENT IDENTIFICATION NUMBER
8c. ADDRESS (City, State, and ZIP Code)	10. SOURCE OF FUNDING NUMBERS PROGRAM ELEMENT NO. / PROJECT NO. / TASK NO / WORK UNIT ACCESSION NO

11. TITLE (Include Security Classification)
Design of Water Tunnel to Measure Wall Pressure Signatures Due to Tunnel Blockage and Wake Effects

12. PERSONAL AUTHOR(S)
Kurt A. Lautenbach, B.S., Capt, USAF

13a. TYPE OF REPORT	13b. TIME COVERED	14. DATE OF REPORT (Year, Month, Day)	15. PAGE COUNT
MS Thesis	FROM _____ TO _____	1988 December	126

16. SUPPLEMENTARY NOTATION

17. COSATI CODES			18. SUBJECT TERMS (Continue on reverse if necessary and identify by block number)
FIELD	GROUP	SUB-GROUP	
14	02		Water Tunnel
01	01		Wind Tunnel Tests

19. ABSTRACT (Continue on reverse if necessary and identify by block number)

Thesis Advisor: Maj Lanson J. Hudson, USAF
Instructor
Department of Aeronautics and Astronautics

This thesis describes the design and construction of a new test section for the AFWAL Aero Propulsion Lab six-inch water tunnel in building 18. The new test section has a ten-inch square cross section and is designed to measure wall pressure signatures caused by solid and wake blockage of the flow due to the separation bubble which forms around bluff bodies immersed in the flow. The wall pressure signature for a spherical model is predicted. Applications of the method and associated requirements for instrumentation are discussed.

20. DISTRIBUTION / AVAILABILITY OF ABSTRACT	21. ABSTRACT SECURITY CLASSIFICATION
☒ UNCLASSIFIED/UNLIMITED ☐ SAME AS RPT. ☐ DTIC USERS	
22a. NAME OF RESPONSIBLE INDIVIDUAL Maj Lanson J. Hudson, USAF	22b. TELEPHONE (Include Area Code) (513)255-2362 / 22c. OFFICE SYMBOL ENY

DD Form 1473, JUN 86 *Previous editions are obsolete.*

SECURITY CLASSIFICATION OF THIS PAGE
UNCLASSIFIED